Title
High-efficiency violet and blue InGaN microcavity light-emitting diodes

Author
Back, Joonho

Publication Date
2021

Peer reviewed|Thesis/dissertation

UNIVERSITY OF CALIFORNIA

Santa Barbara

High-efficiency violet and blue InGaN microcavity light-emitting diodes

A dissertation submitted in partial satisfaction of the

requirements for the degree Doctor of Philosophy

in

Electrical and computer engineering

by

Joonho Back

Committee in charge:

Professor Shuji Nakamura, Chair

Professor Claude Weisbuch

Professor Steven DenBaars

Professor Jonathan Klamkin

March 2021

The dissertation of Joonho Back is approved.

Professor Claude Weisbuch

Professor Steven DenBaars

Professor Jonathan Klamkin

Professor Shuji Nakamura, Committee Chair

March 2021

ACKNOWLEDGEMENTS

Joining the SSLEEC group was big moment to my PhD life. When I recall, it contains lots of life lessons, hard workings, and delightful times. Over six years in UCSB, the life as a graduate student researcher in this group might take 80% of the portion. I was a novice in this graduate school life at the beginning. Though I did not know what is going to happen, I was not worried since I was a good student in undergraduate. In very short time, the illusion got cleared, and I started to face the genuine time as researcher. Finding or studying new things which are not mentioned in the text book or internet was enough to make me lost in the field. Sometimes, I was depressed and frustrated when I could not get any result or even a little hint of something.

However, I have learned as time passes how the professionals should act during those moments. And it has been possible because of the guidance of Prof. Shuji Nakamura. To learn life changing lesson, one needs lots of resources, such as time and supports until it reaches the certain level above the threshold, like a diode. Also, he did not simply keep support my research. Sometimes, he gave critical and constructive feedback when I was off the track. Those have sobered me and guided me to correct direction.

I also would like to thank Prof. Claude Weisbuch. He brought this microcavity LED topic to our group. I could learn the main theories and concepts from his supports and publications. At the beginning of the project, we had several meetings to make the device happened. Also, during the publication process, he commented on many theoretical parts in the drafts. Some of them were critical and could not be found without his helps.

Prof. DenBaars supported all the research resources including the MOCVD growths. Also, he helped all the people in the SSLEEC to be connected even in the pandemic. Actually, he suggested a key process step to achieve the big improvement on MC-LED, which other LED researchers do. I would also like to thank Prof. Jonathan Klamkin for his supports. He always welcomed scheduling the important meetings, such as qualification exam and my defense, though it might not be easy to spend time for other group students. Also, he gave an access of the high frequency measurement lab to us for future study. I believe our future researchers will find the stunning results at there.

I would like to thank all the MC-LED project related researchers, Vince, Camille, Guillaume, Morteza, and Yi chao. Vince joined this topic in November 2020, but he was passionate to learn. This made me to recollect lots of basic concepts and theories of MC-LED. Those were really helpful during the last set of experiment by revisiting ignored points. Also, we could bring up more possibilities of MC-LED, which almost made me feel staying and studying more about it. Camille and Guillaume helped the setting up the angular measurement tool. Though it could not be done, I appreciate their works. And I think working with Morteza and Yi chao would be great for the future researcher of this project. They were very supportive and knowledgeable in measuring the device in different ways.

I appreciate the VCSEL team, Dr. Dan Cohen, Jared, Nate, Ryan Anderson. Without the experience in the team, I could not make the MC-LED happened. I have learned lots of understanding about optoelectronics from Dr. Cohen, growth and processing from Jared. It was great moment when we could demonstrate the first semipolar VCSEL. Nate gave me new view and idea about the VCSEL. And I would like to thank Ryan helping me the growth and maintenance of MOCVD. Actually, the PEC etching and flip-chip bonding which I could learn in this team were key steps to demonstrate the MC-LEDs.

My thanks also go to lab members, Philip, Shereen, Haojun, Hongjian, and Panpan. Especially, Philip and Shereen joined this group at the same time, and we prepared the screening exam together. The fact itself that there are colleagues having similar backgrounds nearby made me feel supported. We had chat about research related and non-related topics. And they also welcomed me to asking sometimes dumb questions about optoelectronics. Changmin, Seunggeun, Sangho who were the previous students in the group supported a lot about the graduate student life in the group and outside of the group, such as studying abroad in US. I also have learned many things about living in Santa Barbara.

Lastly, I should give my thanks to my other lab mates, roommates, friends and families including my fiancé. They made my life during the PhD precious though it could be the tough moments. Their emotional supports in many ways helped me from deep in the mind.

VITA OF Joonho Back
January 2021

EDUCATION

Ph.D. candidate in Electrical and computer engineering, August 2020
Advisor: Shuji Nakamura
University of California, Santa Barbara, CA

M.S. in Electrical and computer engineering, March 2017
Advisor: Shuji Nakamura
University of California, Santa Barbara, CA

B.S. in Electronic engineering, Feb 2013
Dongguk University, Seoul, South Korea

PROFESSIONAL EMPLOYMENT

Graduate student researcher, January 2016 - December 2020
Solid state lighting & energy electronics center (SSLEEC), University of California, Santa Barbara

- Demonstrated ultra-short microcavity light-emitting diodes (MC-LEDs) using semipolar (20-2-1) GaN with the thickness from 110 nm to 290 nm
- Achieved high efficiency 205 nm MC-LEDs with sidewall treatment on semipolar (20-2-1) GaN
- Demonstrated blue, 445 nm wavelength, semipolar vertical-cavity surface-emitting lasers (VCSELs)

Undergraduate student researcher, June 2011 - March 2012
Dongguk University, Seoul, South Korea

- Designed the image processing program for analysis of numerical and graphical results of mouth recognition using OpenCV, C++
- Designed the image processing program using MFC, C++

PUBLICATIONS

- **Back, J.***, et al. (2021); Blue semipolar InGaN microcavity light-emitting diode with a cavity length from 113 nm to 290 nm. Applied Physics Express, accepted
- **Back, J.***, et al. (2021); High efficiency blue InGaN microcavity light-emitting diode with a 205 nm ultra-short cavity. Applied Physics Letters, Vol. 118, No. 3: 031102
- **Back, J.***, et al. (2020); Violet semipolar (20-2-1) InGaN microcavity light-emitting diode with 200 nm ultra-short cavity length. Optics Express, Vol. 28, No. 20: 29991
- Kearns, J. A., **Back, J.***, et al. (2019); Inhomogeneous Current Injection and Filamentary Lasing of Semipolar (20-2-1) Blue GaN-Based Vertical-Cavity Surface-Emitting Lasers with Buried Tunnel Junctions. Phys. Status Solidi A 2019, 1900718

- Kearns, J. A., **Back, J.***, et al. (2019); Demonstration of blue semipolar GaN-based vertical-cavity surface-emitting lasers. Optics Express, Vol. 27, No. 17: 23707
- Mughal, A., Young, E., Alhassan, A., **Back, J.***, et al. (2017); Polarization-enhanced InGaN/GaN-based hybrid tunnel junction contacts to GaN p–n diodes and InGaN LEDs. Applied Physics Express, 10: 121006

AWARDS

Graduate Student Researcher Fellowship, January 2016 - December 2020
University of California, Santa Barbara, CA

Graduate with Honors, February 2013
Dongguk University, Seoul, South Korea

Honors Student, March 2011 - December 2012
Dongguk University, Seoul, South Korea

ABSTRACT

High efficiency GaN-based microcavity light-emitting diodes on semipolar (20-2-1)

by

Joonho Back

III-nitride materials are widely used these days for display, visual light communication, and power electronics from wearable devices to large home appliances. Especially, III-nitride micron-sized light-emitting diodes (µLEDs) in display get wide attentions because of its self-emissivity, small form factor and reliability. These characteristics make µLEDs as one of the best candidates for the next generation displays such as ultra-high resolution near-eye displays for augmented reality (AR) and virtual reality (VR) applications. Because µLEDs have advantages in lifetime, color gamut, form factor size and efficiency unlike the other displays, such as LCDs and OLED. However, there are several downsides of color mixing, color stability, and directionality for those purposes.

The possible solution for those issues would be reducing the thickness of devices. This is basic concept of the microcavity LEDs (MC-LEDs). Therefore, it has been studied for improved directionality, spectrum purity, and thermal stability by minimizing the guided modes in the device. Recently, the ultra-short 200 nm cavity length MC-LEDs with the single mode operation was demonstrated by overcoming the fabrication limit. In this dissertation, the theory of MC-LED and its simulation are explained. Also, I am going to cover the whole

processing steps and results of the electrically injected MC-LEDs grown on GaN semipolar (20-2-1) substrate. Continuously, the device improvement of using sidewall treatment has been achieved. While the previous device has 0.8% of external quantum efficiency (EQE), the second version has peak EQE of 7.3% without the encapsulation. Considering the EQE of the μLEDs without encapsulation is 10.5%, the sidewall treated MC-LEDs reach the similar performance level of conventional ones. This 205 nm MC-LEDs with the wavelength of 430 nm could produce better quality of display, because each device is separated and guided modes are negligible, which cause color mixing. Lastly, with well-designed epitaxial structure and processing steps, the record-thin MC-LEDs with cavity length of 113nm is achieved. We will cover the analysis of these MC-LEDs with different thicknesses, from 110 nm to 290 nm since the light extraction efficiency (LEE) and the directionality are determined by the cavity design in MC-LED. We will see a big potential to use these devices near future. The light can be well controlled by the thickness and active region position.

TABLE OF CONTENTS

1. III-N based light-emitting diodes

III-nitride semiconductors are widely used for various applications spanning from power electronics to optoelectronics. In optoelectronics, there are many uses of as visible light communication, lighting, display and disinfections, despite the nitride materials system having high defect densities and polarization fields[1]–[5]. Especially, micron-sized light-emitting diodes (micro-LEDs) using the III-nitride materials are considered as great candidates for the future displays from near-eye wearable devices to large home appliances[6]–[8]. Micro-LEDs have the main advantages of wide color gamut, high wall-plug efficiency, long operating lifetime and chemical robustness compared to conventional liquid crystal displays (LCDs) and organic light-emitting diodes (OLEDs)[9], [10].

1.1. micro-LED applications

III-nitride materials have been one of the promising semiconductor alloy system by achieving low-resistivity p-type GaN in 1992[11]. Since the Mg-doped GaN is passivated with hydrogen atoms, it could be activated with the thermal annealing at 700 °C which breaks Mg-H bonds[12]. Though there were challenging properties, such as strong polarization which separates electron and hole wave functions and a high defect density, it has been most promising materials emitting light with the improvements of epitaxial growth and processing techniques. Therefore, it has expanded as the major solid-state light source using a phosphor which converts the blue emission to white. Not only used as lighting, but it could also be applied for visual light communications and displays[6]. Common displays are LCDs and OLEDs nowadays. Nevertheless, many displays have been replaced with LEDs because of several advantages of the devices recently. Size of devices decreased as few hundreds to a hundred-micron range. And these are called as mini-LEDs or micro-LEDs. With a few hundred-micron devices, the display of consumer products, such as TV or handheld devices, could achieve high contrast ratio and long operation time without burn-in issues that OLEDs have.

1.2. Light extraction methods

III-nitride LED has high refractive index difference between the semiconductor and the air which is the outside material of conventional case. By Snell's law, the critical angle is narrow around 23°. This caused by low critical angle due to large refractive indices differences, where 2.5 of GaN and 1 of air. We can calculate the light extraction efficiency (LEE) of ~4% considering the emission from top and no encapsulation as shown in figure 1.1.

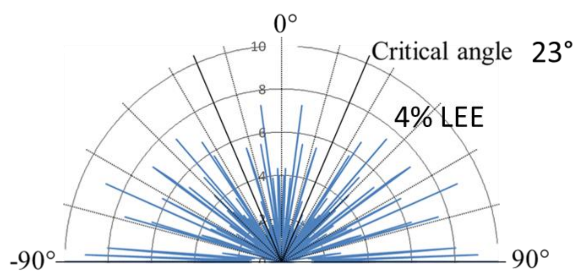

Figure 1.1 The light intensity distribution and light extraction efficiency of conventional top emitting micro-LEDs without encapsulation. The thickness of epitaxial growth is 5 μm on single-side polished sapphire of 500 μm.

To extract the light from the device, various patterns have been applied on either one or more than one parts of LEDs. Both output power and LEE have been improved a lot by surface or backside roughening on c-plane devices. This could be demonstrated by patterned sapphire substrate (PSS) and photoelectrochemical (PEC) etching[13], [14]. These patterns increase the possibility of reflected ray inside the device to be transmitted to low index materials. Since the total internal reflection (TIR) happens when the ray's incident angle from higher refractive index material to lower one is larger than the critical angle at the interface of two materials, the incident angle needs to be lower than the critical angle to escape from high index material. Those cone or pyramid patterns provide various incident angles to the rays within the critical angles at the interface by the geometrical shapes, which helps the light escapes from devices.

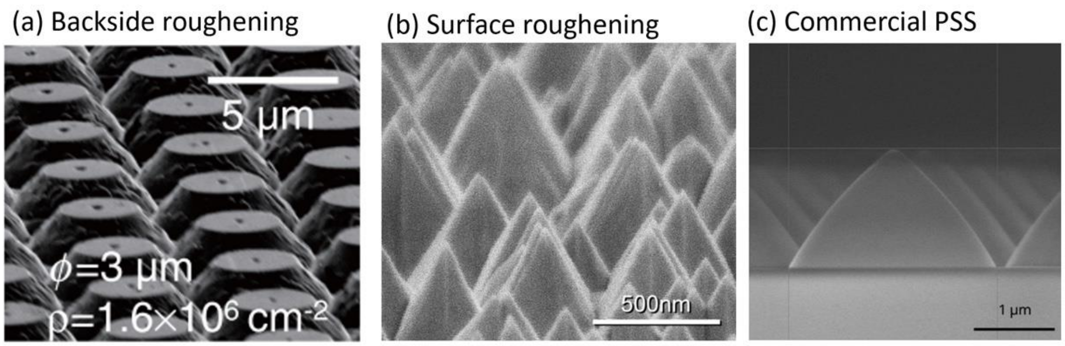

Figure 1.2 SEM images of various light extraction techniques using the patterns. (a) patterned conical features on the backside of the devices[15]. (b) N-faced GaN surface roughneing by KOH-based PEC etching of 10 mins[13]. (c) commercially available PSS which has uniform cone arrays.

These are ways to increase the LEE of LEDs over 80%. However, when the sizes of devices are shrunk, these methods are not usable. Though the LEDs are promising candidates for next generation displays with several advantages as mentioned above, there are big issue to be widely used. Few hundreds micron size of devices is not suitable for display applications. The goal of the next generation displays is ultra-high resolution. To show more vivid colors, TV and handheld devices, such as cell phone or tablet, increases their pixels per inch gradually. Recently, up to 6,000 pixels of LEDs were hybridized to CMOS less than a inch diagonal for augmented reality and compact projection[16]. In this trend of technology, the size of LEDs is too large to be cost effective. To achieve lower cost of transferring devices which is key for high-volume consumer applications, the size of micro-LED needs to be ~9x9 μm^2 for 55” 3840x2160 resolution (4K) TV, which reduces the transferring cost per display under $165[9]. For 5.8” smartphone with 2560x1440 resolution (QHD), micro-LED size target is 3x3 μm^2[9]. This reduces the cost per display under $11. With these cases, micro-LED can be cost competitive with OLED as of 2020.

Recently, Ley at al and Smith et al could demonstrate micro-LED under 10 μm[17], [18]. Using the chemical etching and dielectric passivation of Al_2O_3, the diameter of 2~100 μm micro-LEDs were successfully demonstrated[18]. EQEs of LEDs increase from 8~10% to 12~13.5% with size reduction from 100 μm to 2 μm diameters. From their analysis, the LEE was higher in smaller LED with minimized sidewall damage, which is proved by ray-tracing simulation. Ultra-small micro-LED with diameter of 1 μm also has been demonstrated using the self-aligning fabrication technique[17]. In the former report, the backside LEEs were calculated by Monte Carlo ray tracing. For the diameter of 2, 5, 10, 20, 60, 100 μm cases, the LEEs were 25.1, 17, 14.1, 12.9, 12.3, 12.2% with smooth sapphire substrate and 64.5, 48.8, 41.2, 37.4, 34.7, 34% with rough sapphire. Figure 1.3 shows the two locations where the LEE was measured in their experiment. The results of those LEEs were measured at position of (a) as shown in the figure 1.3.

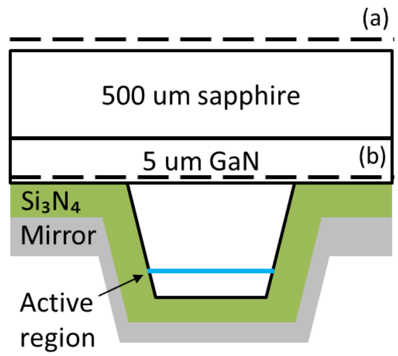

Figure 1.3 Schematic of device structure of backside emitting ultra-small micro-LED showing two different light extraction monitor locations, (a) the monitor above the sapphire substrate (b) the monitor close to mesa[18]

When the monitor was at (b) as in the figure 1.3, the directionality of light was better in smaller diameter devices than larger ones. Because the more rays inside the smaller mesa are reflected by the sidewall mirror and redirect close to normal by the angled sidewall, both directionality and LEE are improved.

This size reduction will solve the current limitation of micro-LEDs to be used as display application. Because the chip sizes of micro-LEDs which is commercially available are over 100 μm, it cannot be used for next generation small displays such as smart phones due to high costs and poor resolution. When the device size is reduced smaller than 3 μm range, the micro-LED can hit cost target for smartphone as mentioned above. This will lead the micro-LEDs as next generation displays such as Augmented reality display and smartphone display which would be a big market near future.

2. Microcavity LEDs

2.1. Advantages over micro-LEDs

As covered in previous section, the micro-LEDs with a size less than 10 μm have been demonstrated, which could make the LEDs cost competitive, especially, when those 3 μm devices are commercially available with the advanced fabrication technique. However, there are several problems, such as color mixing, color purity, directionality, and thermal stability.

First of all, the color mixing is common issue of micro-LEDs with PSS. As shown in figure 1.3, the ultra-small micro-LEDs emit the light to the backside of the devices because of metal mirror covering the mesa. From the Monte Carlo ray tracing, they could find the improved extraction efficiency with the PSS. However, the light goes to different directions since those PSS patterns enhance the extraction efficiency by redirecting the rays in various angles which increase the transmission between higher refractive medium, GaN, and the lower refractive index medium, sapphire. Therefore, the conventional LEDs use the patterned sapphire to extract more light from the devices as shown in figure 2.1[19].

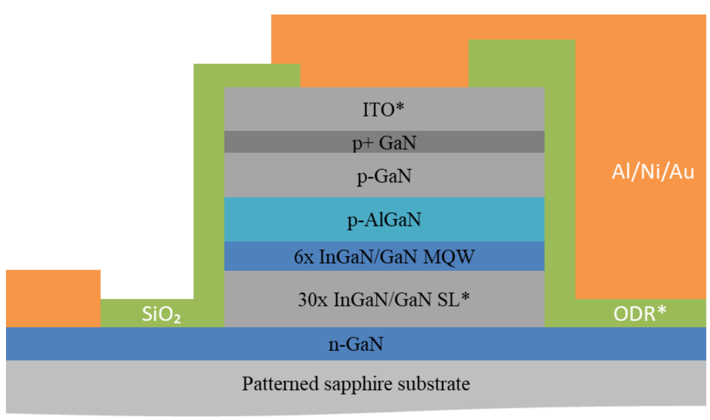

Figure 2.1 Schematic of conventional micro-LED structure with PSS[19].
*ITO: indium-tin oxide current spreading layer, SL: superlattices, ODR: omnidirectional reflector

However, the higher LEE is possible in MC-LED than conventional micro-LED without the PSS. The comparison of light intensity plot with respect to emission angles between micro-LED and MC-LED are shown in figure 2.2. The figure 2.2(a) represents the light intensity plot of conventional micro-LED. For these simulations, the encapsulation on top of the device is not applied, and only the top emission is considered. The critical angle for GaN/air interface is 23°. The light extraction efficiency in the case of conventional micro-LED is 4%. Normally, the device thickness is about 5 μm, and those epitaxial layers are grown on PSS. The conventional LEDs contain lots of optical modes because of the thick epitaxial growth and the substrate thickness. In figure 2.2(b), the result of 113 nm cavity length MC-LED is shown with the strong emission inside the critical angle. The LEE of the MC-LED is 35%, and the light is more directional than conventional micro-LED. Also, the metal contact is very close to the active region which might help the heat dissipation by the metal. However, this needs to be confirmed in future research.

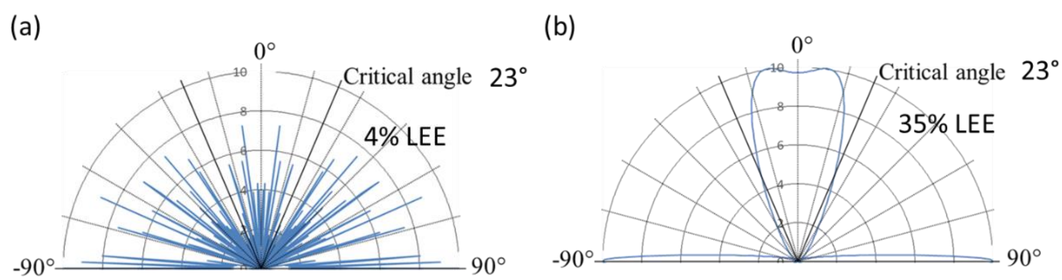

Figure 2.2 (a) The light intensity polar plot with respect to emission angle in conventional micro-LED. For the simulation, the critical angle is set as 23° because of GaN/air interface. Also for the simplicity, we consider only top emission of LED. (b) The light intensity polar plot of 113 nm cavity length MC-LED. The LEE is high as 35%, and the emission is more directional.

Conventional micro-LEDs have uncontrolled light direction since it uses the PSS to increase the light extraction. The extracted light scatters all directions, and this nondirectionality causes color mixing. On the other hand, the MC-LED does not use the PSS for light extraction. The high LEE characteristics come from its thin cavity effect of MC-LEDs.

In conventional LED, there are the similar ways to extract light, backside roughening, surface roughening. All of these techniques can increase the LEE over 80%. But, if the device sizes are reduced less than 3 μm for being cost-effective and high resolution display, then these methods will be unavailable to apply for the same purpose. Because the sizes of roughening are varied from 1~5 μm, those cannot give uniform light extractions for 3 μm sized LEDs. Therefore, conventional thick micro-LEDs without any roughening methods have the low LEE of 4%. The MC-LEDs achieve the superior LEE of 35% without any patterning methods.

Second advantage of MC-LED is color purity. Figure 2.3 shows the comparisons of spectral width. Figure 2.3(a) shows the emission spectra of 205 nm MC-LED grown on semipolar (20-2-1) GaN substrate with various current densities. The red dotted line is a cavity mode with a cavity length of 205 nm at emission angle 0°. And the red solid line is a spectrum with the FWHM of 22 nm at the highest current density. Figure 2.3(b) shows the spectra of conventional micro-LED. The FWHM is wide as 31 nm as shown the red solid line. Therefore, the MC-LED has a narrower spectral width. The difference comes from three reasons. First, MC-LED is grown on semipolar (20-2-1) GaN substrate which has a small polarization effect. Second, the peak wavelength of MC-LED is 435 nm which is shorter than conventional micro-LED of 445 nm. Third, MC-LED emission is determined by overlapping between QW emission and cavity mode. That is why the MC-LED showed better color purity than conventional one.

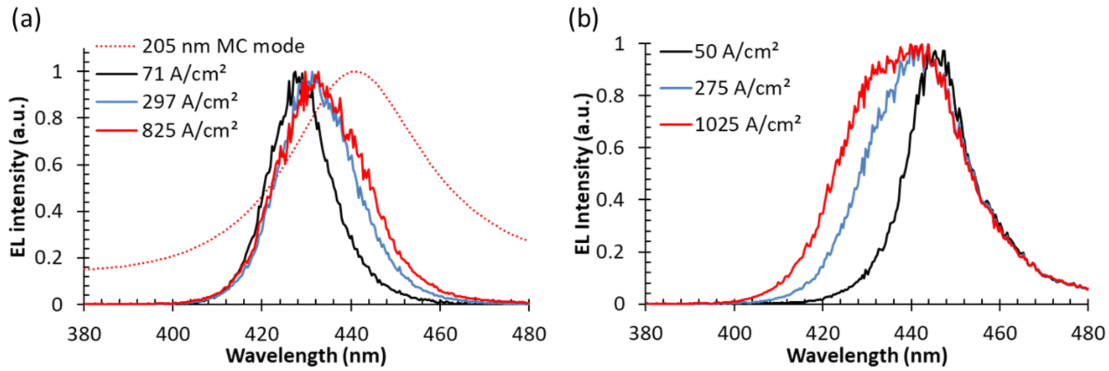

Figure 2.3 (a) Normalized emission spectra of 205 nm MC-LEDs at various current densities. Simulated spectrum of cavity mode of the 205 nm cavity length is shown as red dotted line. (b) Normalized emission spectra of conventional c-plane micro-LEDs at various current densities.

Third one is color stability as shown in figure 2.4. This figure shows the spectra as a function of the current densities. The emission spectra of 290 nm cavity length MC-LED are stable in pulsed operation in figure 2.4(a) because the emission spectra are determined by the overlapping the QW emission and the cavity mode, and the LED are grown on semipolar GaN subatrate . The FWHM in this device is 31 nm which is similar to conventional one shown in figure 2.4(b). The emission spectra, figure 2.4(b), are conventional c-plane micro-LED in pulsed operation. The FWHM is 31 nm in high current density. However, the MC-LED shows stable peak wavelength of 425 nm, while the conventional c-plane LED has peak wavelength at 444 nm with a large blue shift. It comes from the screening effect of the polarization of c-plane LED. We would like to try c-plane MC-LED to confirm the color stability due to the cavity effect in future.

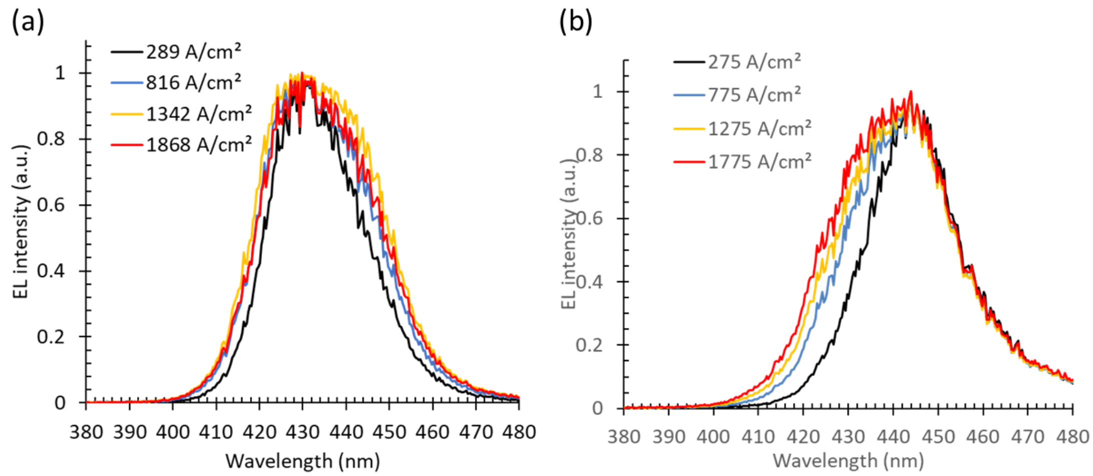

Figure 2.4 (a) Emission spectra of cavity length of 290 nm MC-LED as a function of the current density under pulsed operation with a duty ratio of 2% and frequency of 10 kHz. (b) Emission spectra of conventional micro-LED under pulsed operation with a duty ratio of 2% and frequency of 10 kHz.

2.2. Theory and simulations

To simulate the optical characteristics of MC-LED, we consider the Fabry-Perot cavity with length of L. There is electric field, E_0, traveling from outside of the cavity to the inside of it with incident angle θ as shown in figure 2.5(a). This cavity has top mirror with the reflectance of R_1 and bottom mirror with the reflectance of R_2. The phase shift, 2ϕ, is determined by the cavity length in this model as shown in equation (2.1). n is refractive index of medium, and k_0 is wavevector of light in the vacuum.

$$2\phi = 2nk_0L\,cos(\theta),\ \ k_0 = \frac{2\pi}{\lambda_0} \tag{2.1}$$

$$T_{FP} = \frac{|E_t|^2}{|E_0|^2} = \frac{T_1T_2}{\left(1-\sqrt{R_1R_2}\right)^2}A(\phi) \tag{2.2}$$

$$A(\phi) = \frac{1}{1 + \frac{4\sqrt{R_1 R_2}}{\left(1 - \sqrt{R_1 R_2}\right)^2} sin^2\phi} \tag{2.3}$$

The transmittances of both top and bottom mirrors are T_1 and T_2. The transmission intensity can be calculated by equation (2.2). From this equation, we can derive the A which is Airy function as shown equation (2.3). Airy function represents the resonant wavelength characteristics of the cavity. We can plot this Airy function with respect to wavelength as in figure 2.5(b). The figure 2.5(b) shows the simulation of two different cavity modes at 0° angle, θ=0. The solid line is 200 nm cavity length MC-LED, while the dashed line is 1.36 μm cavity length MC-LED as reference structure of MC-LED. In the figure, 200 nm MC-LED has only one broad wavelength peak while the 1.36 μm MC-LED has five narrow wavelength peaks in the wavelength range from 370 to 490 nm.

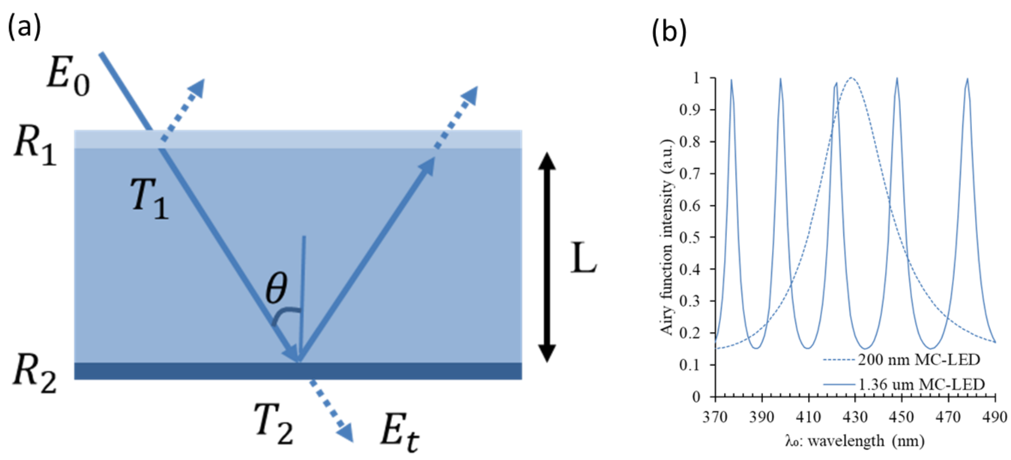

Figure 2.5. (a) Schematic of Fabry-Perot cavity with the length of L. (b) Simulation of Airy function of two cavity modes at 0° incident angle.

To be more realistic, we place active region in the Fabry-Perot cavity. The active region is located at z above the bottom mirror. There are two phase shifts that should be considered.

One phase shift is derived by the cavity length L, equation (2.3). Another one is from the QW position, z, equation (2.4).

$$\phi = nk_0 L\, cos(\theta), \qquad (2.3)$$

$$\phi' = nk_0 z\, cos(\theta) \qquad (2.4)$$

$$I_1 = |E_1|^2 = I_0 \frac{T_1}{\left(1-\sqrt{R_1 R_2}\right)^2} \boldsymbol{A}(\boldsymbol{\phi})\boldsymbol{\zeta}(\boldsymbol{\phi}') \qquad (2.5)$$

The emission intensity above the cavity, I_1, is derived by equation (2.5) which includes the Airy function. There is another term which is the antinode factor, ζ. The antinode factor expresses the coupling efficiency between the emission source and the cavity modes. If we can plot the emission intensity, I_1, with respect to emission angle θ, then the light intensity of the 200 nm cavity length MC-LED with respect to angle would be shown as figure 2.6(b). If we plot in polar plot with the angle from 0 to 180°, the light intensity distribution would be shown more intuitive as shown in figure 2.7(a). There is strong emission of light inside the critical angle (dotted line) which is 23° from the interface between GaN and air in figure 2.6(b). Unlike the strong emission in the air cone, the guided modes outside of the critical angle are weak and not preferred in this cavity design.

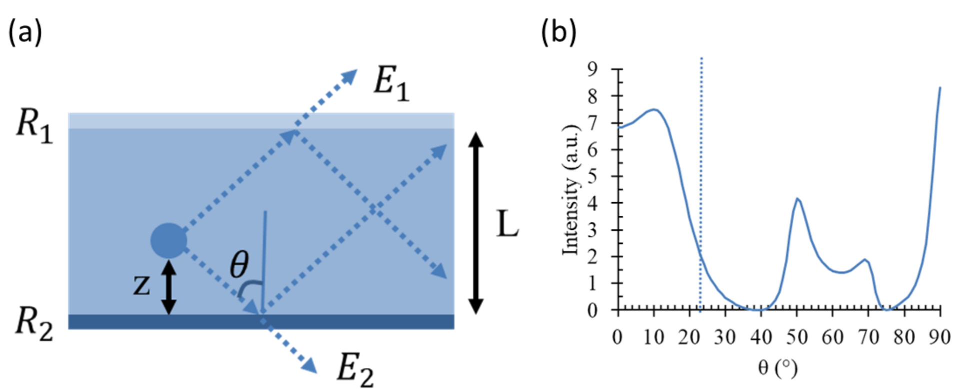

Figure 2.6. (a) Schematic of Fabry-Perot cavity length L with the light source placing at z above the bottom mirror. (b) Simulation of light intensity with respect to emission angle θ in 200 nm cavity length MC-LED.

From the light intensity distribution along the angles, the LEE of the MC-LED could be calculated. The equation is simple, basically light intensity inside the critical angle out of all other angles as equation (2.6). The schematic of the LEE calculation is shown in figure 2.7(a). Because the short cavity MC-LED has strong light emission in the air cone, the MC-LED could achieve the high LEE than the conventional thick LEDs.

$$\eta_{extr} = \frac{\int_{\theta=0}^{\theta_c} I\, sin\theta d\theta}{\int_{\theta=0}^{\pi} I\, sin\theta d\theta} \qquad (2.6)$$

The schematic shown in figure 2.7(b) represents the cavity modes of cavity lengths of 100, 200, 300 nm MC-LEDs. And the phase shift in Ag mirror is considered as the penetration depth which adds effective cavity length on top of the geometrical thickness. As mentioned above, the antinode factor which is coupling efficiency between cavity mode and the emission source is well represented in the figure. To have maximum LEE, we would like to place the QW (active region) on the antinode of cavity modes. By considering all of these factors, the LEE plot according to the cavity thickness and QW relative positions is shown in figure 2.7(c). The simulation has been done by Matioli et al. in 2010[20]. In this simulation, the cavity length of 200 nm MC-LED has the LEE of 31%, while 1.36 μm MC-LED has 15%.

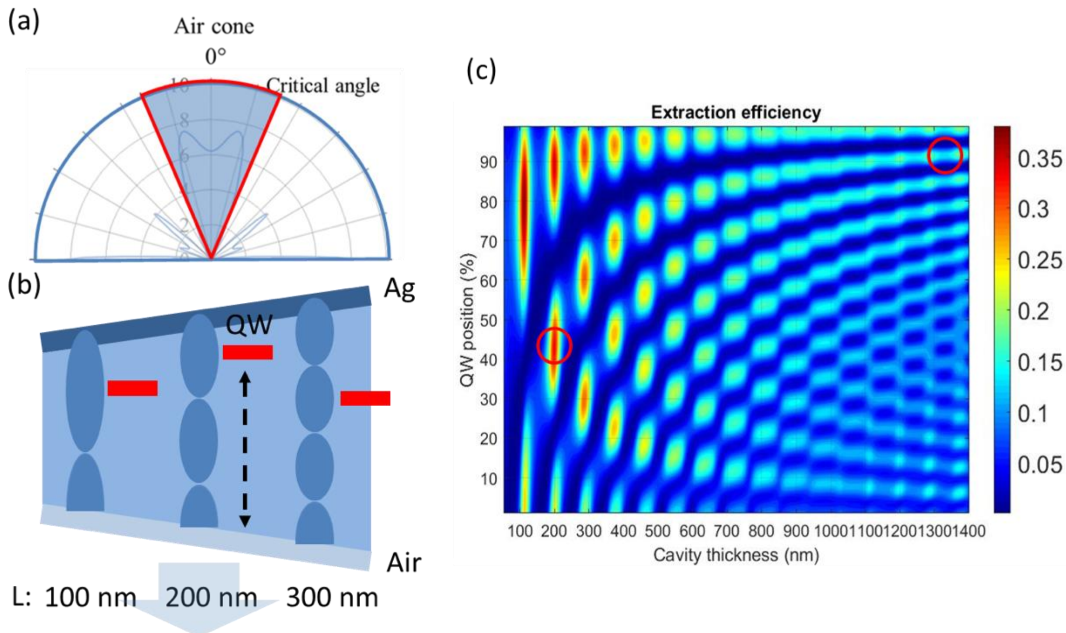

Figure 2.7. (a) Schematic of calculation of the LEE in 200 nm cavity length MC-LED. The LEE is the ratio between the sum of light intensity in the air cone and all other angles. The red line represents the critical angle of 23° at the interface of GaN and air. (b) Schematic of cavity mode shapes and QW positioning. In the microcavity with the Ag mirror, the penetration depth is considered in the calculation of LEE. (c) LEE plot as a function of the cavity thicknesses and the QW positions. The red circle at the cavity thickness of 200 nm is the LEE of 31%, while another red circle at the cavity thickness of 1.36 μm is the LEE of 15%.

2.3. Substrate orientation

For the MC-LED experiment, we have used semipolar (20-2-1) GaN substrates. In 2011, Zhao et al. showed a small blue shift in blue LEDs grown on semipolar (20-2-1) substrate. Because the quantum-confined Stark effect (QCSE) is much smaller than that of LEDs grown on c-plane GaN substrate as shown in figure 2.8(a). It showed a small blue shift in high current density. This is important for MC-LEDs, because the emission spectrum of the MC-LED is determined by the overlapping between the QW emission and the cavity mode. Thus, the QW emission should be constant with changing the current density to keep the constant overlapping. This is why we have used the semipolar (20-2-1) substrate for these devices.

In figure 2.8(b), the spectra of QW emission as dotted line and MC-LED Airy function were shown. The emission spectrum of MC-LED is the result of overlap between the QW emission and the cavity mode. Therefore, if the QW emission wavelength changes, then the LEE will be lower because of low overlapping between those spectra. Conventional c-plane LEDs cause a huge blue shift of the emission spectrum with increasing the current density. Thus, the LEE of the MC-LED is decreased since the overlapping between the QW emission and the cavity mode is reduced. This is why we have used semipolar (20-2-1) GaN substrate for MC-LED this time.

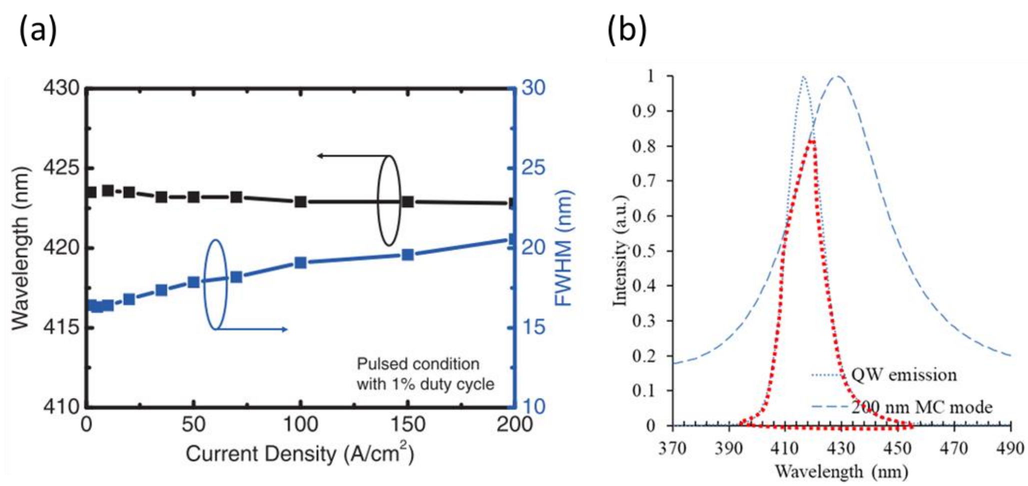

Figure 2.8. (a) Wavelength and FWHM with respect to current density of blue LEDs grown on semipolar (20-2-1) GaN substrate under pulsed operation[21]. (b) Spectra of QW emission (dotted line) and MC mode which is obtained by Airy function (dashed line) of 200 nm cavity length MC-LED[22].

3. Epitaxial wafer growth by MOCVD

3.1. Standard growth condition

All of the growth of epitaxial layers including the tunnel junction (TJ) of MC-LEDs were grown by the MOCVD. And each layer thickness and doping concentration are listed in table 3.1. It starts with the buffer layer of GaN of 1.2 μm. When the buffer layer thickness was thinner or thicker than this, the quick test power were lower than that of 1.2 μm buffer layer thickness case. The sacrificial layers consist of two pairs of InGaN/GaN layer and the InGaN band gap energy should be equivalent to 410 nm photon energy. If the photon energy is larger than 405 nm of the light source of PEC etching, the sacrificial MQWs could not absorb the 405 nm light and then the sacrificial layers are not etched by KOH. Specifically, the sample sit on the KOH beaker upside-down which means the sacrificial MQWs side is facing the lamp. And then, the highly doped n^{++} GaN is grown on top. This layer works as etching stop layer because of high concentration of Si doping[23]. n-GaN layer is follewed by the active region growth which is InGaN/GaN single quantum well (SQW) with each thickness of 12 nm and 3 nm, respectively. The emission wavelength of the SQW is targeted to be 420 nm. The 5 nm thickness undoped GaN barrier layer is followed by p-AlGaN layer. The Al composition of p-AlGaN is graded with the higher Al composition at p-side of the epitaxial wafer to maximize the electron blocking. Highly doped p^{++} GaN is grown as a contact layer. The Mg-doped p-type layers are activated at 600 °C in oven for 15 min with an air ambient. After the quick test of the epi-wafers, the sample is dipped in the heated aqua regia in 10 min for three times to remove the indium dots used for the quick test contact. To remove the residual Mg deposition on the surface of p^{++}-GaN [24]for next growth of TJ, the sample was submerged in BHF for 5 min right before the regrowth of n^{++} GaN by MOCVD. When the regrowth of the TJ is done, the epitaxial wafer is ready for the device processing.

Table 3.1. The device structure of 205 nm cavity length MC-LED grown on semipolar (20-2-1) GaN substrate.

Layer	Thickness (nm)	Doping concentration (cm^{-3})
n^{++} GaN[a]	10	Si: 1.4×10^{21}
p^{++} GaN	10	Mg: 3×10^{20}
p-GaN	67	Mg: 5×10^{19}
p-AlGaN/ graded AlGaN	5/ 5	Mg: 3.8×10^{18}
GaN cap	5	UID[b]
InGaN/ GaN SQW	12/ 3	UID
n-GaN	75	Si: 1.3×10^{19}
n^{++} GaN	12	Si: 4×10^{20}
2x InGaN/GaN (sacrificial MQW)	5/ 5	UID
n-GaN Buffer	1200	Si: 3×10^{18}
Substrate	330 μm	UID

[a]The epitaxial growth was interrupted after p^{++} GaN, and then n^{++} GaN layer of the TJ was grown after the quick test.

[b]UID: unintentionally doped.

3.2. Epitaxial thickness series

Figure 3.1 shows the quick test results of epitaxial wafers of 290 nm, 200 nm and 110 nm cavity thickness MC-LEDs which target emission wavelength is 420 nm. As shown in the figure, the MC-LED epi-wafer with thicker cavity have relatively higher output power than shorter ones. The output power of 290 nm MC-LED epi-wafer is about 7 mW, while that of the 110 nm MC-LED is about 4 mW. That of 200 nm epi-wafers is about 5 mW. This difference of the output power would be caused by thin n-type and p-type layers thicknesses. Since the MC-LED structure is very limited to meet the requirement of ultra-short thickness, the n-type or p-type layer thickness is not enough to have a stable output power as conventional LED epi-wafer. Considering about the output power results of Fig. 3.1, the cavity thickness is larger the better. Further growth optimization is required for the short cavity of 200 nm and 110 nm.

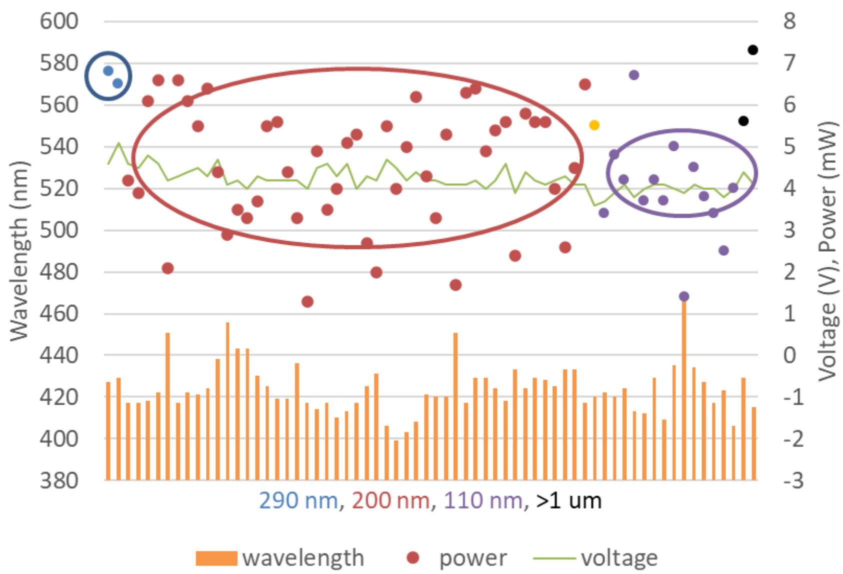

Figure 3.1. Emission wavelength in orange histogram, output power (blue, red, violet dots) and voltage (green line) by quick test of various epitaxial wafers. 290 nm cavity length epi-wafers are marked as blue dots in the blue circle. 200 nm cavity length ones are red dots in red circle. 110 nm cavity length epi-wafers are violet dots in violet circle. These epi-wafer growths are in the order of 290 nm, 200 nm, 110 nm cavity length.

4. Fabrication of MC-LED

To achieve ultra-short MC-LEDs, the flip-chip bonding structure was selected. Since the control of cavity length is important in microcavity regime, the substrate removal technique using the photoelectrochemical (PEC) etching is the best way to have the designated cavity thickness. The MOCVD growth rate can be calibrated easily by growing each layer as same growth condition as in the epitaxial structure. It also can be calibrated by X-ray diffraction. each layer thickness of the device structure is quite in the range of the growth rate in the period of about 2 months. Because the growth rate fluctuates less than 10% between each maintenance cycle, we can expect less than 2.5% growth rate fluctuation within 2 months.

4.1. General MC-LED process

In this section, the whole process flow of MC-LED will be covered. Figure 4.1 shows device cross section schematics and mask design for each step. The thickness of each layer could be variable for different MC-LEDs with a different cavity thickness of 113, 205 and 290 nm, respectively.

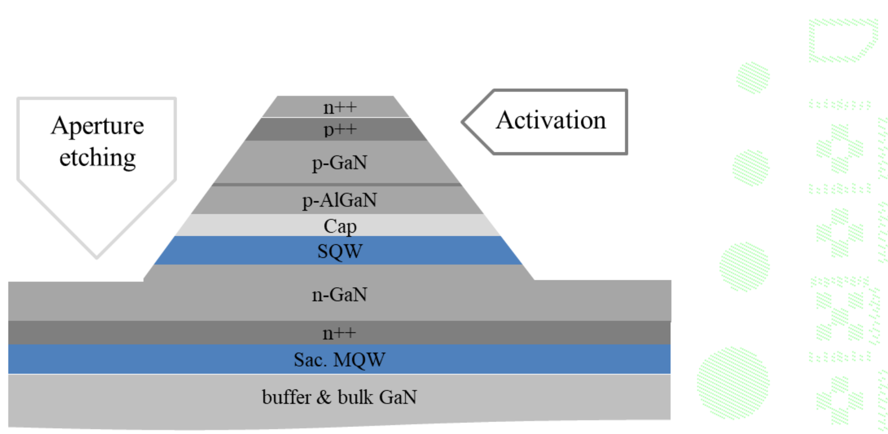

(a) Aperture etching and TJ activation: 20 mins at 720 C

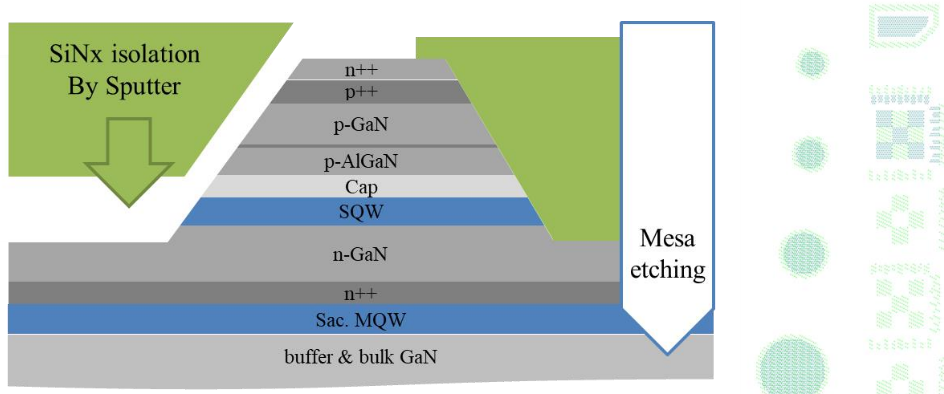

(b) Isolation (+sidewall passivation) and mesa etching

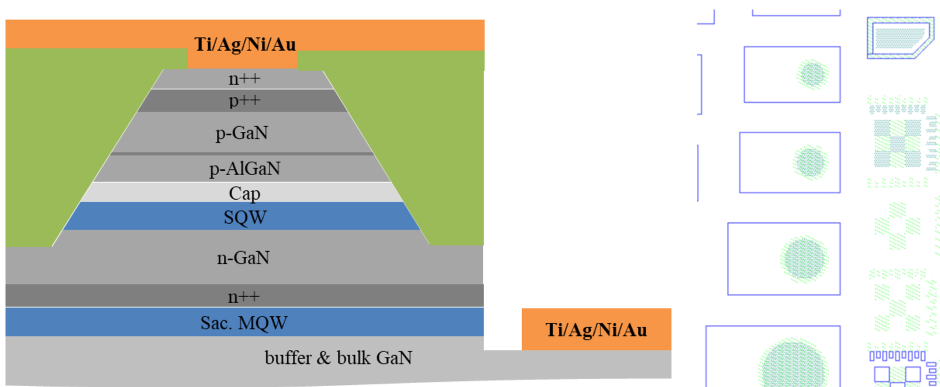

(c) p-side Ti/Ag/Ni/Au deposition

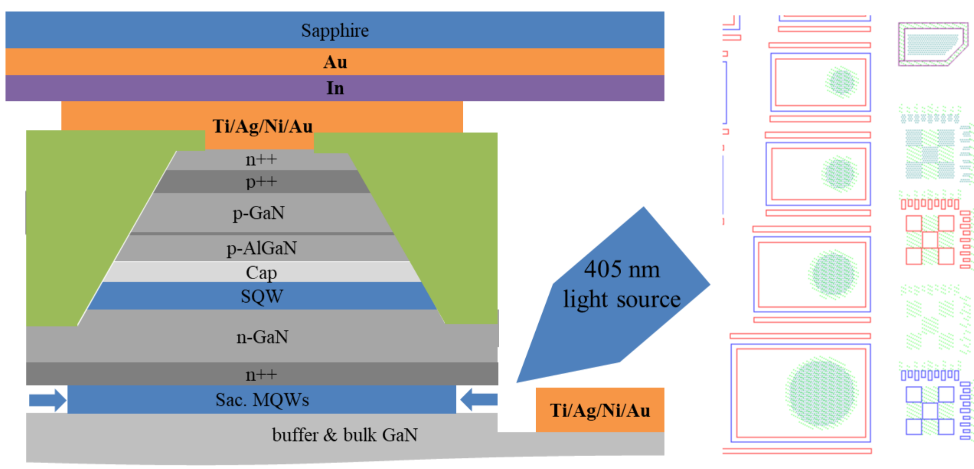

(d) Flip-chip bonding (solid-liquid interdiffusion bonding) and PEC etching

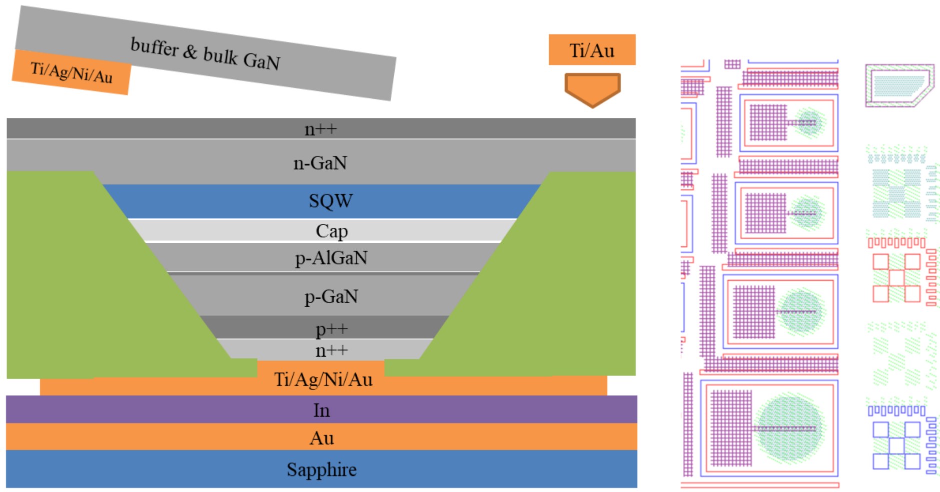

(e) GaN substrate removal and n-contact deposition

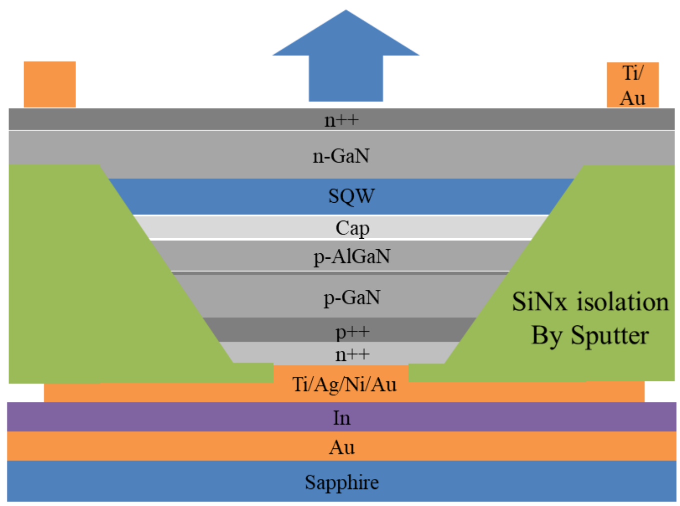

(f) Final device

Figure 4.1 Schematic cross section of device structure at each fabrication process step and mask designs at each step, respectively. Light emission of MC-LED is shown as a blue arrow in (f)

First step shown in figure 4.1 (a) is n^{++} regrowth on epitaxial wafer to form TJ by MOCVD. Since the quick test is performed using the indium contact after the p^{++}-GaN epitaxial growth, a treatment to remove the indium dots is required for next growth of TJ. The treatment: aqua regia, the mixture of 3:1 HCl: HNO_3 is placed on 120 °C hotplate for 5 min. Epi wafers are submerged in the mixture for 10 min. This will be repeated for three times with new mixture of chemicals at each iteration. After the aqua regia, 5 min of buffered HF (BHF). This BHF pre-treatment cleans the surface of epitaxial wafer, which improves TJ contact by removing Mg deposition on the surface of p^{++}-GaN [24]. Then, the sample is rinsed with DI, dried with N_2, and vacuum sealed. Then, regrowth of n^{++}-GaN of TJ is performed by MOCVD.

To make the aperture, we have used reactive-ion etching (RIE) as a dry etcher. For example, the etching depth should be deeper than SQW position since the dielectric layer needs to cover the QW from KOH etching during photoelectrochemical (PEC) etching. Therefore, the etching time varies depending on MC-LED structures. With the etching gas of silicon-tetrachloride ($SiCl_4$), the etching time is ~6 min 40 sec since the etching rate is ~21 nm/min for semipolar (20-2-1) GaN. After the etching, the sample is submerged in 80 °C N-methyl-2-pyrrolidone (NMP) with ultrasonic cleaning for 10 min to get PR removal. In later experiment set, we found keeping the PR could improve the device performance by preventing the damage from following treatments. This will be mentioned in later section 6, conclusion and future works. Then, we put the sample in BHF 5 min to remove the Si-based residue originated from the $SiCl_4$ dry etch of RIE. Then, the sample was submerged in H_3PO_4 for 30 min at room temperature (RT) to remove the sidewall etching damage. The sample was sonicated in DI for 5 min to remove remained H_3PO_4 etchant which has a high viscosity and dried by N_2 gun. To activate the TJ, we loaded the sample in rapid thermal annealing (RTA) system. Annealing condition was at 720 °C for 25 min with the ambient gas of N_2 and O_2 which have the flow ratio of 80% and 20% respectively. Kuwano et al activated the ~55 μm width from the edge of the aperture of the p-type layers of TJ with 720 °C, 30 min[25]. From considering about their results, ~50 μm width of p-type layers from the edge of aperture could be activated at the same temperature for 25 min annealing. However, considering about the high forward voltage of our MC-LEDs mentioned later using this activation method, further improvements of p-type activation are required.

Second step is shown in figure 4.1(b). This step contains the isolation deposition and mesa etch. To isolate p-type layers and n-type layers, we have deposited dielectric layer with some area opening on aperture. The first trial was with silicon dioxide (SiO_2). But it has been replaced to silicon nitride (Si_3N_4) later because KOH etches SiO_2 during the PEC etching. This will be covered in next section. The sputter was used for the deposition of ~100 nm of Si_3N_4. The isolation layer also protects QW from the KOH during PEC etching, which is important to be operational at the end. Then, the mesa is formed by RIE to expose the sacrificial QWs for PEC etching later. This etching uses the etching gas of chlorine (Cl_2) which has the etching rate of 112 nm/min for semipolar (20-2-1) GaN. The mesa etching depth was ~2 μm. Since the MC-LED device structure is flip-chip, the mesa height needs to be higher than the position of sacrificial QWs. To perform the flip-chip bond, p-type and n-type of epitaxial layers need metal pads for each side. When both metal pads connect each other on the submount, PEC etching yield becomes poor because of the short circuit between those contacts. Also, the flip-chip bonding is Au-In solid-liquid inter diffusion (SLID) bonding[26]. Therefore, the good bonding between n-type metal and the submount prevents the separation from substrate after the PEC etching.

In Fig. 4.1(c), we deposit Ti/Ag/Ni/Au for the contact and bottom mirror using E-beam deposition tool. The thicknesses of each layer are 1.8 nm/ 150 nm/ 100 nm/ 1000 nm. Since the Ag has a good reflectance at the wavelength of 420 nm, we use the Ag a high reflection mirror. For adhesion layer between Ag and GaN,1.8 nm of Ti is deposited. 100 nm of Ni is used for diffusion barrier between Ag and Au. The thick 1000 nm of Au is required for Au-In

SLID bonding to Ti/Au/In/Au deposited on sapphire submount. The metal deposition of Ti/Au with each thickness of 40 nm/ 600 nm on the submount was performed by E-beam deposition. And the following stack of In/Au is performed by thermal evaporator while the thickness is 1500 nm/ 210 nm.

Step four is showing in figure 4.1(d). In this step, the processed sample is placed upside down on the prepared submount. The hand-tightened graphite fixture holds both the sample and submount. After the 230 °C oven for two hours, the SLID bonding between the sample and submount is performed. Then, the bonded sample is submerged in 1M KOH which is in -1.5 °C iced bath. To avoid the surface roughening by the KOH for PEC etching, the bath temperature has been set as low as -1.5 °C [25]. The light source for PEC etching is 405 nm which is shorter than the sacrificial QWs wavelength. Because the epitaxial wafer is bonded and faces down, the light is irradiated above the sample. Then, the holes and electrons are excited in the InGaN layer by the light and then, the holes are accumulated at the surface of n-type InGaN layers of sacrificial layer. After the substrate is removed, we clean the surface of flip-chipped devices using the cotton tip swabbing. During the PEC etching, Ga_2O_3 and In_2O_3 are produced and remain during the etching. These particles could work as scattering points which are detrimental to the LEE of MC-LEDs[27]. Using the cotton tip, the sample is swabbed in diluted tergitol detergent. Figure 4.2 shows the result of the PEC etching. Figure 4.2(a) is microscope image of various device sizes of MC-LEDs, while (b) is SEM image of bird-eye view of various sizes of MC-LEDs. As shown in the figure 4.2, the PEC etch shows good yield in the separation of various mesa sizes of devices mostly. The length of MC-LEDs is from 72 μm to 131 μm, while the widths are from 36 μm to 65 μm as shown in Fig. 4.2.

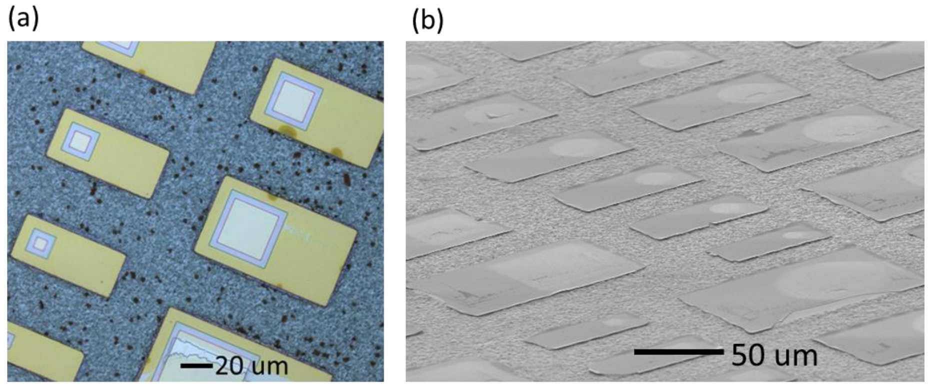

Figure 4.2 Images of the samples after the PEC etching. (a) Microscope image shows various sizes and shapes of devices were transferred on the submount. (b) SEM image shows the bird-eye view of transferred MC-LEDs on the submount.

However, there is more room to be improved in PEC etching condition. Figure 4.3 show the SEM images of various mesa sizes of MC-LEDs. As shown in figure 4.3 (a), the largest device with the mesa width of 131 μm was not fully separated. The aperture area has broken part which indicates non-completed separation from the substrate. The smaller devices shown in figure 4.3 (b) are fully separated.

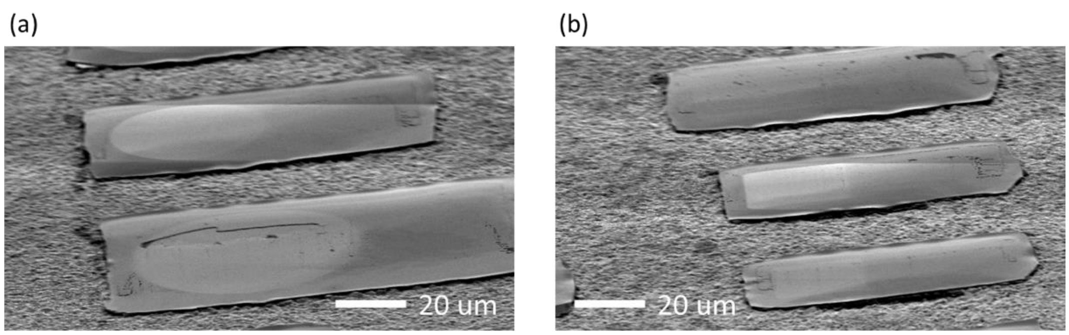

Figure 4.3 SEM images of various devices after the PEC etching. (a) Two relatively large devices with the mesa widths of 110 μm (top) and 131 μm (bottom). (b) Three relatively small devices with the mesa widths of 82 μm (top), 88 μm (middle) and 94 μm (bottom)

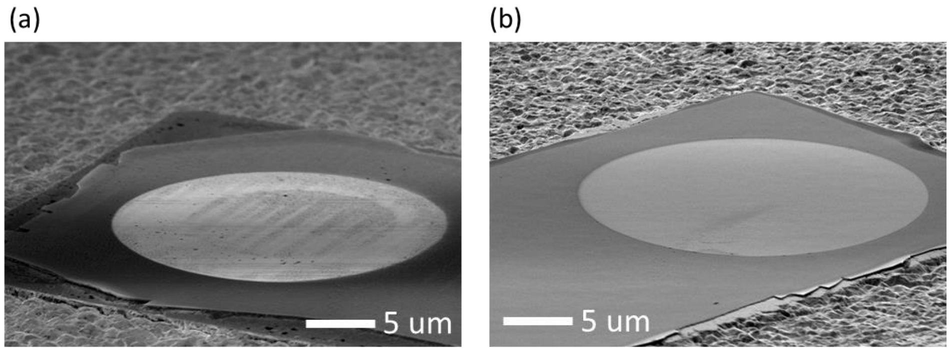

Figure 4.4 SEM image of the samples after the PEC etching, (a) without the swabbing in tergitol, (b) with swabbing in tergitol

Figure 4.4 is showing the difference between with swabbing in tergitol and without of it. Those particles which were originated during the PEC etching were removed by the cotton tip swabbing in tergitol detergent.

Step five is shown in figure 4.1 (e). Ti/Au metal contact is deposited by E-beam deposition. The thickness of Ti is 40 nm, while that of Au is 600 nm. Figure 4.1 (f) is the finalized device structure. Since the cavity thickness range is from 113 nm to 290 nm depending on the epitaxial structure, the process of making the smaller apertures is easier than the conventional thick, ~5 μm, micro-LEDs. The thin cavity length is beneficial when the apertures of LEDs are required to be small in view of dry etching. Because the longer etching time using the dry etcher causes additional etching on aperture and non-flat etching profile on edge of the aperture.

4.2. Isolation dielectrics

To isolate the p-type layers and n-type layers of device, the dielectric film is needed. Figure 4.5 shows the SEM image of samples without the isolation film and with the film.

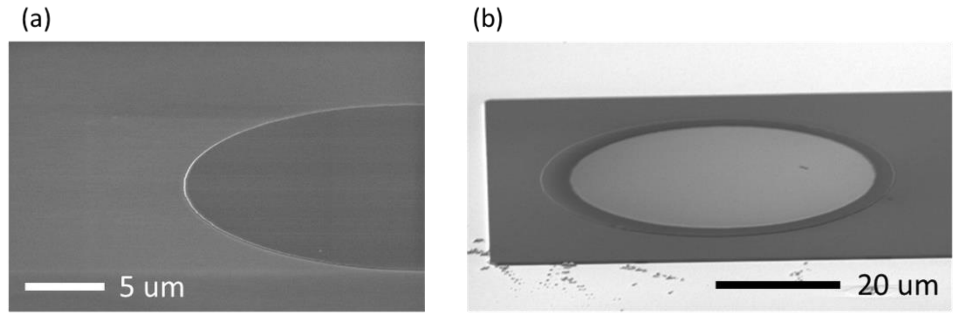

Figure 4.5 SEM images of MC-LED samples. (a) Image of the sample before the isolation layer deposition. (b) Image of the sample after the isolation layer deposition.

With the isolation film, the leakage path on the sidewall is reduced by the passivation. The purpose of this layer is not only preventing the short circuit but also protecting the active region from the KOH during the PEC etching. On the early stage of MC-LED, the SiO_2 film was deposited as the isolation layer by the sputter. Figure 4.6 shows the images of devices after the PEC etching, which have SiO_2 isolation layer. The silver contacts are exposed without covering epitaxial layers on the outside of apertures in figure 4.6 (a). In the same image, the outer circle of aperture is showing height difference between top of epitaxial wafer and bottom of the aperture dry etched front. The inner circle of aperture is where the silver metal mirror is directly deposited on the epitaxial wafer. The outside of the inner circle is covered by the isolation dielectric and followed by the silver metal on the epitaxial wafer. In figure 4.6 (b), the partial area of aperture is colored as the violet. This could indicate the damaged epitaxial layers of III-nitrides. As shown in figure 4.6, SiO_2 was not suitable for the isolation film of device since it was etched by KOH during PEC etching. It is important to be not etched because the next step of the processing is the deposition of n-side metal contact. Without the dielectric layer between p-side and n-side, the device will be short circuit. Also, the aperture area where the InGaN SQW is placed should not be etched, which is the source of emission.

The dielectric layer covers the aperture while protecting it from the KOH during the PEC etching. Therefore, the dielectric film should not react with KOH.

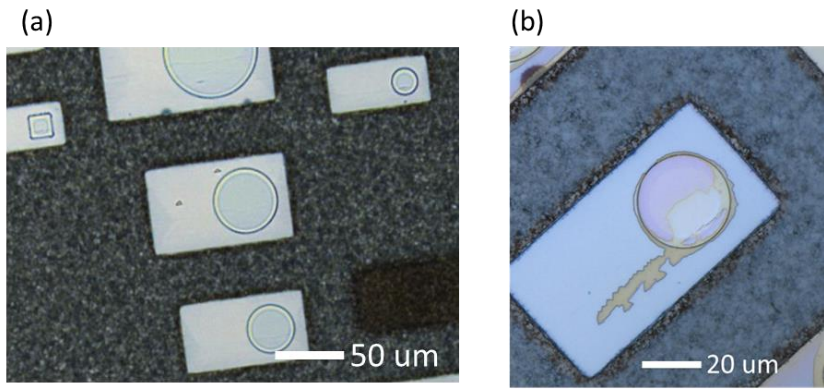

Figure 4.6 Microscope images of samples with SiO_2 isolation layer after the PEC etching. (a) The silver contact metal was left after the PEC etching. (b) The partial III-nitride epitaxial layers were left inside and outside of the aperture.

Silicon nitride, Si_3N_4, is used as the isolation layer for the next generation of MC-LEDs. It was deposited also by the sputter. In SEM, the sample looks similar to the samples with SiO_2 as shown in figure 4.5. However, the result of PEC etching is different as shown in figure 4.7. The figure 4.7 (a) shows the device after the PEC etching. Though some portion of device is broken because of unfinished PEC etching, the aperture area is not etched. Figure 4.7 (b) is representing the fully detached device from substrate without any damage. The color difference comes from the epitaxial layer thicknesses of 113 nm (figure 4.7 (a)) and 205 nm (figure 4.7 (b)). As it is shown in figure 4.8, there are two boundary lines on aperture. The inner boundary line represents the boundary between epitaxial wafer with and without the dielectric layer. Inside of the inner boundary line is epitaxial wafer with the silver metal contact directly. Between the inner boundary and the outer boundary line, the epitaxial wafer is covered by the dielectric layer as isolation layer and the silver metal contact on top of it. Figure 4.8 (b) shows the outer line of aperture which is the boundary between the epitaxial wafer with dry etching (outside of the line) and without the etching (inside of the line). During the first step of the process, figure 4.1 (a), the epitaxial wafer was etched by RIE. As a reminder, this step was for TJ activation and exposing the active region of device to get the isolation layer in step two of the processing as shown in figure 4.1 (b).

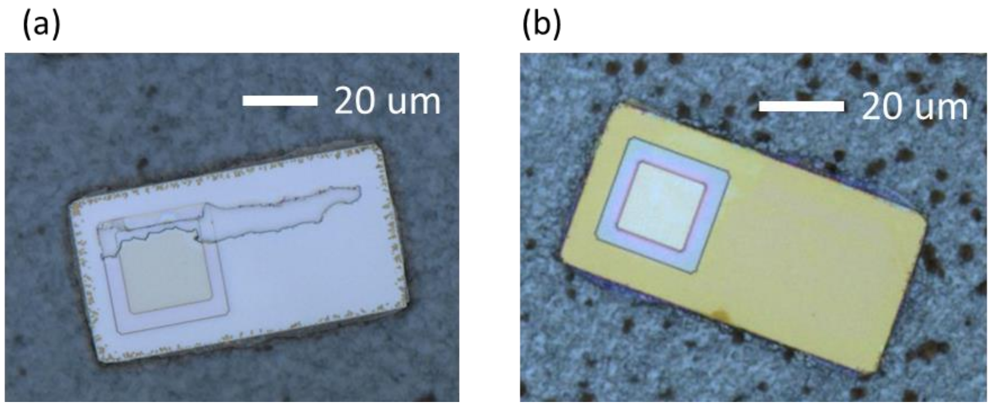

Figure 4.7 Microscope images of sample with Si_3N_4 isolation layer after the PEC etching. (a) The partial area of device was not separated from the substrate because of not enough submerging time during PEC etching. (b) The whole device was separated from the substrate without the damage of KOH.

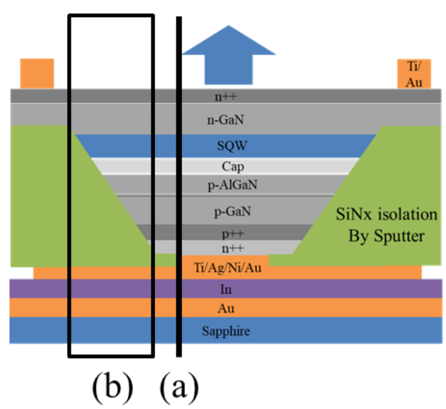

Figure 4.8 Schematic of device structure of MC-LEDs with two boundary lines. (a) inner boundary line indicates the layer difference between the bare epitaxial wafer and the dielectric layer on top of the epi. (b) outer boundary line indicates the layer difference between the epitaxial wafer with and without dry etching.

In summary, the purposes of isolation deposition were to isolate the p-type semiconductor and n-type semiconductor not to be short circuit and protect the active region from the KOH. The material of isolation layer is changed from SiO_2 to Si_3N_4. This change is important to get the devices without any damage from KOH during the PEC etching. The SiO_2 was etched and the yield of the process was low. However, using the Si_3N_4 solved the problem and the process yield increased from the no reaction between the dielectric film and KOH.

4.3. Metal stacks

The MC-LED structure is based on flip-chip bonding design since it provides high level of controlling the cavity thickness. Using the sacrificial MQWs, the designated cavity thickness during the MOCVD growth is well defined after the substrate removal as well. Since there is no additional dry etching to thinning the thickness of device to achieve the ultra-short cavity, we could demonstrate the various cavity thicknesses of MC-LEDs as intended without any issue related to cavity length. However, the flip-chip bonding requires the optimized conditions for both PEC etching and SLID. With respect to PEC etching, the low temperature bath was applied for 1M KOH. It was set as -1.5 °C. For (20-2-1) semipolar GaN, the 1M KOH in RT led the surface roughening issue which increases the scattering loss in MC-LEDs. This issue could be solved by the low temperature KOH. In addition, the bonding metal needs to be optimized. The sample images were shown in figure 4.9. Figure 4.9 (a) is the submount with the metal stack of Ti/Au/In/Au, 40/300/1500/240 nm. The device transfer yield was around 10% in the experiment set. However, when the submount metal stack is changed as Ti/Au/In/Au, 40/300/1500/180 nm, the yield went up as 90%. To bond the epitaxial wafer and the submount, Au-In SLID bonding is applied. The reduced Au thickness on submount helped the SLID bonding a lot.

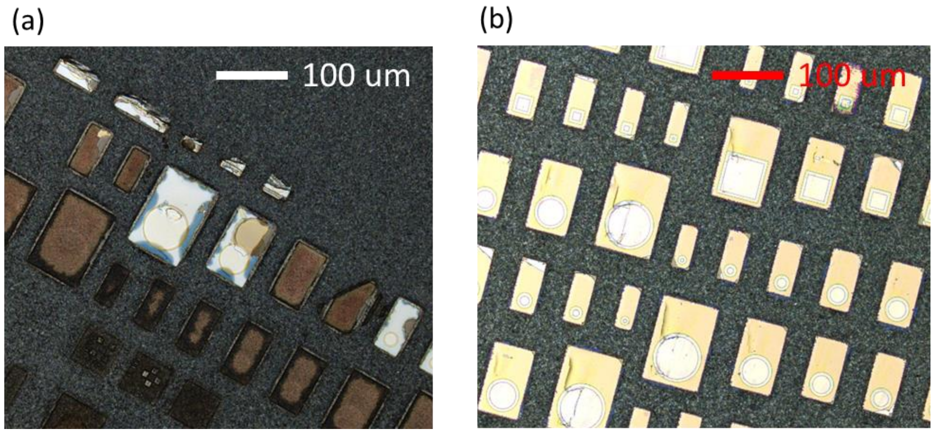

Figure 4.9. Microscope images of flip-chipped devices of MC-LEDs after the PEC etching. (a) Low bonding yield: the submount has the thick gold deposition. About 10% of devices were bonded on the submount (mostly the edges of the epitaxial wafer). (b) High bonding yield: the submount has the thin gold deposition. About 90% of devices were bonded on the submount (uniform distribution of the epitaxial wafer).

4.4. Process images of FIB and SEM

In this section, some of finalized devices images by focused ion beam (FIB) and SEM images of sidewall treated sample will be shown. In figure 4.10, those images show the FIB-SEM of different points on the device. Figure 4.10(a) is the whole aperture with the 16 μm width. Figure 4.10(b) is the image where the aperture is etched, which shows the inclined sidewall well. Also, the black thin layer marked as (1) in figure 4.10(b) represents the Si_3N_4 isolation layer of 105 nm which matches with the actual dielectric layer deposition of ~108 nm by sputtering. The etching depth to form the aperture is measured as 143 nm marked as (2) in figure 4.10(b), which is similar to targeted depth of 145 nm. The thickness of (3) in figure 4.10(b) is 308 nm representing the actual thickness epitaxial growth which was targeted 290 nm. Though it is 6% off from the target thickness, this difference could be reduced by checking the growth rate of each layer of the device using the calibration runs before the epitaxial growth. Also, when the total thickness of epitaxial growth of MC-LED is ultra-short, such as 113 nm, the thickness gap between the target and the actual could be lower. Figure 4.10(c) shows at the point of aperture where the boundary is between the isolation deposited area and without it. The black line, the dielectric isolation layer, is continued from the left end in the image (c) and stopped at the middle of the image (c). (2) of image (c) is representing the metal deposition layer of Ag, 146 nm which is very close to the target thickness of 150 nm. (1) of image (c) is metal deposition of Ni, 83nm which is little different to the target thickness of 100 nm. If the layer blocks the diffusion between Ag and Au, then it is okay. (3) of image (c) is Au layer of 508 nm which is targeted as 1 μm thickness. This is because Au-In SLID bonding was performed for the flip-chip bonding. Therefore, the Au layer thickness is various from 360~1000 nm as shown in the figure 4.10 images. Figure 4.10(c) represents clearly the p-side metal contact of Ti/Ag/Ni/Au with the thickness of 2/150/100/1000 nm, except the Ti 2 nm.

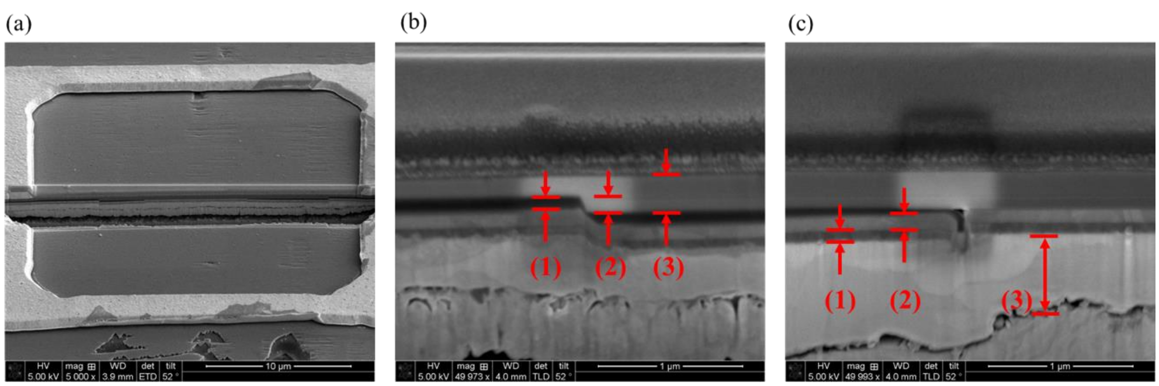

Figure 4.10. SEM images of cross section of 290 nm cavity length MC-LED. (a) SEM image of whole aperture with the width of 16 μm. (b) SEM image at the aperture cliff. (c) SEM image at the boundary between the isolation covered area and without covering.

Figure 4.11. shows another sample with different dry etching condition which used the $SiCl_4$ instead of Cl_2. The thicknesses of the Si_3N_4 isolation layer, aperture etching depth, and total epitaxial growth are 105, 152, and 301 nm, which are marked as (1), (2), (3) in figure

4.11, respectively. And the target numbers for those were 105, 145, 290 nm, respectively. For this sample, the total thickness of epitaxial growth was less than 4% off. Again, this can be resolved by the calibration runs right before the epitaxial growth or shorter epitaxial growth, such as 113 or 200 nm. However, the sidewall angle in this figure is different from the previous case, figure 4.10(b). Here, the angle is ~40° while the angle in figure 4.10(b) was ~70°. The $SiCl_4$ etching gas made the sidewall angle lower than that of Cl_2 etching. This came from the difference of etching rates and the by-products generated during the etching. This will be covered in later of this section. In figure 4.11(b), the thickness of epitaxial layers which is outside of aperture area is marked as (1) and 155 nm. At the aperture etch cliff in figure 4.11(a), the remaining thickness is calculated as 149 nm. This difference might come from the low resolution of the measurement tool or growth/etching variation along the position in the wafer. However, the difference is less than 4% which is little difference. Also, the remaining layer works as current conducting layer for n-side contact, which means no emission related area. A layer (2) in figure 4.11(b) has the thickness of 105 nm matched with the thickness of (1) in figure 4.11(a). The layer, (3) in figure 4.11(b), is n-side metal contact. The actual thickness by the SEM is 832 nm which was targeted 640 nm at the E-beam deposition tool. Though this is 30% over deposition than the target, it is not critical for MC-LED operation. Actually, the thicker metal pad prevents the brakeage of this ultra-thin device during the probing for measurement.

Figure 4.12(a), (b) are sidewall images after the aperture etching with RIE using $SiCl_4$, Cl_2 etching gas, respectively. When the epitaxial wafer is etched by $SiCl_4$, there are significant Si-based residue build-ups on the inclined sidewall. This is generated during the etching process by the re-deposition of by-products. Figure 4.12(b) is the result of Cl_2 etching with the same tool. As shown in the image, the sample's sidewall does not have any Si-based residue since the etching gas of Cl_2 does not contain any Si-atoms in the etchant.

(a) (b)

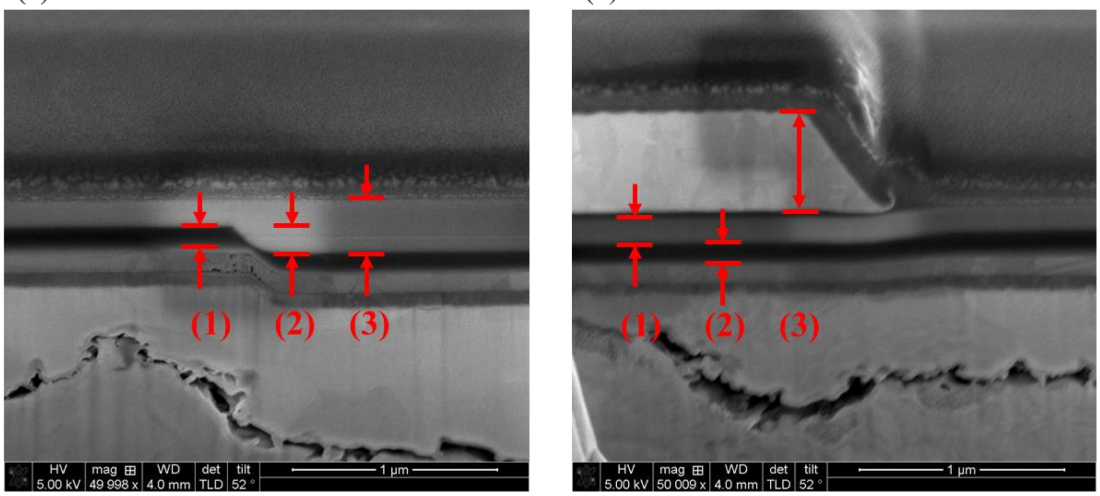

Figure 4.11. SEM images of cross section of 290 nm cavity length MC-LED. (a) SEM image at the cliff of aperture. The dry etching gas was $SiCl_4$ instead of Cl_2 for this set of devices. (b) SEM image at the boundary between the area of n-side metal contact and without the contact.

(a) (b)

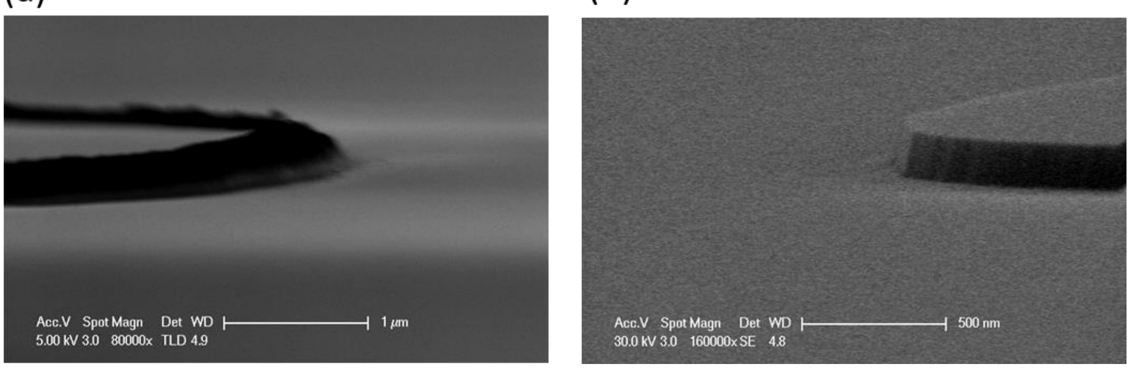

Figure 4.12. SEM images of dry etching results by RIE. Both samples have been etched for aperture formation with the etching depth of ~145 nm. (a) The image of sample etched with $SiCl_4$. (b) The image of sample etched with Cl_2.

Figure 4.13(a), (b) clearly show the difference of etched samples between without BHF dip and with it. (a) is the SEM image of the sample after the aperture etching by RIE with $SiCl_4$ etching gas. It correlates with the result shown in figure 4.12(a) which is also the sample etched by $SiCl_4$ gas. These build ups could be cleaned by the BHF dip for 5 mins. Figure 4.13(b) is the SEM result when the sample shown in (a) was dipped in BHF. The BHF cleans the Si-based residue caused by the $SiCl_4$ totally. This is important step for the MC-LEDs. Because the following process steps, such as isolation deposition, p-side metal deposition, will cover the device to prevent the KOH etching during the PEC etching. However, if the Si-based residue with the height of 500~1000 nm remained on the sidewall, then the stiff hill of the residue could be the path of KOH wet etchant because of the potholes in epitaxial layers. Since the KOH etches the SiO_2 layer, the build-ups on the sidewall cannot be protecting layer.

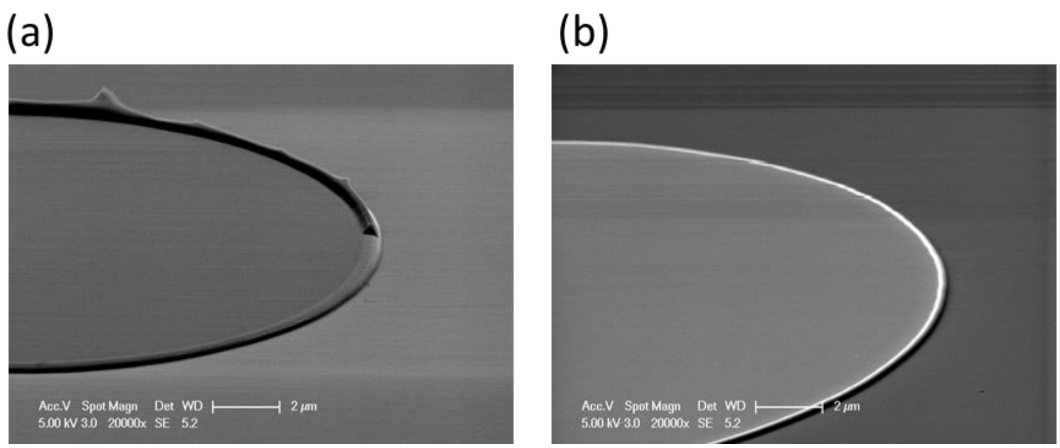

Figure 4.12. SEM images of dry etching results by RIE. Both samples have been etched for aperture formation with the etching depth of ~145 nm. (a) The image of sample etched with $SiCl_4$. (b) The image of sample etched with Cl_2.

Figure 4.13 represents the dry etched samples without H_3PO_4 treatment and with H_3PO_4. (a) is the dry etched sample for aperture formation by $SiCl_4$ etching gas in RIE. (b) is the same sample, but it was submerged in H_3PO_4 for 30 min in RT. As shown in the image, figure

4.13(b), the sidewall profile is changed because of the slow wet etch process of H_3PO_4. During the process, the dry etch damage which was caused by RIE gets cleaned. The result of the treatment was mainly the leakage current reduction and higher EQE than without the sidewall treatment. Figure 4.14 shows the results of several different treatments, without treatment (a), with H_3PO_4 treatment (b), with KOH long time (c), with KOH short time (d), respectively. The faceting problem occurs on samples with KOH, even with short time. However, it does not happen when the sample is treated with H_3PO_4. This comes from the differences of the GaN etch rate and etch preference in certain facets on these chemicals[28]. For example, the dodecagonal pyramids which have twelve facets with {20-2-3} and {22-4-5} are shown by H_3PO_4 treatment due to its kinetic-limited process. However, the hexagonal pyramids are formed when the sample is treated under KOH.

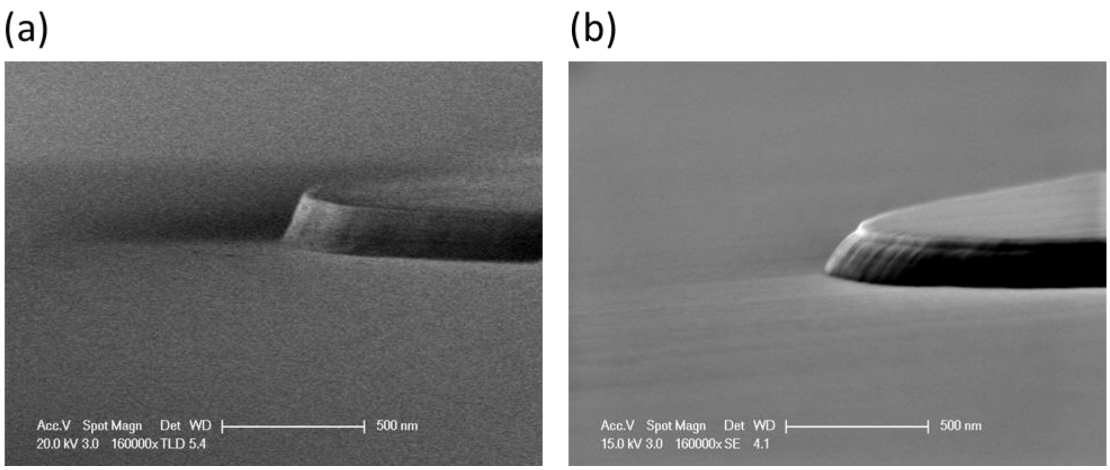

Figure 4.13. SEM images of dry etched samples with $SiCl_4$ etching gas in RIE (a) The image of sample etched with $SiCl_4$. (b) The image of sample etched with $SiCl_4$ and dipped in H_3PO_4 30 min in RT.

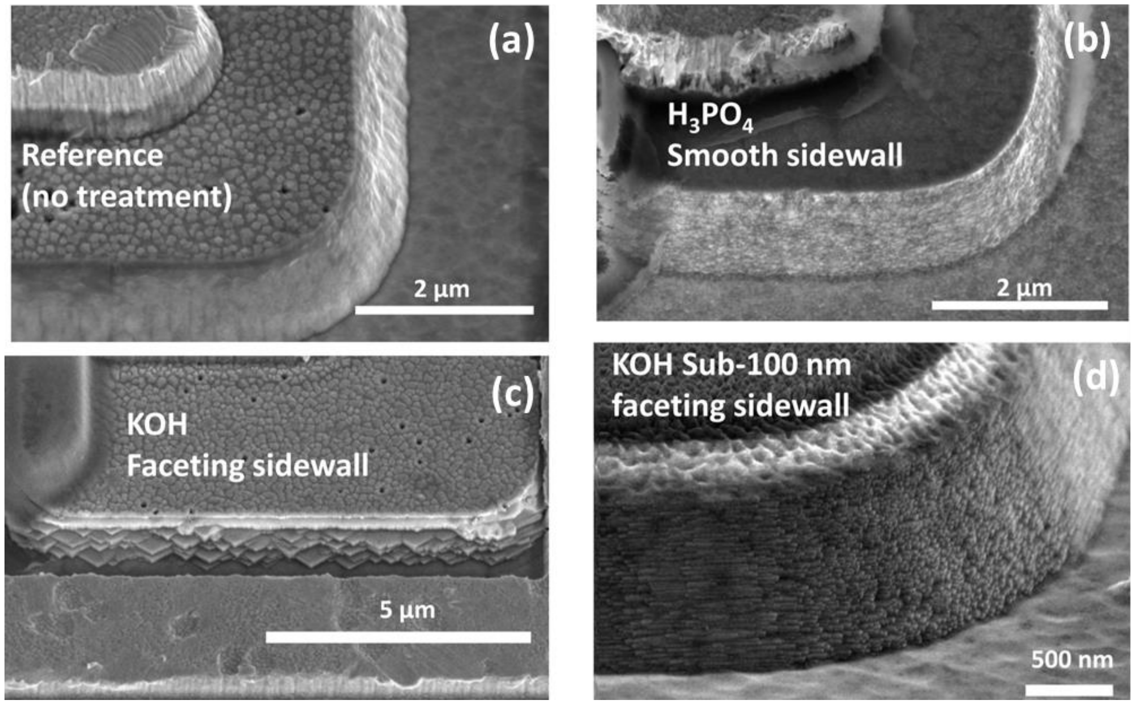

Figure 4.14. SEM images of dry etched samples (a) The image of sample without treatment. (b) The image of sample with H_3PO_4 treatment. (c) The image of sample with long KOH etch time (d) The image of sample with short KOH etch time.

5. Demonstration of MC-LEDs

In this section, there are three sets of demonstration of MC-LEDs. The first demonstration of 200 nm MC-LEDs which were achieved in January 2020. In this time, the EQEs were low EQE. At 1 mA, while the conventional micro-LEDs had 4.4% of EQE, the MC-LEDs had 0.8% of EQE since the leakage current was main issue in the devices. In the I-V characteristics, 200 nm cavity length of MC-LEDs showed large leakage in low voltage. At this time, we used SiO_2 isolation layer. However, it can be etched by the KOH during the PEC etching. Therefore, the isolation layer was etched, and epitaxial layers got damage by KOH which caused the leakage path in the devices. The problem is solved by using Si_3N_4 as isolation layer and sidewall treatment in next demonstration.

In second demonstration, high efficiency MC-LED with sidewall treatment has been achieved in October 2020. From the EQE result, we could find the conventional micro-LEDs had the EQE of 10.5% and MC-LEDs had the EQE of 7.3% at 22 A/cm^2, which is improved a lot. The I-V characteristics presented the electrical improvement, no leakage, unlike the previous MC-LED. This comes from the sidewall treatments using the H_3PO_4. It removed the damages on sidewall originated from the dry etching which can be leakage paths of device. Wong et al[29] showed size independent EQE of micro-LEDs with KOH sidewall treatment in 2019. However, KOH treatment makes faceting on sidewall because of high etching rate of GaN. H_3PO_4 showed smooth sidewall profile because of slow etching rate. Using the sidewall treatment, we could effectively remove the leakage paths by the dry etching damage. Additionally, dipping the sample in BHF for 5mins helps remove the Si based residue on the sidewall by $SiCl_4$ dry etching. With these treatments, the second MC-LED demonstration showed better efficiency than the first one.

Lastly, we have compared various MC-LEDs with different QW positions and cavity thicknesses since the LEE of MC-LEDs is determined by those factors. The simulation of LEE has been achieved with respect to cavity length and active region position. There were several cavity modes in the simulation, such as MC1 with 290 nm cavity length, MC2 with 205 nm, MC3~5 with 113nm with different QW positions. These MC-LEDs could be achieved by changing the length of epitaxial layers of p-GaN and n-GaN during the MOCVD growth. From the EQE results, The 290 nm cavity length MC-LED showed the peak EQE of 6.8%. The EQE of 4.8%, 2.5% have been achieved from 205 nm, 113 nm cavity length MC-LEDs respectively. Also, among 113 nm MC-LEDs, the MC4 which has LEE of 24% has the EQE of 2.5% while the MC3 with LEE of 7% has only 0.6% of EQE. This showed good match between the LEE and EQE of devices. And we couldn't get the 113 nm cavity length MC-LED with the QW position of 75%, MC5 in the simulation, because of processing fault. However, once the device processing is optimized, the MC5 could have the highest LEE of 35%.

5.1. First demonstration of 200 nm MC-LED

Violet semipolar (20-2-1) InGaN microcavity light-emitting diodes (MC-LED) with 200 nm ultra-short cavity length were demonstrated. The emission wavelength was 419 nm with a spectrum width of 20 nm. The external quantum efficiency (EQE) of MC-LED was constant at 0.8% for a forward current from 0.5 to 2 mA with the emitting area of $30\times30\ \mu m^2$. With increasing forward current, the peak wavelength and spectrum width of the emission showed almost no changes. For epitaxial growth, metal-organic chemical vapor deposition (MOCVD) was used. Substrate removal and tunnel-junction with an Ag-based electrode made possible the fabrication of the ultra-short 200 nm thick cavity MC-LED. This is more than a factor of 2 improvement compared to previous MC-LEDs of 450 nm cavity thickness sustaining 5 modes.

Semipolar (20-2-1) GaN was selected here over *c*-plane GaN to fabricate the MC-LEDs because the blueshift of the emission wavelength of semipolar LEDs with increasing current is less than that of *c*-plane LEDs which show a large blueshift with increasing forward current due to the screening of the polarization fields with current injection[21], [30], [31]. MC-LEDs require a constant emission wavelength to retain a good overlapping between the InGaN QW emission and the cavity mode in the air cone to achieve constant light extraction efficiency.

Here, we demonstrate 200 nm cavity violet III-Nitride based semipolar MC-LEDs. To achieve the shortest cavity of 200 nm, substrate removal and tunnel-junction (TJ) were used to fabricate the MC-LEDs. The MC effect is caused by the multiple reflections of the InGaN QW emission between the air/GaN top interface and the GaN/Ti/Ag contact interface acting as a back mirror. Having here demonstrated the feasibility of single mode MC-LED, we expect that their ultimate properties such as single-mode extraction efficiency in the 40% range are within reach with optimization of growth and materials parameters.

A. Experiments

The device structure shown in Table 5.1 was grown by metal-organic chemical vapor deposition (MOCVD) for all the epitaxial growth including n^{++} GaN layer of the TJ. The simplified device processing sequence is shown in figure 4.1. The growth starts with a GaN buffer layer on freestanding semipolar (20-2-1) GaN substrate. Sacrificial layers consist of two 5 nm barriers and 5 nm InGaN quantum wells with 15% indium incorporation. The targeted QW wavelength was 410 nm so that QWs would absorb the 405 nm LED array illumination during photo-electrochemical (PEC) etching[32]–[34]. Heavily doped n^{++} GaN layer grown on the sacrificial layers were followed by 76 nm of n-GaN. The Si concentration of n^{++} GaN layer was 4.5×10^{19} cm^{-3} and worked as an etch stop layer for the PEC etching and as an n-side Ohmic contact[23]. A single quantum well (SQW) active layer with a thickness of 12 nm was grown, and it was followed by 3 nm barrier and 5 nm capping layer with unintentionally doped (UID) GaN. 5 nm of Mg doped p-AlGaN was grown on the active region and graded 5 nm on the p-GaN side to minimize the hetero-junction barrier heights[34], [35]. 64 nm p-GaN was followed by 8 nm heavily doped p^{++} GaN with 2×10^{20} cm^{-3} to finish the first growth. After taking the wafer out from the MOCVD reactor, it was dipped in buffered HF for 5 mins. Then 10 nm n^{++} GaN was grown by MOCVD to form the TJ. Buffered HF pre-treatment was done for surface cleaning to improve the TJ contacts[24]. The simplified final device structure is shown in Fig. 1(f). The center of the InGaN QW is located at 106 nm above the bottom mirror out of 200 nm total thickness, i.e. at 47% of cavity thickness from the top surface. The antinodes of the standing wave are not located at the geometrical center of the cavity by adding to the geometrical cavity thicknesses of 200 nm a penetration depth of 55 nm calculated by considering the phase shift of the reflection light at an Ag mirror [36]. Considering about the Matioli and Weisbuch's simulation results of Fig. 14 of reference[20], the highest light extraction efficiency of 200 nm MC is obtained at the QW location at 40~50% from the top surface because of the mirror phase shift and of the optimizing detuning. Using the fluorescent microscope, we did not observe any dark regions in InGaN QW that would indicate misfit dislocations.

Table 5.1. The device structure of MC-LED grown on semipolar (20-2-1) GaN substrate. Back, J., Wong, M. S., Kearns, J., DenBaars, S. P., Weisbuch, C., Nakmaura, S., (2020). Violet semipolar (20-2-1) InGaN microcavity light-emitting diode with a 200 nm ultra-short cavity length. Optics Express, 28(20), 29991. https://doi.org/10.1364/OE.401640 © 2020

Layer	Thickness (nm)	Doping concentration (cm^{-3})
n^{++} GaN[a]	10	Si: 4.5×10^{20}
p^{++} GaN	8	Mg: 2×10^{20}
p-GaN	64	Mg: 3.8×10^{18}
p-AlGaN/ graded AlGaN	5/ 5	Mg: 3.8×10^{18}
GaN cap	5	UID[b]
InGaN/ GaN SQW	12/ 3	UID
n-GaN	76	Si: 3×10^{18}
n^{++} GaN	12	Si: 4.5×10^{19}
2x InGaN/GaN (sacrificial MQW)	5/ 5	UID
n-GaN Buffer	1200	Si: 3×10^{18}
Substrate	330 μm	UID

[a]The device growth was stopped after p^{++} GaN, and a second growth was used to make the n^{++} GaN for the TJ.

[b]UID: unintentionally doped.

The aperture of MC-LEDs was square with an emitting area of 30×30 μm^2 as shown in figure 5.1 (a). Reactive ion etching (RIE) was used to make the aperture of 150 nm height while exposing the TJ and active region and the etching was down to the n-GaN. During the etching, the sidewall is etched with ~30° angle. By using the BCl_3 etch gas with positive photoresist mask, the aperture sidewall is ~30° while Cl_2 etch gas forms ~90° angle.

The purpose of the angled etching is to extract the guided modes of MC-LED to increase the light extraction efficiency. The light in the guided mode is reflected into the aperture by the total internal reflection, which could increase the light extraction efficiency. After angled etching, SiO_2 dielectric layer was deposited by atomic layer deposition (ALD). This is important to passivate the etching damage of the sidewall[19]. This layer also prevents the etching of active region by KOH during PEC etching.

After depositing another SiO_2 by sputtering, RIE was performed to etch deep mesas in the n-GaN. After opening a window at p-side contact area, 3 nm-Ti/Ag/Ni/Au was deposited as p-side contact by electron beam deposition as shown in figure 4.1 (c). At first, 3 nm thickness titanium (Ti) was deposited as an adhesion layer between silver (Ag) and the n^{++} GaN of TJ. The Ti/Ag was used as the back mirror of the MC-LED, the front mirror being the GaN/air interface. With 3 nm-Ti, the reflectance of the Ti/Ag mirror becomes significantly smaller than that of an Ag mirror, which diminishes the light extraction efficiency. We have not measured the real reflectance of 3 nm-Ti/Ag mirror experimentally. We use R = 83% from reference [37]. In a next phase, we plan to use only Ag as a mirror without Ti after finding good adhesion conditions. Thick gold was used for bonding to the submount. After bonding to the sapphire submount, the PEC etching of InGaN/GaN sacrificial layer was performed as shown in figure 4.1 (d)[38], [39]. Then, Ti/Au Ohmic contacting on n-GaN was performed as shown in figure 4.1 (e). The final operating device is shown in figure 5.1 (a). We checked an uniformity of the emission in the aperture of MC-LED with the cavity length of 200 nm at the forward current of 0.27 mA and 8 mA, as shown in figures 5.1 (b) and 5.1 (c). We observed a uniform emission in the aperture. A great advantage of TJ is improving the current spreading dramatically. Yonkee et al.[24] demonstrated the wall-plug-efficiency of more than 70% of conventional blue *c*-plane LEDs with the TJ by improving the current spreading and minimizing the droop of the efficiency. Figure 5.1 (d) shows the scanning electron microscopy (SEM) image of various sizes and shapes of MC-LEDs transferred to submount.

Two kinds of MC-LEDs were tested. One is a short cavity MC-LED with a cavity length of 200 nm. Another one is a long cavity MC-LED with a cavity length of 1.36 μm. We used different (20-2-1) semipolar substrates for each growth of short and long cavity MC-LEDs.

The device structure of the long cavity MC-LED is the same as that of the short cavity MC-LED except for the n-GaN thickness of 1.236 μm. The cavity length was estimated from the growth rate of each layer.

All of the characteristics of MC-LEDs were tested under direct current (DC) biased conditions at room temperature. A calibrated Si-photodiode was used to measure the output power. The Si-photodiode with a diameter of 1 cm was placed just above the MC-LED at a distance of 2-3 mm. The useful emission used for external quantum efficiency (EQE) purpose is coming only from the top air cone within ± 19° due to MC effect, compared to the ± 23° angle corresponding to the full half-space. Thus, the Si-photodiode collects most of the emission from an emitting area of 30×30 μm^2 with this geometry. For the spectrum measurement, an optical fiber was placed at the same location, which was connected to an Ocean Optics USB2000 spectrometer. We could not perform the angular electroluminescence measurement due to a lack of access to the equipment at this time. All testing was done by using an unpackaged bare chip of MC-LED or conventional *c*-plane LED grown on patterned sapphire substrate (PSS) without any high refractive index encapsulant. An ITO contact was used for the p-type layer of *c*-plane LED instead of the TJ.

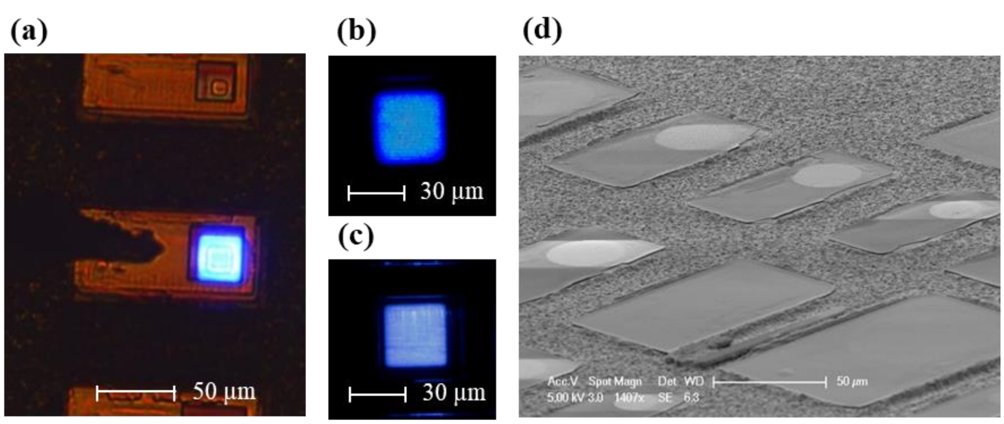

Figure. 5.1. (a) Microscope image of electroluminescence (EL) from finalized device. (b) Emission from aperture of MC-LED with the cavity length of 200 nm at the forward current of 0.27 mA. (c) Emission from aperture of MC-LED with the cavity length of 200 nm at the forward current of 8 mA. (d) Bird's-eye view of SEM image of various flip-chipped MC-LEDs on sapphire submount after PEC etch. [Back, J., Wong, M. S., Kearns, J., DenBaars, S. P., Weisbuch, C., Nakmaura, S., (2020). Violet semipolar (20-2-1) InGaN microcavity light-emitting diode with a 200 nm ultra-short cavity length. Optics Express, 28(20), 29991. https://doi.org/10.1364/OE.401640

Before the device fabrication, a quick test of epitaxial wafers was performed using indium dots as the electrodes. The emission wavelength of the epitaxial wafer of short cavity MC-LED was 417 nm with a FWHM of 15 nm and that of long cavity MC-LED was 414 nm with a FWHM of 17 nm. Our MC-LED was designed for 420 nm. For the wavelength tuning, a number of epitaxial growth runs were required. But it was limited due to a tight growth period during the recent pandemic.

B. Results and discussion

The output power and external quantum efficiency (EQE) as a function of forward current characteristics of the short and long cavity MC-LEDs are shown in figure 5.2. As a reference, conventional *c*-plane LEDs grown on a PSS with an emission wavelength of 450 nm were also tested. The MC-LEDs have the same emitting area of 30×30 μm^2, while the conventional *c*-plane LED is 20×20 μm^2. The EQE of the short cavity MC-LED is 0.8% at a forward current of 1 mA. The long cavity MC-LED shows an EQE of 1.4% at the same forward current. The EQE of the conventional c-plane LED is 4.4%. The EQE of the long cavity MC-LED was about two times higher than that of the short cavity MC-LED.

Figure 5.3 shows I-V curves for short and long cavity MC-LEDs and conventional *c*-plane LEDs. The relatively large leakage current is observed at a current less than 0.1 mA on the short cavity LED in the inset of figure 5.3. Also, at current less than 0.1 mA in figure 5.2, the short cavity MC-LED has a weak emission intensity not seen in a linear scale. The excess leakage current is due to a carrier recombination in depletion regions through trap levels presumably associated with crystal defects[40]. It is assumed that the etching damage caused by PEC etching for the substrate removal could penetrate past the thin 88 nm n-GaN (76 nm)/n^{++} GaN (12 nm) into the active layer of InGaN QW because the large leakage current is not observed for the long cavity MC-LED with a thickness of 1.248 μm of n-GaN (1.236 μm)/n^{++} GaN (12 nm). To improve on this, we would have to remove the etching damage by changing the etching conditions or to passivate the etching damage by depositing passivation materials on the etched surface.

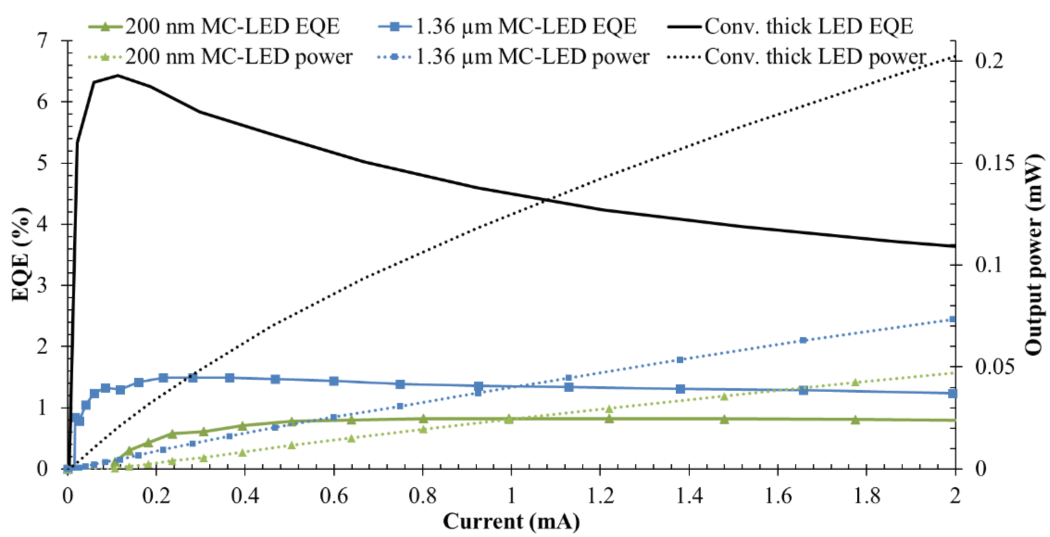

Figure 5.2. EQE (solid lines) and output power (dotted lines) vs. forward current of short and long cavity MC-LEDs, and conventional *c*-plane LEDs grown on PSS substrate at room temperature. Emitting area of MC-LEDs is 30×30 μm^2, and that of conventional *c*-plane LED is 20×20 μm^2. [Back, J., Wong, M. S., Kearns, J., DenBaars, S. P., Weisbuch, C., Nakmaura, S., (2020). Violet semipolar (20-2-1) InGaN microcavity light-emitting diode with a 200

nm ultra-short cavity length. Optics Express, 28(20), 29991. https://doi.org/10.1364/OE.401640 © 2020 Optical Society of America] Users may use, reuse, and build upon the article, or use the article for text or data mining, so long as such uses are for non-commercial purposes and appropriate attribution is maintained. All other rights are reserved.

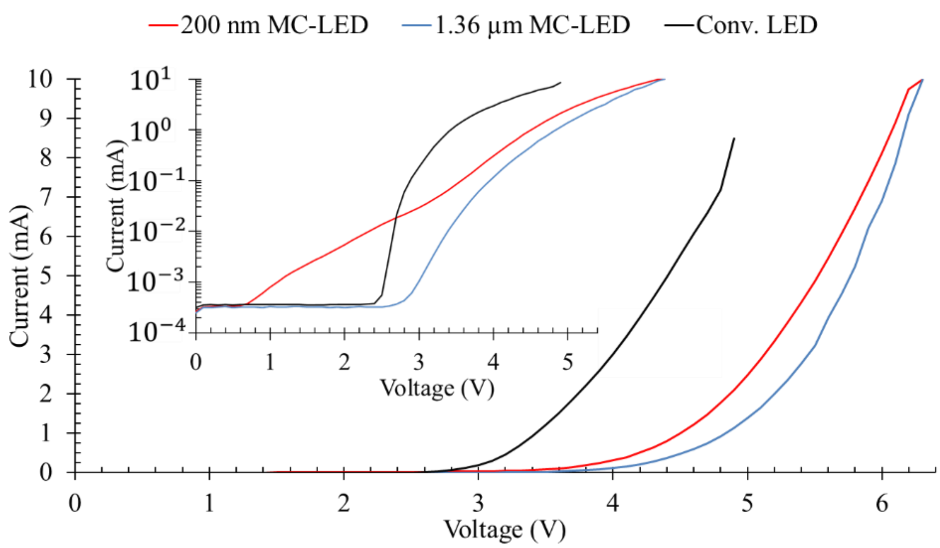

Figure 5.3. I-V curves for short and long cavity MC-LEDs and conventional *c*-plane LED. Inset shows I-V curve with a log scale to enhance the leakage current at a low current region. [Back, J., Wong, M. S., Kearns, J., DenBaars, S. P., Weisbuch, C., Nakmaura, S., (2020). Violet semipolar (20-2-1) InGaN microcavity light-emitting diode with a 200 nm ultra-short cavity length. Optics Express, 28(20), 29991. https://doi.org/10.1364/OE.401640 © 2020 Optical Society of America] Users may use, reuse, and build upon the article, or use the article for text or data mining, so long as such uses are for non-commercial purposes and appropriate attribution is maintained. All other rights are reserved.

The voltage of short and long cavity MC-LEDs and conventional *c*-plane LED is 5.3 V, 5.6 V and 4.2 V at a forward current of 4 mA, respectively as shown in figure 5.3. The voltage of short and long cavity LEDs is relatively large in comparison with that of conventional *c*-plane LED. The reason of the high voltage of MC-LEDs is considered to be due to a poor hole concentration of p-GaN. When the hole concentration is small, the depletion width of the TJ under reverse biased condition becomes wider. It is difficult to activate Mg-doped p-type GaN covered by n-type GaN of TJ by thermal annealing[41]. Recently, we have developed a new technology to activate p-type GaN of the TJ[42]. The voltage of the conventional *c*-plane LED is relatively small because of the use of an ITO contact instead of the TJ.

Matioli and Weisbuch[20] simulated the extraction efficiency of III-Nitride based MC-LEDs with a wavelength of 420 nm and a cavity length of 198 nm. The simulated emission in air cone was a single mode emission and the intensity was stronger than that of thick LEDs. Here, we refer their simulation results.

We used for all of simulations of figures 5.5, 5.6, 5.8, 5.9 and 5.10 an effective cavity length by adding to the geometrical cavity thicknesses of 200 nm and 1.309 μm a penetration depth of 55 nm calculated by considering the phase shift of the reflection light at an Ag mirror[36]. The angular dependence of the InGaN QW emission intensity of short and long cavity MC-LEDs was simulated using theoretical equations of Airy function and antinode factor[43], [44] as shown in Figs. 10 and 11. The angular dependence of the InGaN QW emission intensity was obtained by a product of Airy function and the antinode factor in reference[43]. The light extraction efficiency (LEE) was obtained as a ratio of the sum of emitted light intensity within the air cone and the total sum of the emission intensity of all of the modes included the guided modes[43].

Let us analyze the spectra from both microcavity LEDs. The short cavity MC-LED has a single peak at 419 nm with a spectrum width from 20 nm to 22 nm at current from 0.16 mA to 7.1 mA in figure 5.4 (a) as shown in figure 5.5 (a) and mentioned in reference[20] because only one cavity mode exists in the air cone. The spectrum width of 20-22 nm is determined by the spectral overlap between InGaN QW emission and the single cavity mode in air cone.

With increasing the current, the peak position and shape of the emission spectrum do not change because the variation of the emission wavelength of (20-2-1) semipolar LEDs with increasing current is very small[21], [30], [31].

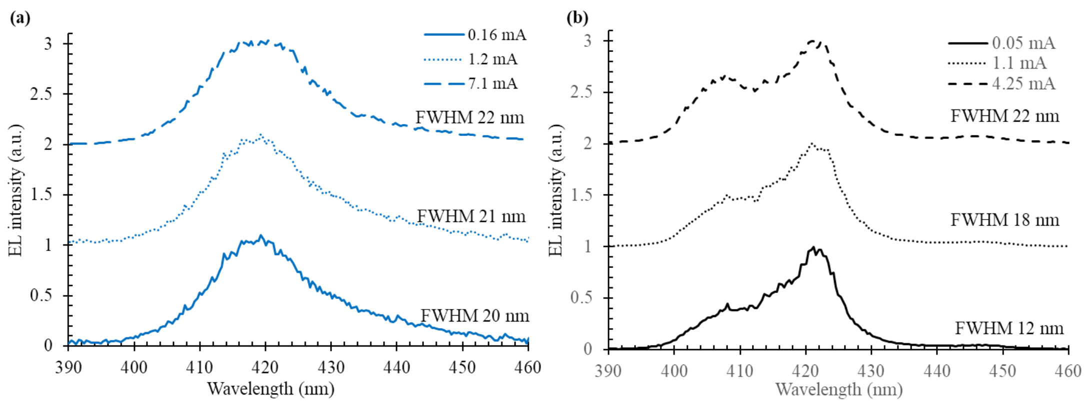

Figure 5.4. Electroluminescence (EL) spectra of short and long cavity MC-LEDs with various current. (a) The short cavity MC-LED has single peak at 419 nm with a spectrum width of 22 nm at 7.1 mA. (b) The long cavity MC-LED has three peaks. The spectrum width is 22 nm at a forward current of 4.25 mA, with three peaks at 408, 422 and 448 nm. [Back, J., Wong, M. S., Kearns, J., DenBaars, S. P., Weisbuch, C., Nakmaura, S., (2020). Violet semipolar (20-2-1) InGaN microcavity light-emitting diode with a 200 nm ultra-short cavity length. Optics Express, 28(20), 29991. https://doi.org/10.1364/OE.401640 © 2020 Optical Society of America]

We simulated the cavity modes of the short and long cavity MC-LEDs using the Airy function (pp.32 of reference[43]) which modulates the QW emission by the electromagnetic response function of the MC and compare with the experimental results of figure 5.4. The 200 nm short cavity has a broad cavity mode width with a FWHM of 50 nm as shown in figure 5.5(a). The single cavity mode shows a detuning of 13 nm with the InGaN QW emission at 417 nm and has a FWHM of 15 nm as shown in figure 5.5(a). The InGaN QW emission overlaps well with the broad cavity mode in the air cone, however with a reduction of the intensity due to the wavelength detuning. This detuning decreases the LEE from the valued obtained by the simulation of Fig. 10(a) by another 24%.

Our designed peak wavelength of short cavity MC-LED was 420 nm with a designed cavity thickness of 195 nm. The peak wavelength of cavity mode is 430 nm, which is caused by the grown 200 nm cavity length and the phase-shift of the mirror, which both causes a detuning of cavity. Figure 5.6(a) shows the spectrum obtained by multiplying the normalized intensity of optical cavity mode of figure 5.5(a) with the normalized spectrum of the InGaN QW emission measured by the quick test. In this simulation, we changed cavity length from 200 nm to 201 nm to obtain the spectrum in figure 5.6(a), which peak wavelength of 419 nm is same as that of figure 5.4(a). Such a shift compared to designed thickness is well within thickness or growth fluctuations.

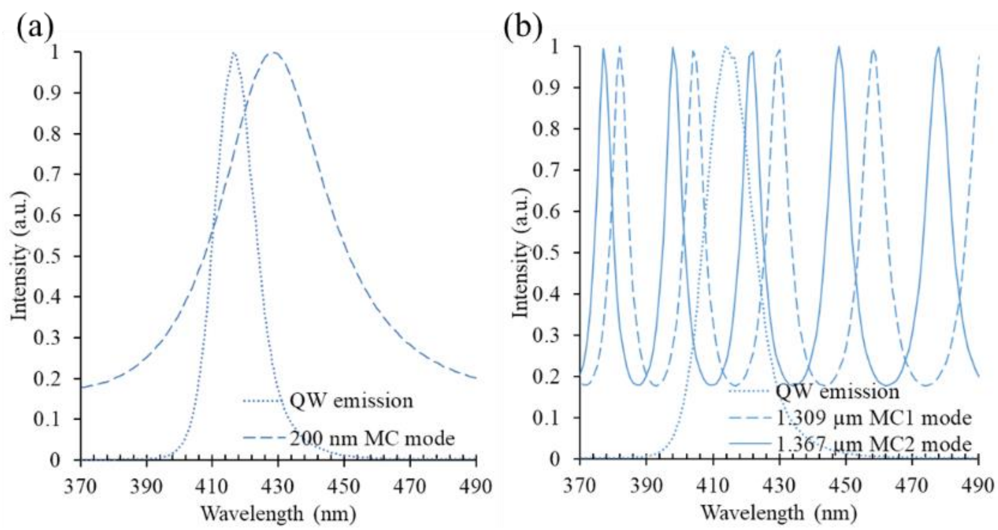

Figure 5.5. Schematics of simulated cavity mode behavior (dashed lines). Measured InGaN QW emission spectrum (dotted lines) by the quick test is shown by overlapping it with the cavity modes. (a) Cavity modes of 200 nm cavity length. (b) Modes of MC1 (dashed line) and MC2 (solid line) with cavity lengths of 1.309 µm and 1.367 µm, respectively. [Back, J., Wong, M. S., Kearns, J., DenBaars, S. P., Weisbuch, C., Nakmaura, S., (2020). Violet semipolar (20-2-1) InGaN microcavity light-emitting diode with a 200 nm ultra-short cavity length. Optics Express, 28(20), 29991.

https://doi.org/10.1364/OE.401640 © 2020 Optical Society of America] Users may use, reuse, and build upon the article, or use the article for text or data mining, so long as such uses are for non-commercial purposes and appropriate attribution is maintained. All other rights are reserved.

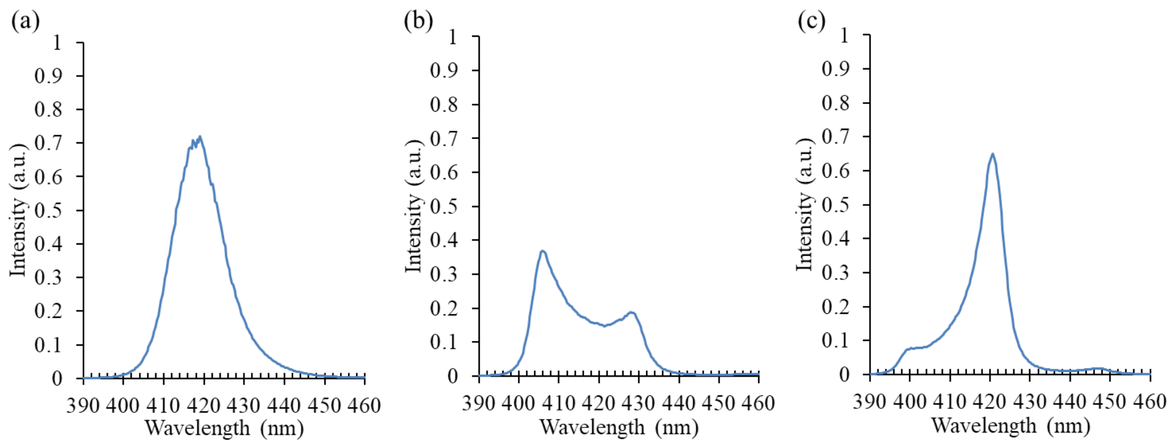

Figure 5.6. (a) Simulated spectrum obtained by multiplying the normalized intensity of cavity mode by the normalized intensity of measured InGaN QW emission by the quick test assuming that the cavity length is 201 nm. (b) Simulated spectrum obtained by multiplying the normalized MC1 modes of Fig. 6(b) with the normalized measured InGaN QW emission. (c) Simulated spectrum obtained by multiplying the normalized MC2 modes of Fig. 6(b) with the normalized measured InGaN QW emission. [Back, J., Wong, M. S., Kearns, J., DenBaars, S. P., Weisbuch, C., Nakmaura, S., (2020). Violet semipolar (20-2-1) InGaN microcavity light-emitting diode with a 200 nm ultra-short cavity length. Optics Express, 28(20), 29991. https://doi.org/10.1364/OE.401640 © 2020 Optical Society of America] Users may use, reuse, and build upon the article, or use the article for text or data mining, so long as such uses are for non-commercial purposes and appropriate attribution is maintained. All other rights are reserved.

We now turn to the 1.36 µm long cavity MC-LED. We first observe that the three observed peaks at 408, 422 and 448 nm are not in a sequence of mode wavelengths corresponding to a single MC, which would be, in a first approximation, equidistant. This can be explained as inspection of the device structure in figure 5.7 shows that there are actually 3 cavities to consider: a central cavity, MC1, between the back contact and top air/GaN interface; two side cavities, labelled MC2 and MC3, corresponding to reflections on the SiO_2/back contact interface and GaN/SiO_2 interface, respectively. We will neglect MC3 emission as the reflectivity of the GaN/SiO_2 interface is much smaller than that at the contact interface. To fit the observed spectrum, we first assume that the cavity length of MC1 is 1.309 µm, reduced by 51 nm from the nominal cavity length of 1.36 µm. Such a variation is again within growth speed uncertainty. The simulated MC1 cavity modes shown in figure 5.5(b) have a main peak at 404 nm and a smaller one at 430 nm, with FWHMs of 7 nm and 8 nm respectively. The main peak is observed around 422 nm in figure 5.4(b). In order to obtain the main peak at 422 nm, we considered MC2 modes as shown in figures 5. 5(b) and 5.7. The MC2 has a cavity length of 1.367 µm by adding 58 nm as an equivalent GaN thickness of 100 nm SiO_2 to the MC1 cavity length of 1.309 µm as 100 nm thickness SiO_2 equals 58 nm GaN thickness given the refractive indices of GaN and SiO_2. The simulated MC2 modes are shown in figure 5.5(b), with a FWHM of 8 nm and 9 nm at 422 and 448 nm, respectively, similar to the positions and FWHM of each sharp peak of figure 5.4(b).

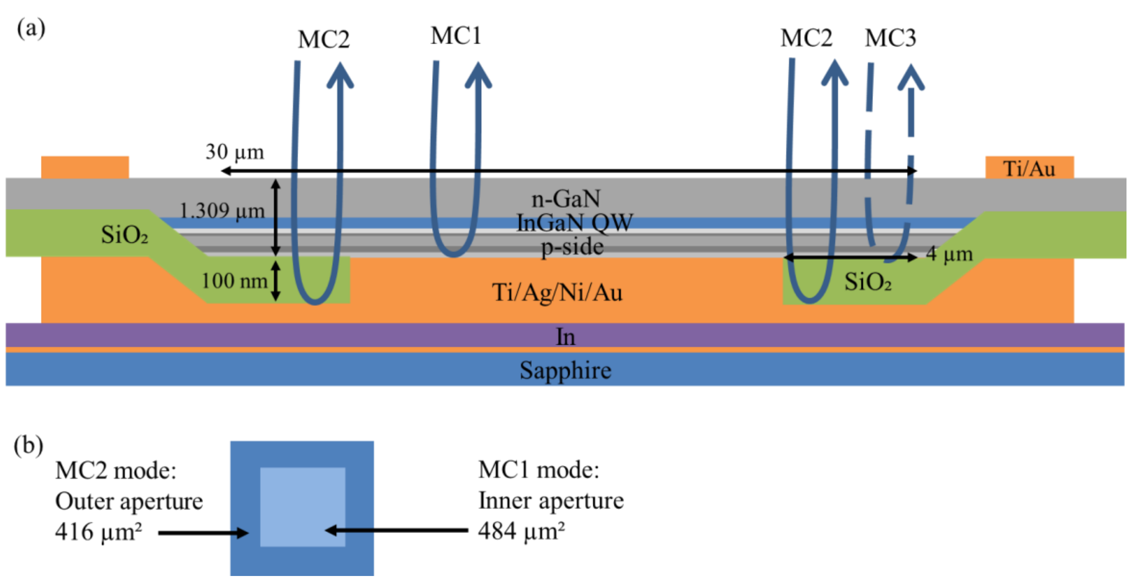

Figure 5.7. (a) Schematic cross-section of long cavity MC-LED. There are three microcavities, MC1, MC2 and MC3 in the aperture. MC1 has a cavity length of 1.309 µm. MC2 has a cavity length of 1.367 µm. The effect of MC3 is neglected due to the low reflection coefficient of the GaN/SiO_2 interface (b) Emitting areas of MC1 and MC2. The area of MC2 is only 14% less than that of MC1. [Back, J., Wong, M. S., Kearns, J., DenBaars, S. P., Weisbuch, C., Nakmaura, S., (2020). Violet semipolar (20-2-1) InGaN microcavity light-emitting diode with a 200 nm ultra-short cavity length. Optics Express, 28(20), 29991. https://doi.org/10.1364/OE.401640

The spectrum of the measured InGaN QW emission by the quick test is shown as a dotted line in figure 5.5(b). Figure 5.6(b) shows the simulated spectrum obtained by multiplying the MC1 modes of figure 5.5(b) with the measured InGaN QW emission. Figure 5.6(c) shows the simulated spectrum obtained by multiplying the MC2 modes of figure 5.5(b) with the measured InGaN QW emission.

The simulated full spectrum is obtained by adding the weighted contributions of MC1 and MC2 according to their emitting areas, as shown in figure 5.8(a). It somewhat overemphasizes the emission at 430 nm. However, it should be remarked that another source of upwards emission is provided by some of the QW light first emitted in guided modes: it can be extracted to outside through two mechanisms: when the guided modes hit the GaN/SiO_2 sidewall at 30°, light is reflected towards the top surface. Also, when a fraction of the guided modes enter the air/GaN/SiO_2 waveguide atop the SiO_2 isolation, a strong radiation out of the waveguide occurs[45]. By adding a 10% fraction of the unmodified QW emission spectrum to the MC1+MC2 spectrum, we recover in figure 5.8(b) a better agreement with figure 5.4(b). Also, we assumed that the QW emission in figure 5.8 has a peak wavelength is 414.7 nm which is 0.7 nm longer than that of the measured QW emission to obtain the good agreement with the spectra of figure 5.4(b). At this point, it is difficult to get a better agreement to the measured spectrum, as there are too many uncontrolled parameters.

The peak intensity at 408 nm is increasing with increasing the forward current in figure 5.4 (b). Zhao et al.[21], observed that a peak wavelength of semipolar LED with an emission wavelength of 423 nm showed a small blueshift (about 1 nm) with increasing the forward current density from 2 A/cm^2 to 200 A/cm^2[21]. Considering about their results of the small blueshift of 1 nm to our MC-LEDs, the small blueshift (1 nm) of the QW emission decreases the spectrum overlapping between the QW emission and 422 nm peak of the MC2 modes and increases the spectrum overlapping between the QW emission and 408 nm peak of the MC1 modes with increasing the forward current density from 6 A/cm^2 (current: 0.05 mA) to 472 A/cm^2 (current: 4.25 mA). As a result, the peak intensity of 408 nm increases and the peak intensity of 422 nm decreases with increasing the forward current as seen in figure 5.4(b).

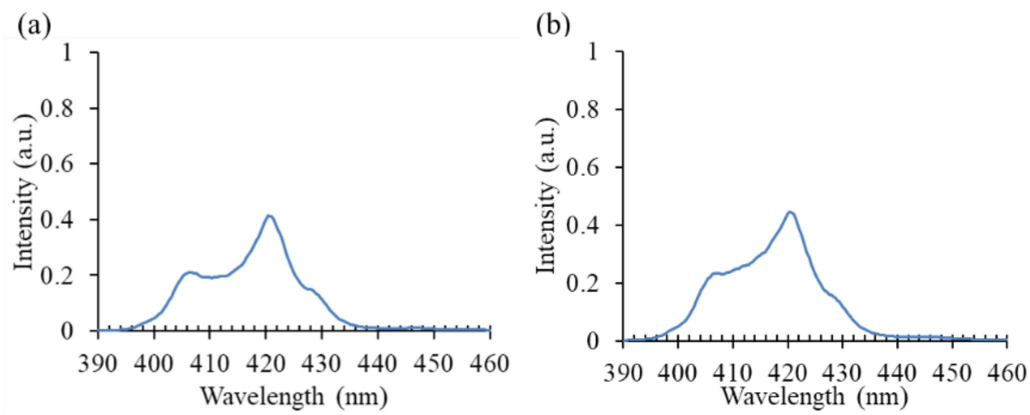

Figure 5.8. Simulated emission spectra of long cavity MC-LEDs. It is assumed that the QW emission has a peak wavelength of 414.7 nm and FWHM of 17 nm to obtain the spectra of (a) and (b). (a) The simulated full spectrum is obtained by adding the weighted contributions of MC1 and MC2 according to their emitting areas. (b) The simulated full spectrum is obtained by adding 10% intensity of unmodified QW emission to the MC1+MC2 spectrum of (a). [Back, J., Wong, M. S., Kearns, J., DenBaars, S. P., Weisbuch, C., Nakmaura, S., (2020). Violet semipolar (20-2-1) InGaN microcavity light-emitting diode with a 200 nm ultra-short cavity length. Optics Express, 28(20), 29991.

https://doi.org/10.1364/OE.401640 © 2020 Optical Society of America] Users may use, reuse, and build upon the article, or use the article for text or data mining, so long as such uses are for non-commercial purposes and appropriate attribution is maintained. All other rights are reserved.

Figure 5.9(a) shows the angular dependence of emission of our 200 nm short cavity MC-LED with a LEE of 24%, the emission wavelength of 417 nm, the InGaN QW position at 47% from the top surface and a low reflectance 3 nm-Ti/Ag mirror with R = 83% computed from reference [37]. Figure 5.9(b) is for an ideal 200 nm short cavity MC-LED with LEE of 33%, the emission wavelength of 420 nm, the InGaN QW position at 41% from the top surface and a high reflectance Ag mirror of 97%[37]. A single mode emission is observed in air cone for both simulated emissions. Due to a poor reflectance of mirror and a detuning of the wavelength and the position of InGaN QW from those of the ideal structure of figure 5.9(b), the LEE of our short cavity MC-LED is decreased to 24%.

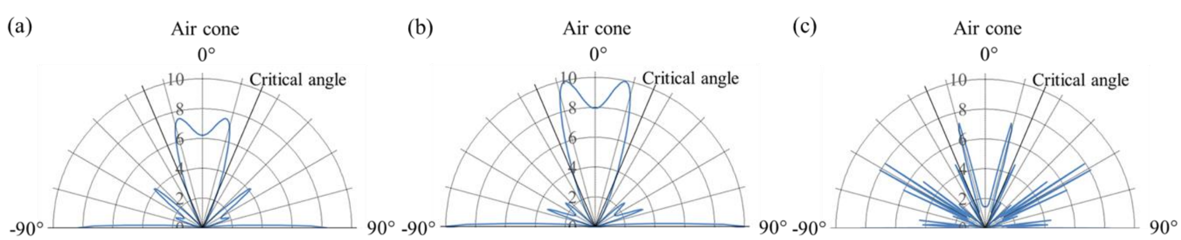

Figure 5.9 Simulated angular dependence of light emission intensity from the InGaN QW emission. The air cone is within ±23°. (a) Cavity length: 200 nm, LEE: 24%, wavelength: 417 nm, QW position: 47%, and mirror: 3 nm-Ti/Ag (R = 83%). (b) Cavity length: 200 nm, LEE: 33%, wavelength: 420 nm, QW position: 41%, and mirror: Ag (R = 97%) (c) Cavity length: 1.309 µm, LEE: 14%, wavelength: 414 nm, QW position: 92%, and mirror: 3 nm Ti/Ag (R = 83%). [Back, J., Wong, M. S., Kearns, J., DenBaars, S. P., Weisbuch, C., Nakmaura, S., (2020). Violet semipolar (20-2-1) InGaN microcavity light-emitting diode with a 200 nm ultra-short cavity length. Optics Express, 28(20), 29991. https://doi.org/10.1364/OE.401640 © 2020 Optical Society of America] Users may use, reuse, and build upon the article, or use the article for text or data mining, so long as such uses are for non-commercial purposes and appropriate attribution is maintained. All other rights are reserved.

Figure 5.9(c) shows our long cavity MC-LED with a LEE of 14%, an emission wavelength of 414 nm, an InGaN QW position at 92% from the top surface and a low reflectance 3 nm-Ti/Ag mirror of 83%. Here, we used the cavity length of 1.309 μm by reducing the 51 nm thickness from the estimated cavity length of 1.36 μm obtained by the growth rate, as mentioned above. We would obtain a higher LEE of 18% using the emission wavelength of 414 nm, the InGaN QW position at 92% from the top surface and a higher reflectance Ag mirror of 97% as an ideal structure. Matioli and Weisbuch[20] already obtained similarly small values of LEE of long cavity MC-LEDs. In the air cone, there are two strong modes. There are many guided modes outside of air cone shown in figure 5.9(c). The long cavity MC-LED has a low light extraction efficiency due to its high cavity order, leading to many guided modes. That is a reason why a short cavity MC-LED should have an advantage for highly efficient, directional LED.

The low value of EQE of both MC-LEDs in comparison with conventional *c*-plane LED grown on PSS is probably caused by poor internal quantum efficiency (IQE) or poor injection efficiency due to small thickness of tunnel-injecting structure MC-LEDs. In figure 5.2, The EQE of the long cavity MC-LED varies from 1.5% to 1.2% at the forward current from 0.5 mA to 2 mA. The EQE of the short cavity is almost constant of 0.8% at the same current range. As discussed above, our short cavity MC-LED has a simulated LEE of 24% while that of the long cavity MC-LED is 14%. Thus, the joint value of IQE and injection efficiency of the short cavity MC-LED can be evaluated as 3%. That of the long cavity MC-LED is 9-11%. The IQE would be 3% for short cavity and 9-11% for long cavity assuming the injection efficiency is 100%. We have not measured the injection efficiency of these small thickness

LEDs. There is a high possibility that the injection efficiency is relatively small due to a small thickness of electron blocking layer and the poor hole concentration of p-type.

Returning to the spectrum of the short microcavity of figure 5.4(a), we have considered only MC1 to obtain the results of figures 5.5(a) and 5.6(a). Figure 5.10 shows the angular dependence of emission of the short cavity MC2 with a cavity length of 258 nm (200 nm plus 58 nm as an equivalent GaN thickness of 100 nm SiO_2). Other parameters used for simulation to obtain the results of figure 5.10 are the same as those used for figure 5.9(a) except for the cavity length. Within the air cone, there is no strong emission. The light extraction efficiency of 0.7% is almost negligible in comparison with the 24% of short cavity MC1 with a cavity length of 200 nm as shown in figure 5.9(a). Thus, we do not need to consider the MC2 modes for the short cavity MC-LED emission.

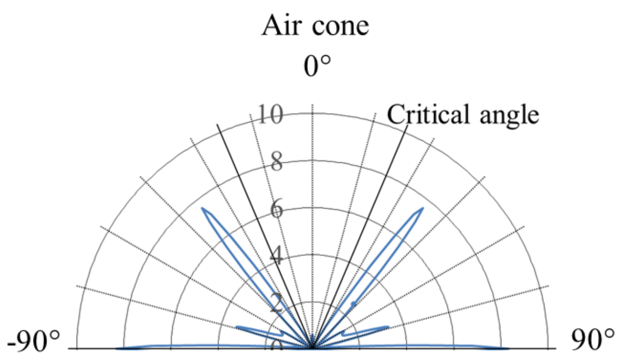

Figure 5.10. Simulated angular dependence of light emission intensity from the InGaN QW emission for the MC2 cavity of the short microcavity 200 nm LED. The air cone is within ±23°. Cavity length: 258 nm, LEE: 0.7%, wavelength: 417 nm, QW position: 36%, and mirror: 3 nm-Ti/Ag (R = 83%). [Back, J., Wong, M. S., Kearns, J., DenBaars, S. P., Weisbuch, C., Nakmaura, S., (2020). Violet semipolar (20-2-1) InGaN microcavity light-emitting diode with a 200 nm ultra-short cavity length. Optics Express, 28(20), 29991. https://doi.org/10.1364/OE.401640 © 2020 Optical Society of America] Users may use, reuse, and build upon the article, or use the article for text or data mining, so long as such uses are for non-commercial purposes and appropriate attribution is maintained. All other rights are reserved.

C. Conclusion

A 200 nm ultra-short cavity lowest order MC-LED was demonstrated using semipolar (20-2-1) GaN, flip-chip bonding. We used the combination of TJ and PEC etch for the first time in the fabrication of our MC-LEDs. The EQE was constant of 0.8% at a forward current from 0.5 mA to 2 mA with an emitting area of 30×30 μm^2. The emission spectrum showed a single peak with a single cavity mode in the air cone. With increasing the current, almost no changes of the peak and spectrum width of the emission were observed. The efficiency could be improved from better mirrors, materials, fabrication processes and optimizing the cavity detuning.

5.2. High efficiency MC-LED with sidewall treatments

High-efficiency blue InGaN-based semipolar (20-2-1) ultra-short microcavity light-emitting diodes (MC-LEDs) with a cavity length of 205 nm were demonstrated. A peak external quantum efficiency (EQE) of 7.3%, which value is almost same as 10% of conventional *c*-plane micron-sized micro light-emitting diodes (μLEDs) with a device thickness of ~5 μm grown on sapphire substrate, was achieved. The emission wavelength is 431 nm at the current density of 297 A/cm^2. In order to obtain high-efficiency MC-LEDs, a sidewall treatment was performed by using buffered hydrofluoric acid (BHF) and phosphoric acid (H_3PO_4) to remove the dry etching residue and the surface damage. The demonstration of MC-LEDs with a high EQE and a single mode emission should pave the way for the application to display and others.

In the past, Pattison et al. demonstrated cavity length of 375 nm InGaN-based MC-LEDs, and Choi et al. demonstrated 450 nm MC-LEDs with a cavity order of five[46], [47]. However, there is no external quantum efficiency (EQE) report on both papers. Using 40-pairs of AlInN-

GaN distributed Bragg reflectors (DBRs), Dorsaz et al. demonstrated EQE of 2.6% MC-LEDs emitting 450 nm wavelength with a cavity length of ~900 nm with a cavity order of nine[48]. Recently, we demonstrated MC-LEDs with the cavity length of 200 nm MC-LED, which however had a poor EQE of 0.8% with a single mode emission[22]. These previous reported MC-LEDs could not be used for display application due to a poor EQE in comparison with that of conventional *c*-plane µLEDs.

When the size of *c*-plane µLEDs becomes small (especially smaller than 40 µm), the EQE decreases dramatically[29]. This decrease is due to surface recombination and the sidewall damage of the mesa from the plasma-assisted dry etching, which contribute to increased Shockley-Read-Hall non-radiative recombination at small dimensions[49]–[51]. Potassium hydroxide (KOH) has been used to improve the electrical performance of GaN based devices by removing the plasma-damaged material on the device side walls[29], [52], [53].

Here we demonstrate high-efficient InGaN semipolar (20-2-1) ultra-short 205 nm cavity MC-LEDs with a single mode emission and the peak EQE of 7.3% which value is almost the same as that of conventional *c*-plane µLEDs by removing the dry etching residue and the sidewall damage using buffered hydrofluoric acid (BHF) and phosphoric acid (H_3PO_4). Semipolar (20-2-1) GaN was selected here over *c*-plane GaN to fabricate the MC-LEDs because the blueshift of the emission wavelength of semipolar LEDs with increasing current is less than that of *c*-plane LEDs[31], [54].

A. Experiments

Figure 5.11(a) shows the schematics of device structure. The growth conditions of epitaxial layers grown by metal-organic chemical vapor deposition (MOCVD) are similar to previously reported MC-LEDs, except for the thickness of four layers[22]. The layer thicknesses of p^{++} GaN (from 8 nm to 10 nm), p-GaN (from 64 nm to 67 nm), p-AlGaN (from 10 nm to 11 nm) and n-GaN (from 76 nm to 75 nm) were changed from the previous ones. Because the light extraction efficiency (LEE) improves with the optimized position of active layer, those layers are changed as shown in figure 5.11(a). Also, there are two different sidewall treatments of MC-LEDs done after the aperture etching process shown in Fig. 1(a) of reference[22]: dipping in BHF for 5 mins removes the etching residue on sidewall. After the BHF dipping, the sample is submerged in H_3PO_4 for 30 mins in RT to remove the sidewall damage caused by reactive ion etching (RIE)[28]. Other groups have used KOH etching to improve the electrical performance of GaN based devices by removing the plasma-damaged material on the device sidewalls[29], [52], [53].

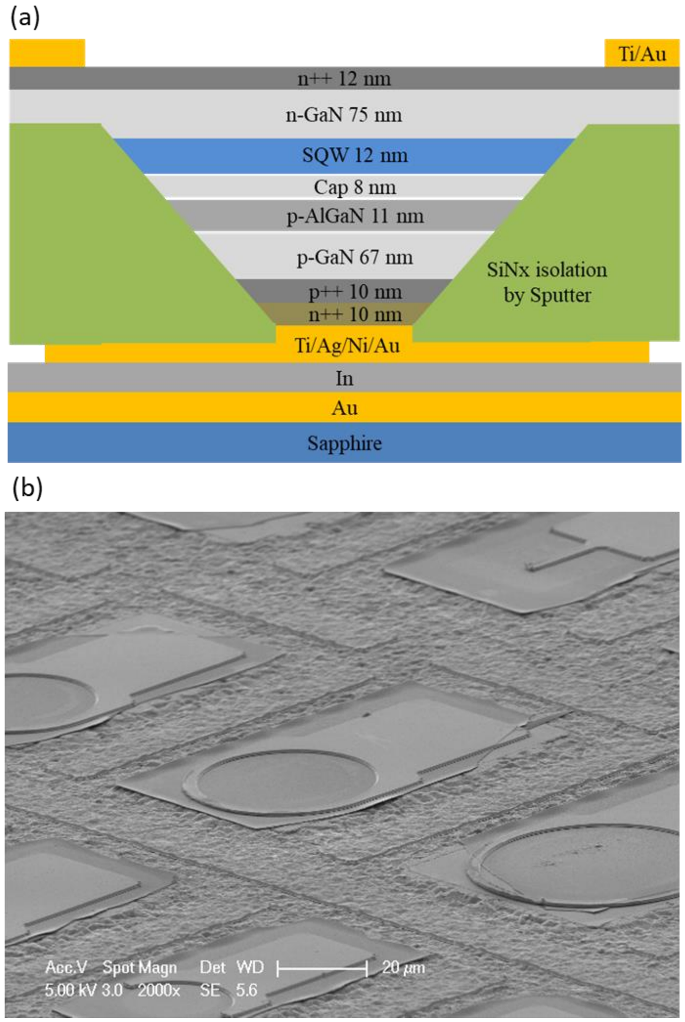

Figure 5.11. (a) Schematics of the cross section of MC-LEDs (b) SEM image of bird's-eye view of finalized MC-LEDs with various size and aperture shapes. Reproduced from [Back, J., Wong, M. S., DenBaars, S. P., Weisbuch, C., Nakamura, S. (2021). High efficiency blue InGaN microcavity light-emitting diode with a 205 nm ultra-short cavity. Applied Physics Letters, 118(3), 031102. https://doi.org/10.1063/5.0039773] with the permission of AIP Publishing.

This time, we used H_3PO_4 instead of KOH. Silicon dioxide (SiO_2) was replaced with silicon nitride (Si_3N_4) for isolation of metal contacts and protection of aperture from photoelectrochemical (PEC) etching as shown in figure 5.11(a). The p-side metal consists of 1.8 nm of Ti followed by 150 nm Ag. Thick 150 nm Ag was deposited for p-contact and bottom mirror to increase the reflectance[55]. The reflectance 97% of 1.8 nm-Ti/150 nm-Ag mirror was measured by using Filmetrics F40-UV, which value matches other groups measurements[37]. Other device fabrication processes are the same as those of the previous report[22]. The circular shape aperture of MC-LED has a 30 μm diameter. The conventional *c*-plane μLED is a rectangular emitting area of 20 × 20 μm described in details of fabrication process in reference[29]. A Si-photodiode was used to measure the output power of MC-LEDs and conventional *c*-plane μLEDs from the top surface of the device on wafer. A diameter of 1 cm Si-photodiode was located 2-3 mm above the MC-LED and conventional *c*-plane LED. For the spectrum measurement, an optical fiber connected to an Ocean Optics USB2000 spectrometer was placed at the same location. All of the measurements were done at RT under DC current by using the bare chip of the device on wafer without encapsulation as shown in figure 5.11(b). The measurement method is described in details in our previous paper.[22]

B. Results and discussion

The angular dependence of the InGaN QW emission intensity of MC-LEDs was simulated using theoretical equations of Airy function and antinode factor as mentioned in our previous paper[22]. The angular dependence of the InGaN QW emission intensity was obtained by a product of Airy function and the antinode factor in reference[43]. The light extraction efficiency (LEE) was obtained as a ratio of the sum of emitted light intensity within the air cone and the total sum of the emission intensity of all of the modes, including guided modes[43]. We used for all of simulations of figures 5.12 and 5.14 an effective cavity length by adding to the geometrical cavity thicknesses of 205 nm a penetration depth of 59 nm calculated by considering the phase shift of the reflected light at an Ag mirror[36].

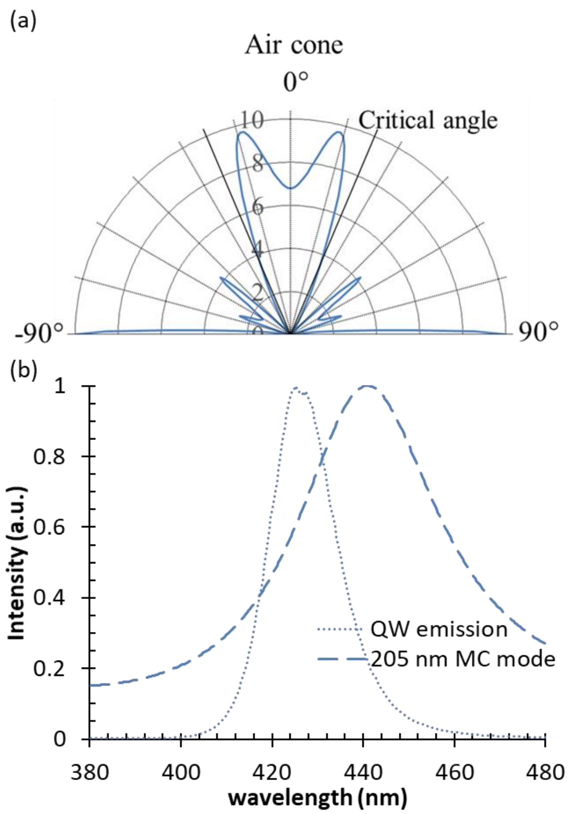

Figure 5.12. (a) Simulated angular dependence of light emission intensity from the InGaN QW emission represented by a monochromatic line at the peak wavelength, 425nm. The air cone is within ±23°. Cavity length: 205 nm, LEE: 31%, wavelength: 425 nm, QW position: 45%, and mirror: 1.8 nm-Ti/150 nm-Ag (R = 97%). (b) Simulated spectrum of the vertical cavity mode of 205 nm cavity length MC-LED (dashed lines) with a peak wavelength of 440 nm and a spectral width of 40 nm. The measured InGaN QW emission spectrum by the quick test with a peak wavelength of 425 nm and a spectral width of 17 nm is shown (dotted lines). Reproduced from [Back, J., Wong, M. S., DenBaars, S. P., Weisbuch, C., Nakamura, S. (2021). High efficiency blue InGaN microcavity light-emitting diode with a 205 nm ultra-short cavity. Applied Physics Letters, 118(3), 031102. https://doi.org/10.1063/5.0039773] with the permission of AIP Publishing.

Figure 5.12(a) shows the simulated angular dependence of light emission intensity from the InGaN QW emission of 205 nm cavity length MC-LEDs with bottom 1.8 nm-Ti/150 nm-Ag mirror with a reflectance of 97% and QW position of 45% from the top surface as shown in figure 5.11(a). There is a strong emission within the critical angle of 23°. From the figure

5.12(a), LEE was obtained as 31%. The previous LEE was 24% due to a poorer mirror reflectance (83%) and non-optimum InGaN QW position in the microcavity[22]. Figure 5.12(b) shows the spectral positions of the 205 nm cavity mode obtained by the Airy function and of the InGaN quantum well (QW) emission obtained by a quick test measurement on the epitaxial wafer before MC fabrication. The quick test emission of the InGaN QW showed a peak wavelength of 425 nm and a spectrum width of 17 nm as shown in figure 5.12(b). The peak wavelength of 205 nm cavity mode of the MC-LEDs is 440 nm. As can be seen in figure 5.12 (a), the detuning of 15 nm is about optimum to extract most of emission spectrum as the peak emission occurs at the middle between the vertical direction and the critical angle[56], [57].

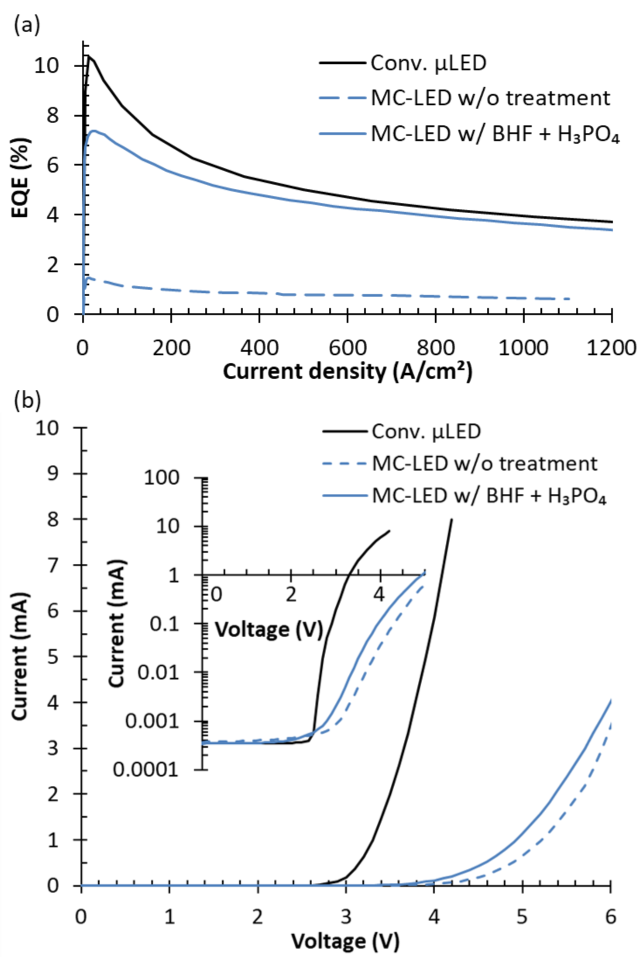

Figure 5.13. (a) EQE vs. current density of MC-LEDs without sidewall treatment and with BHF and H_3PO_4 treatments, and conventional µLEDs. (b) Current vs. voltage (I-V) characteristics of MC-LEDs and conventional µLEDs. Inset shows I-V curves on a log scale. Reproduced from [Back, J., Wong, M. S., DenBaars, S. P., Weisbuch, C., Nakamura, S. (2021). High efficiency blue InGaN microcavity light-emitting diode with a 205 nm ultra-short cavity. Applied Physics Letters, 118(3), 031102. https://doi.org/10.1063/5.0039773] with the permission of AIP Publishing.

EQE vs. current density characteristics of 205 nm MC-LEDs are shown in figure 5.13(a), for MC-LEDs without sidewall treatment or with the BHF and H_3PO_4 treatment. At a current density of 100 A/cm^2 (current of 0.65 mA for MC-LEDs), MC-LEDs with BHF and H_3PO_4 treatment showed 6.6% of EQE while those without treatment showed 1.1%. Our previous 200 nm cavity MC-LED showed an EQE of 0.8% at a current density of 100 A/cm^2[22]. Without any treatment, the EQE increased from 0.8% to 1.1% at the same current density of 100 A/cm^2 by a possible combination of improving the LEE (from 24%[22] to 31%), internal quantum efficiency (IQE) and injection efficiency (IJE). The RIE dry etching of the MC-LED used $SiCl_4$ gas, which forms Si-based residue after dry etching. The dry etching residue was removed from the sidewall with BHF treatment. Then, H_3PO_4 etching removed the sidewall damage, increasing the EQE from 1.1% to 6.6%, which value is close to 7.7% of our conventional c-plane 20 × 20 µm µLEDs at a current density of 100 A/cm^2. From figure 5.12(a), the LEE was obtained as 31%. Thus, the joint value of IQE and IJE of MC-LEDs with BHF and H_3PO_4 treatment at the current density of 100 A/cm^2 can be evaluated as 21% which is much higher than the 3% of our previous 200 nm cavity length MC-LEDs[22]. The peak EQE is 7.3% for MC-LEDs and 10 % for our conventional c-plane µLEDs at a current density of 22 A/cm^2 and 13 A/cm^2, respectively. The conventional *c*-plane 20 × 20 µm µLEDs used here are the same as the µLEDs with a sidewall treatment of KOH

+ Atomic layer deposition (ALD) described in reference[29]. We used commercially available epiwafers to fabricate µLEDs for a fast feedback of results[29]. The peak EQE of 20 × 20 µm µLEDs of the reference[29] is about 25% which was measured by using an encapsulated LED chip after singulation of each chip from the wafer. Then, the output power was measured in an integrating sphere which also captures the sidewall emission of the guided modes. Using an encapsulation with resin of refractive index 1.5, the EQE of our µLEDs would become about two times higher with the increase of the LEE[29]. Therefore, our measurement results of the peak EQE of 10% of the conventional *c*-plane µLEDs made from wafers similar to Ref [29] is reasonable by considering that our measurement does not include the sidewall emission of guided modes as we use devices on wafer, and as we measure µLEDs without encapsulation. The Si-photodiode with a diameter of 1 cm located 2-3 mm above conventional *c*-plane LED on wafer indeed collects a major fraction of the emission within the air cone or critical angle from the top surface of *c*-plane µLEDs[22].

Current vs. voltage (I-V) characteristics of 205 nm MC-LEDs are shown in figure 5.13(b). ITO was used for the p-type contact of conventional c-plane µLEDs[29]. A tunnel junction (TJ) was used for MC-LEDs. The voltages of MC-LEDs with BHF and H_3PO_4 treatment and conventional *c*-plane LEDs were 5.7 V and 3.7 V at a forward current of 3 mA (current density 423 A/cm^2 for MC-LED, 830 A/cm^2 for *c*-plane µLEDs), respectively as shown in figure 5.13(b). The voltage of MC-LEDs is relatively large in comparison with that of conventional *c*-plane LED. The high voltage of MC-LEDs is due to a poor hole concentration of p-GaN which induces a wide depletion width in the reverse biased TJ. The poor hole concentration is due to the difficulty to activate the Mg-doped p-type GaN by thermal annealing since it is covered by Si-doped n-type GaN[41]. The high voltage of the TJ will be decreased dramatically by using the selective area growth of the TJ[58]. As the microcavity has a weak top mirror due to the GaN/air interface, light makes very few roundtrips before escaping to an air. Therefore, the p-GaN absorbing effective length is comparable or smaller than the length in usual patterned sapphire substrate (PSS) grown LEDs with 200 nm thick p-layers, where light also makes 2-3 roundtrips before escaping leading to p-GaN absorption loss of 2%[59]. The main loss mechanism in a MC-LED is the strong metal absorption where the cavity mode amplitude at the GaN/metal interface is much larger than with a far metal.

The forward leakage current of all of the MC-LEDs is as small as 4×10^{-4} mA at forward bias of 2.0 V as shown in the inset of figure 5.13(b). The previous 200 nm cavity length MC-LEDs had a forward leakage current of 1×10^{-2} mA at forward bias of 2.0 V[22]. This time, SiO_2 isolation layer was replaced with Si_3N_4 as shown in figure 5.11(a). During the PEC etching of the sacrificial layer of InGaN layers for the substrate removal as shown in Fig. 1(d) of ref. [22], the etchant of KOH dissolved the SiO_2 isolation layer and then a leakage path was formed on the surface of sidewall of the mesa. In contrast, Si_3N_4 does not react with KOH.

Figure 5.14 shows the emission spectra of MC-LEDs with BHF and H_3PO_4 treatment and *c*-plane µLEDs at different current densities. The peak wavelength of the MC-LED is almost constant around 430 nm with increasing the current density as previously reported on semipolar LEDs[21]. The peak wavelength/spectral width of MC-LEDs are 427 nm/ 16 nm, 431 nm/ 20 nm, and 432 nm/ 22 nm at current densities of 71, 297, 825 A/cm^2, respectively; those of conventional *c*-plane µLEDs are 444 nm/ 16 nm, 442 nm/ 25nm, and 438 nm/ 31nm at current densities of 50, 275, 1025 A/cm^2, respectively. Using the semipolar (20-2-1) GaN for the MC-LED, the blue shift due to the screening of the polarization fields with current injection is minimized[31], [54]. The difference of EQE between conventional *c*-plane µLED and MC-LED with the treatment is 1.1% at current density of 100 A/cm^2, and 0.4% at a current density of 650 A/cm^2. The reason would be that semipolar LED has a small efficiency droop in comparison with that of *c*-plane µLED[31], [54]. The emission spectra of conventional *c*-plane µLEDs show a blue shift of the peak wavelength with increasing the current density from 445 nm to 437 nm due to the screening of the polarization fields with current injection[31], [54].

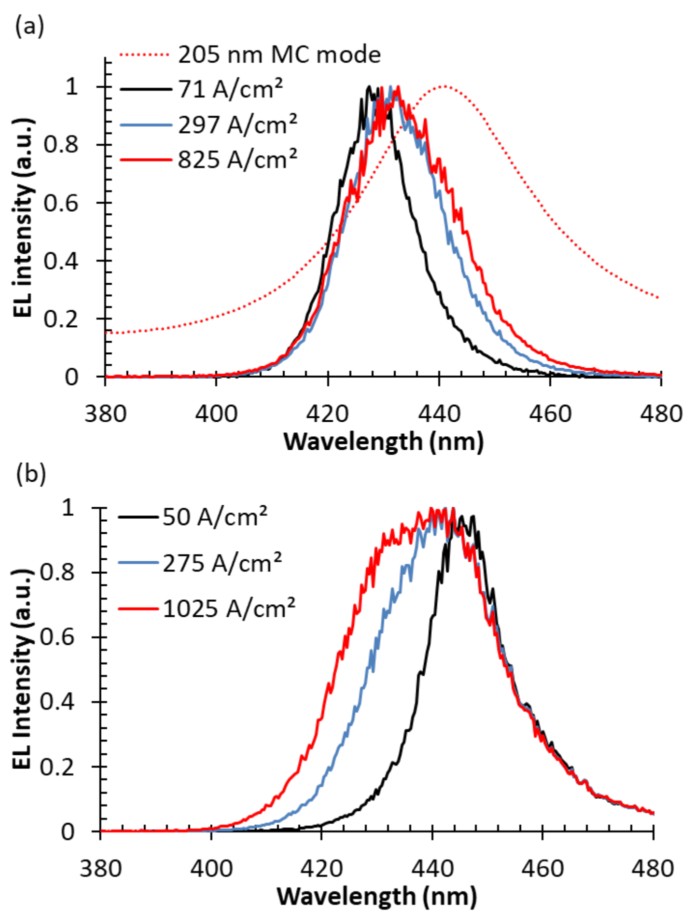

Figure 5.14. (a) Normalized emission spectra of 205 nm MC-LEDs with BHF and H_3PO_4 treatments at various current density. Simulated spectrum of cavity mode of 205 nm cavity length in Fig. 2(b) is also shown. (b) Normalized emission spectra of conventional *c*-plane µLEDs at various current density. Reproduced from [Back, J., Wong, M. S., DenBaars, S. P., Weisbuch, C., Nakamura, S. (2021). High efficiency blue InGaN

microcavity light-emitting diode with a 205 nm ultra-short cavity. Applied Physics Letters, 118(3), 031102. https://doi.org/10.1063/5.0039773] with the permission of AIP Publishing.

Let us put our results in perspective by comparing them to state of the art µLEDs. Fully packaged *c*-plane µLEDs with sizes from 10 µm to 100 µm showed peak EQEs from 40.2% to 48.6%[49]. The LEE was estimated to be about 87% using the Monte Carlo ray-tracing Synopsys LightTools software[49]. From the peak EQE of 7.3% of our 205 nm MC-LEDs, the IQE is 24%, assuming the LEE of 31% and the IJE of 100%. The highest peak EQE of packaged semipolar blue LED fabricated with backside roughening has been reported to be from 52%[15] to 55%[21]. Assuming that their LEE is as high as 87%[49] and the IJE is 100%, the IQE is obtained from 60% to 63%[15], [21]. Considering the 24% IQE of our 205 nm cavity length MC-LED, the EQE of a 205 nm cavity length MC-LED would increase up to 19% by increasing the IQE from our 24% to the previously reported 63%. Also, using the encapsulation with the refractive index of 1.5, we could increase the LEE from 31% to 39% with increasing the critical angle from 23° to 37° of figure 5.12(a)[57], [60]. In that case, the EQE of our 205 nm cavity MC-LED would become from 19% to 24%. We can also expect that using c-plane wafers with IQEs in the 85% range[61] would further increase the IQE to 35% and then, the EQE would become from 24% to 32%, with better directionality than c-plane µLEDs.

One of the big differences between the conventional *c*-plane µLED and the MC-LED is the device thickness. The thickness of *c*-plane LEDs is 4~5 µm and that of MC-LEDs is 100~200 nm. The LEE of the conventional *c*-plane µLED with a size of 10 µm to 100 µm is as high as 87%[49]. This high LEE of 87%[49] is obtained through using the PSS while roughening of the nitrogen (N) polar GaN surface yields an LEE of 70%[61] after removing the substrate. When the device size of µLEDs becomes less than 1~3 µm, it is difficult to use these methods in order to increase the LEE because the size of cones used for roughening or patterned size of PSS are micron sized[13], [49], [61], [62]. In addition, during the device fabrication process, each chip has to be separated by deep mesa etching due to the 4~5 µm device thickness, which causes etching of the edge of the top surface, and reduces the area of the top surface[17]. This is a severe problem when the device size becomes less than 1~3 µm[17] to extract the light from the top surface. In the case of MC-LED, the device fabrication with thin device thickness of 100~200 nm is a simple process as mentioned in our paper[22] even for the device size less than 1~3 µm.

C. Conclusion

A size of ~3 × 3 μm^2 is required for smartphone applications to meet the cost targets to be competitive with organic LED displays[9]. Their 2020 goal is 3 µm size red, green and blue µLEDs with an IQE of 25%[9]. As discussed above, this is within reach using the MC-LED with 205 nm cavity length, keeping in view the simplicity of device fabrication, while such sizes would be very hard to reach with µLEDs.

5.3. Comparison of various MC-LEDs with different cavity lengths

Blue semipolar InGaN microcavity light-emitting diodes (MC-LEDs) with cavity lengths of 113 nm, 205 nm and 290 nm were fabricated, demonstrating the feasibility of ultra-thin MC-LEDs. Precise positioning of the active layer in the cavity is shown to be possible. The 113 nm cavity length MC-LED should have the highest light extraction efficiency (LEE) of 35% but showed no emission due to a high leakage current caused by the device fabrication process. The 290 nm cavity length MC-LED had the highest peak external quantum efficiency

(EQE) of 6.7%. The peak wavelength was almost constant at 430 nm at a current density from 289 A/cm^2 to 1868 A/cm^2 under pulsed operation.

A. Experiments

Figure 5.15(a) shows the schematics of a device structure of a MC-LED with a cavity thickness of 290 nm, as named MC1. The growth conditions of epitaxial layers grown by metal-organic chemical vapor deposition (MOCVD) are similar to previously reported MC-LEDs, except for the thickness of four layers[22]. The layer thicknesses of p^{++}GaN (from 8 nm to 10 nm), p-GaN (from 64 nm to 71 nm), p-AlGaN (from 10 nm to 11 nm) and n-GaN (from 76 nm to 156 nm) were changed from the previous report.

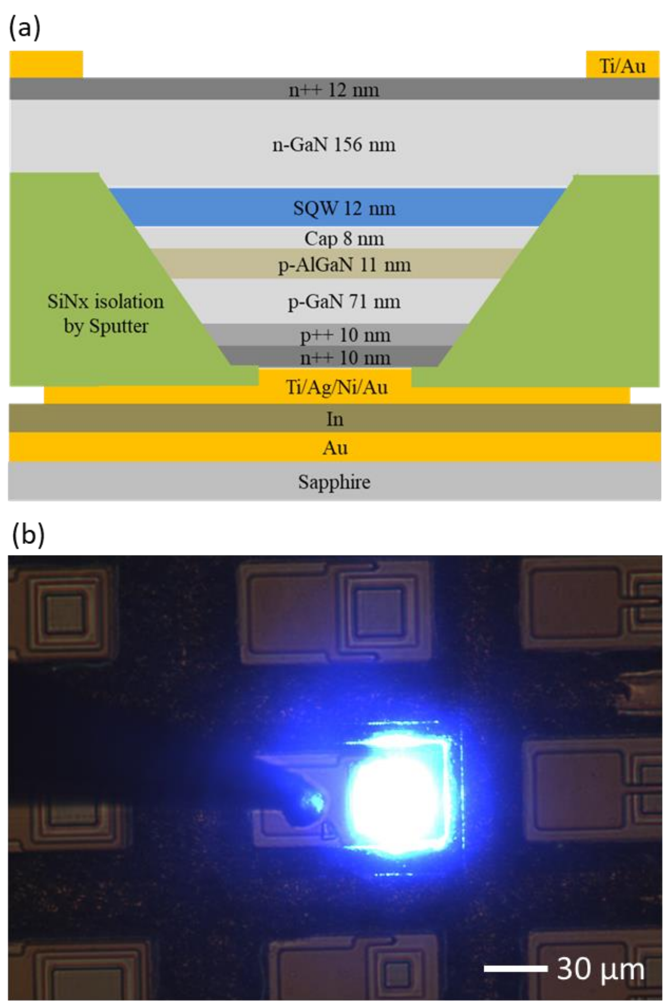

Figure 5.15. (a) Schematics of the cross section of MC-LED with the cavity length of 290 nm. (b) Microscope image of finalized MC-LEDs with various sizes and shapes of apertures. One MC-LED is operated at a forward current of 25 µA. This is the Accepted Manuscript version of an article accepted for publication in [Applied Physics Express]. IOP Publishing Ltd is not responsible for any errors or omissions in this version of the manuscript or any version derived from it. The Version of Record is available online at [https://doi.org/10.35848/1882-0786/abebb3].

After p^{++}GaN growth of the tunnel junction (TJ) in figure 5.15(a), the epitaxial wafer was taken out from the MOCVD reactor. Then, the wafer was annealed to activate the p-type layers at a temperature of 600 °C in air for 15 minutes. Then, a quick test of epitaxial wafers was performed using an indium dot as an electrode. After the quick test, the sample was dipped in aqua regia for 10 minutes, 3 times, and then dipped in BHF for 5 minutes for cleaning of the surface[41]. Then, the epitaxial wafer was placed back inside the MOCVD reactor and the n^{++}GaN layer of the TJ was grown.

There were two different sidewall treatments of MC-LEDs done after the aperture etching process shown in Fig. 1(a) of reference[22]: dipping in BHF for 5 mins removes the etching residue on the sidewall. After the BHF dipping, the sample is submerged in H_3PO_4 for 30 mins in room temperature (RT) to remove the sidewall damage caused by reactive ion etching (RIE)[28].

The reflectance of 97% of 1.8 nm-Ti/150 nm-Ag mirror was used as a high reflection mirror and contact. The size of the square shape aperture of MC1 is 26 µm × 26 µm as shown in figure 5.15(b). For the spectrum measurement, an optical fiber connected to an Ocean Optics USB2000 spectrometer was placed 2~3 mm above the MC-LEDs. A Si-photodiode with a diameter of 1 cm was used to measure the output power of MC-LEDs from the top surface of the device on wafer. All of the measurements were done at RT under DC current except for the spectra measurements by using the bare chip of the device on wafer without encapsulation as shown in figure 5.15(b). The measurement method is described in detail in our previous paper[22].

B. Results and discussion

The angular dependence of the InGaN QW emission intensity of MC-LEDs was simulated using theoretical equations of Airy function and antinode factor as mentioned in our previous paper[22]. The angular dependence of the InGaN QW emission intensity was obtained by a product of the Airy function and the antinode factor found in reference[43]. The LEE was obtained as a ratio of the sum of emitted light intensity within the air cone and the total sum of the emission intensity of all of the modes, including guided modes as shown in figures 5.16(a) and 5.16(b)[43].

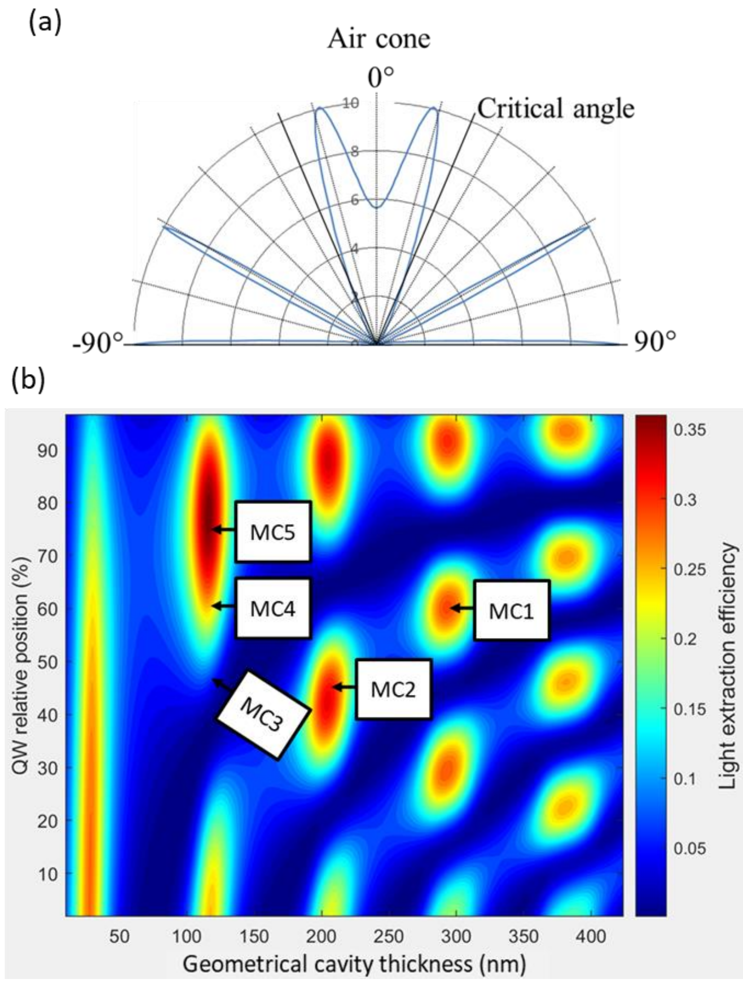

Figure 5.16. Simulated angular dependence of light emission intensity from the InGaN QW emission represented by a monochromatic line at the peak wavelength, 425 nm. The air cone is within ±23°. Mirror: 1.8 nm-Ti/150 nm-Ag (R = 97%). (a) MC1 with cavity length: 290 nm, LEE: 29%, wavelength: 425 nm, and QW position: 60%. (b) Simulated LEE versus InGaN QW relative position and geometrical cavity thickness. The QW position and LEE of each MC-LED: MC1: 60%, 29%, MC2: 45%, 31%, MC3: 46%, 7.6%, MC4: 60%, 24%, MC5: 75%, 35%. This is the Accepted Manuscript version of an article accepted for publication in [Applied Physics Express]. IOP Publishing Ltd is not responsible for any errors or omissions in this version of the manuscript or any version derived from it. The Version of Record is available online at [https://doi.org/10.35848/1882-0786/abebb3].

We used for all of the simulations of figure 5.16 an effective cavity length by adding to the geometrical cavity thicknesses of 113 nm, 205 nm and 290 nm a penetration depth of 58 nm calculated by considering the phase shift of the reflected light at an Ag mirror[36]. In this section, we use the modified internal quantum efficiency (MIQE) = current injection efficiency (CIE) × internal quantum efficiency (IQE), where the MIQE includes the eventual non-unity current injection efficiency (CIE).

Figure 5.16(a) shows the simulated angular dependence of light emission intensity from the InGaN QW emission of MC1 with a bottom 1.8 nm-Ti/150 nm-Ag bottom mirror with a reflectance of 97% and QW position of 60% from the top surface as shown in figure 5.15(a). There is a strong emission within the critical angle of 23°. From the figure 5.16(a), LEE was obtained as 29%. The LEE of the 205 nm cavity MC-LED is 31% with the same high reflection mirror of 97% and the optimum InGaN QW position is named MC2[22].

Figure 5.16(b) shows simulated LEE versus InGaN QW relative position and the geometrical cavity thickness. The values of LEE of each cavity length of figure 5.16(b) is obtained by using the simulation result of figure 5.16(a) for each MC-LED. We have fabricated five MC-LEDs wafers with different cavity lengths and QW positions in this study. Each device is shown as MC1~MC5 in figure 5.16(b). Each LED structure is the same except for the thickness of n-GaN and p-GaN which was varied to obtain each cavity thickness after putting the QW position at the target position. MC5 has the shortest cavity length of 113 nm and an optimum QW position at 75% of the cavity height counted from the top of the device, which should lead to the highest LEE of 35%.

In figure 5.16, we plot the LEE of MC-LED as determined by both the Airy function and antinode factor[43]. The Airy function indicates the resonant characteristics of the cavity, i.e. the amplitude of the standing modes of the cavity, maximum when the cavity length (its geometrical length added with the effective penetration depth of 58 nm) is equal to (λm)/(2n) (λ: emission wavelength of 420 nm, n: refractive index, m: integer called the cavity order).

The antinode factor indicates the coupling efficiency of QW to the cavity modes, which depends on the position of the QW relative to the antinode of a given mode. For example, when m equals to 2, (λm)/(2n) becomes 168 nm which is 110 nm + 58 nm. Thus, a geometrical cavity length of 113 nm of MC3~MC5 corresponds to m≈2. Therefore, to obtain the maximum LEE, the QW should be placed on the antinode of the cavity mode to maximize the LEE, i.e. at 75% from the top of the device of figure 5.15(a), like for MC5. Conversely, with the QW position at the node of the cavity mode as for MC3 at 46%, the emission is strongly decreased in spite of the cavity being resonant.

Table 5.2. Room-temperature quick test results of epitaxial wafers of MC1~MC5 at a forward current of 20 mA. Each estimated MIQE was obtained assuming that MC1 has an MIQE of 23% and the relative output power is proportional to the MIQE. Estimated EQE was obtained by using the estimated MIQE and the LEE of Fig. 2(b). This is the Accepted Manuscript version of an article accepted for publication in [Applied Physics Express]. IOP Publishing Ltd is not responsible for any errors or omissions in this version of the manuscript or any version derived from it. The Version of Record is available online at [https://doi.org/10.35848/1882-0786/abebb3].

	Voltage (V)	Relative output power (mW)	Estimated MIQE (%)	LEE by simulation (%)	Estimated EQE (%)	Peak EQE (%)
MC1	4.4	6.5	23	29	6.7	6.7
MC2	4.3	6.6	23	31	7.1	4.8
MC3	4.1	4.2	15	7.6	1.1	0.6
MC4	3.8	6.7	24	24	5.8	2.5
MC5	3.6	5.2	18	35	6.3	-*

*No emission by short circuit

Table 5.2 shows the quick test results of the MC1~MC5 epi-wafers before the n^{++} regrowth. Assuming the LEE of epi-wafer of MC1~MC5 is constant at about 4%, each relative output power of Table 5.2 is proportional to each MIQE of MC1~MC5. Each MIQE is obtained assuming that the MIQE of the MC1 epi-wafer is 23% which value is almost the same as our previous result of 24%[63]. Then, we obtained the estimated EQE using the value of LEE of figure 5.16(b). All of the MC1~MC5 epi-wafers have a reasonable quick test forward voltage of 3.6~4.4 V and a reasonable relative output power of 4.2~6.7 mW as shown in table 5.2. Considering the quick test results, all of the LEDs are acceptable and similar including the MC5 epi-wafer with a cavity thickness of 113 nm.

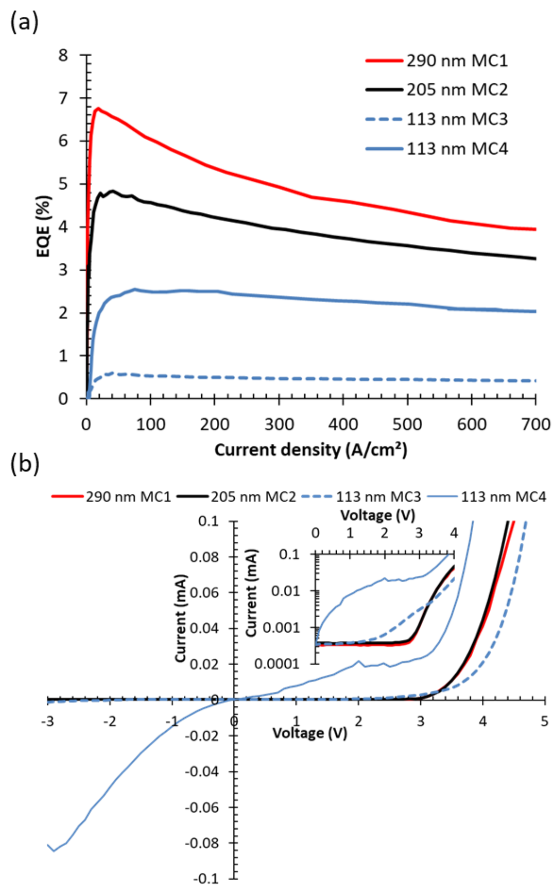

Figure 5.17 (a) EQE of MC1~MC4 as a function of current density. (b) I-V curves of MC1~MC4. Inset shows the I-V curves in log scale. The I-V curves were measured under DC biased conditions. This is the Accepted Manuscript version of an article accepted for publication in [Applied Physics Express]. IOP Publishing Ltd is not responsible for any errors or omissions in this version of the manuscript or any version derived from it. The Version of Record is available online at [https://doi.org/10.35848/1882-0786/abebb3].

Figure 5.17(a) shows the EQEs of the fabricated MC1~MC4 LEDs as a function of the current density. The peak EQE of MC1~MC4 is 6.7 %, 4.8%, 0.6% and 2.5%, respectively, as shown in Table I. We have grown several MC5 devices, but all devices showed a short circuit and no emissions after the device fabrication process. The MIQE of MC1 is obtained to be 23% using the LEE of 29% in figure 5.16(b) and the peak EQE of 6.7% of figure 5.17(a). Using each estimated MIQE shown in Table I and the LEE in figure 5.16(b), each estimated EQE of MC1~MC5 is as shown in Table 5.2. The value of peak EQE of MC2~MC4 of figure 5.17(a) and Table 5.2 is lower than that of the estimated EQE. We however recover the very low EQE of MC3 as predicted from the poor placement of the QW within the microcavity as predicted in figure 5.16(b). The lower peak EQEs, their uneven relative values and the short circuit of MC5 are considered to be caused by the device fabrication process.

Figure 5.17(b) shows the I-V curves of MC1~MC4. The high voltages of the MC-LEDs are due to a poor hole concentration of p-GaN of the TJ, which induces a wide depletion width in the reverse biased TJ. The poor hole concentration is due to the difficulty in activating the Mg-doped p-type GaN by thermal annealing since it is covered by Si-doped n^{++}-type GaN[41]. This high TJ voltage could be decreased dramatically by using the selective area growth of the TJ[58]. MC3 and MC4 had a leakage current of 0.6 μA and 20 μA, respectively, at the forward voltage of 2.0 V. Due to the leakage current path, the peak EQE of MC3 and MC4 should indeed be low as mentioned above. The forward leakage current of MC1 and MC2 is less than 0.3 μA, which is the detection limit of our experimental setup, at forward bias of 2.0 V as shown in the inset of figure 5.17(b), which leads to EQEs near their expected values.

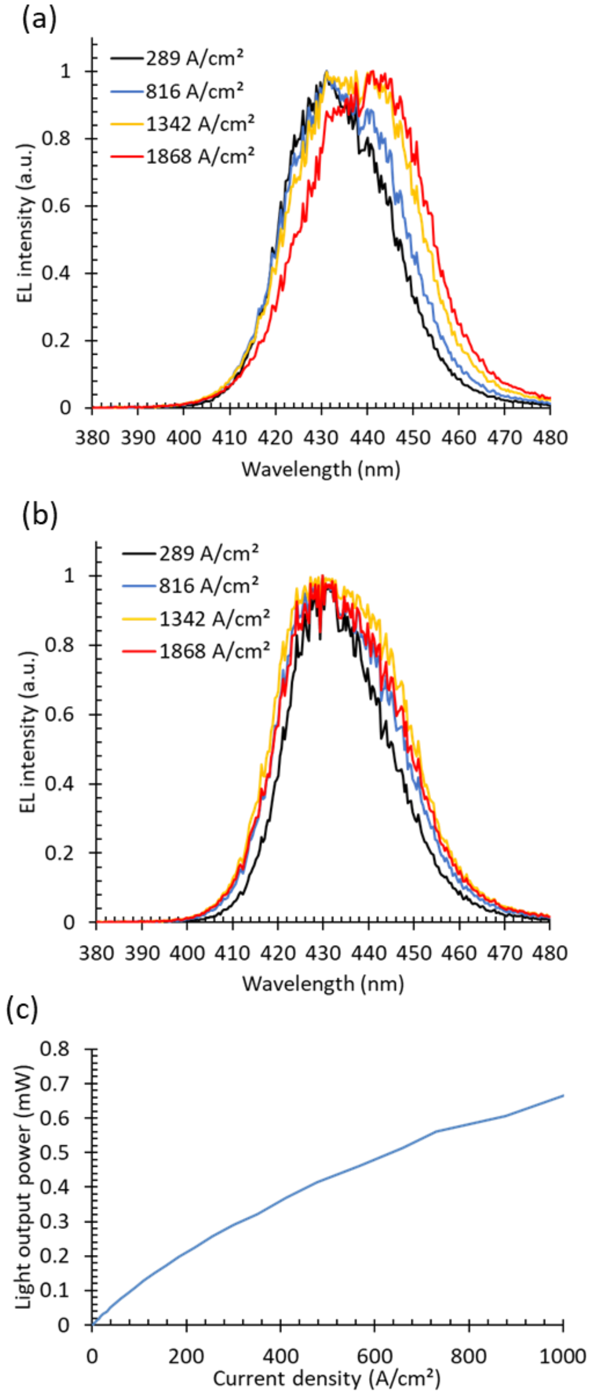

Figure 5.18. Emission spectra and light output power of MC1 with a cavity length of 290 nm as a function of the current density. (a) Emission spectra under DC operation. (b) Emission spectra under pulsed operation with a duty ratio of 2% and frequency of 10 kHz. (c) Light output power under DC operation. This is the Accepted Manuscript version of an article accepted for publication in [Applied Physics Express]. IOP Publishing Ltd is not responsible for any errors or omissions in this version of the manuscript or any

version derived from it. The Version of Record is available online at [https://doi.org/10.35848/1882-0786/abebb3].

Figure 5.18 shows the emission spectra of MC1 under DC and pulsed operations. The peak wavelength is almost constant around 430 nm with increasing the current density from 289 A/cm^2 (current: 1.1 mA) to 816 A/cm^2 (current: 3.1 mA), and then suddenly redshifts to around 440 nm from the current density from 1342 A/cm^2 (current:5.1 mA) to 1868 A/cm^2 (current: 7.1 mA) due to the heat generation under DC operation as shown in figure 5.18(a). The heat sink of our device is not working well at current densities more than 1342 A/cm^2 (current: 5.1 mA). Under pulsed operation, the peak wavelength is constant at 430 nm for the whole current density range as shown in figure 5.18(b). This is due to our use of semipolar (20-2-1) GaN for the MC-LED, the blue shift due to the screening of the polarization fields with current injection being minimized[31], [54]. This constant emission wavelength with changing the current density as shown in figure 5.18(b) should prove useful for real application. Figure 5.18(c) shows the light output power of MC1 as a function of the current density. The light output power increases almost linearly with increasing the current density though the deviation of the light outpower from linear increase is observed with increasing the current density, which is called as an output power droop. The EQE droop of MC1 is observed in figure 5.17(a)

The peak EQEs of MC2~MC5 are smaller than that of their estimated EQE as mentioned above, with MC5 having no emission due to a short circuit after device fabrication. How to improve the device fabrication process? The p-side thickness of MC1~MC5 is 110 nm, 106 nm, 54 nm, 39 nm and 22 nm, respectively, the n-side thicknesses of MC1~MC5 being 168 nm, 87 nm, 47 nm, 62 nm and 79 nm, respectively. The leakage currents of

MC1~MC5 are ≤0.3 μA, ≤0.3 μA, 0.6 μA, 20 μA, and short circuit, respectively, at the voltage of 2.0 V, as shown in figure 5.17(b). The quick test relative output powers of epitaxial wafers of MC1~MC5 are normal as shown in Table 5.2. Thus, it looks like a small p-side thickness is related to the origin of the leakage. After the RIE etching process as shown in Fig. 1(a) of Ref. [22], the sample is submerged in H_3PO_4 for 30 mins at RT to remove the sidewall damage caused by RIE[28]. As shown in Fig. 1(a) of Ref. [22], the top layer of the TJ is not covered by any mask to protect the etching during the H_3PO_4 treatment. There is a possibility that the top layer of the TJ and thin p-GaN layers are etched through pinholes, and that then a leakage path is formed through the TJ and the p-type layers. To avoid the degradation of the thin p-type layers, a fabrication process should protect the TJ before the H_3PO_4 treatment etching.

C. Conclusion

We have demonstrated the feasibility of ultimate-sized MC-LEDs in the nitride materials system. Precise positioning of the active layer in the cavity was shown possible by the quick test results. A lower damage MC-LEDs fabrication process should provide the quantitative results in order to compare performance with theory.

6. Future works and conclusion

6.1. Extraction of guided modes by angled sidewall

One of future works could be extraction of guided mode. Figure 6.1 show light intensity plots on 113 nm cavity length MC-LED. There are strong light extraction of 35% in the air cone when the QW position is 75% of the cavity from the top of the device. But this means there are 65% of light is guided inside the device. We can extract this guided mode by optimizing the sidewall angle. By Snell's law, we can have much more extraction by redirecting the light. This needs further study about the sidewall angles to maximize the extraction of the guided mode in MC-LEDs. In figure 6.1(a), the light intensity polar plot shows how well the light is distributed in certain angles. When the QW position is placed at 46% of the device from the top, which is black shape in figure 6.1(a), the angles of 15°, 58°, and 90° are the major light directions in the MC-LED. Among those angles, only the angle of 15° can be extracted. We need to redirect the angles of 58° and 90°, which requires complicated device geometry. However, when the QW position of MC-LED is 75%, it shows already the 35% light lays extraction without adding any pattern. Also, another 65% of the emission is highly concentrated at 90°, which makes the device geometry relatively easier than the previous case of multiple light angles as shown in figure 6.1(b).

The angled sidewall can be worked as tapered waveguide structure. Marcuse showed this theory in 1980[45]. When the waveguide refractive index changes abruptly, the guided mode is lost from the tapering structure of waveguide. Figure 6.2(a) showed the optical loss in the waveguide when it had step-tapered channel waveguide. From the result, the shorter length which had abrupt change of refractive index lost more radiation than the longer length waveguide. This loss is disadvantageous for the purpose of waveguide. However, as an emitter aspect, this is additional extraction of the light from the device. Therefore, the angled sidewall can be considered as the structure of tapered waveguide which extracts more guided modes. Figure 6.2(b) showed the radiation power of the channel waveguides with different taper lengths. As shown in the figure, the waveguide of short taper length, for example 30 μm case, emits about six times more radiation than the longer ones, 100 μm case. From the result, we could conclude the additional extraction of light from MC-LED. However, the angular dependence of the sidewall has not been studied yet. Using the simulation, Monte Carlo ray-tracing Synopsys LightTools software, and experiment of sidewall angle etching series will determine the optimized angle for the MC-LEDs.

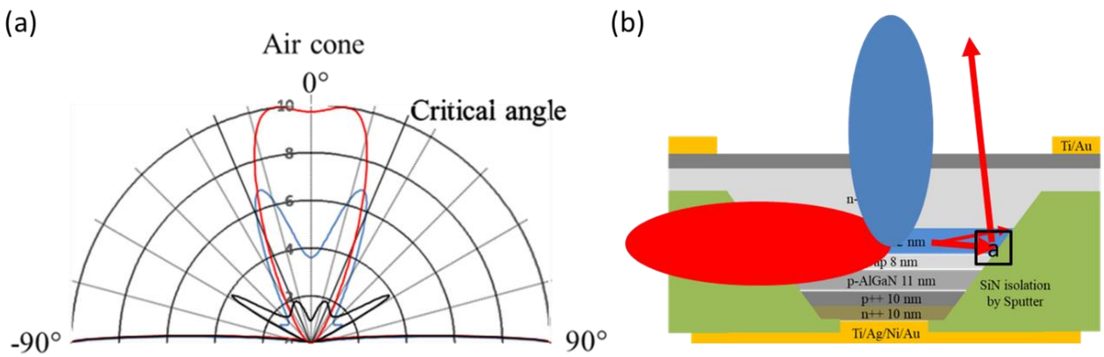

Figure 6.1. Schematics of light intensity plots in various 113 nm MC-LEDs and cross sectional device structure. (a) Light intensity plots of QW position of 75% (red), 60% (blue), 46% (black) in 113 nm MC-LEDs. (b) Schematic of light intensity in QW position of 75% (red) of 113 nm MC-LED. Extracted mode is 35% while the guided mode is 65% near 90°. Red arrows show light's redirection by the angled sidewall which reflects the light of guided modes to the air cone.

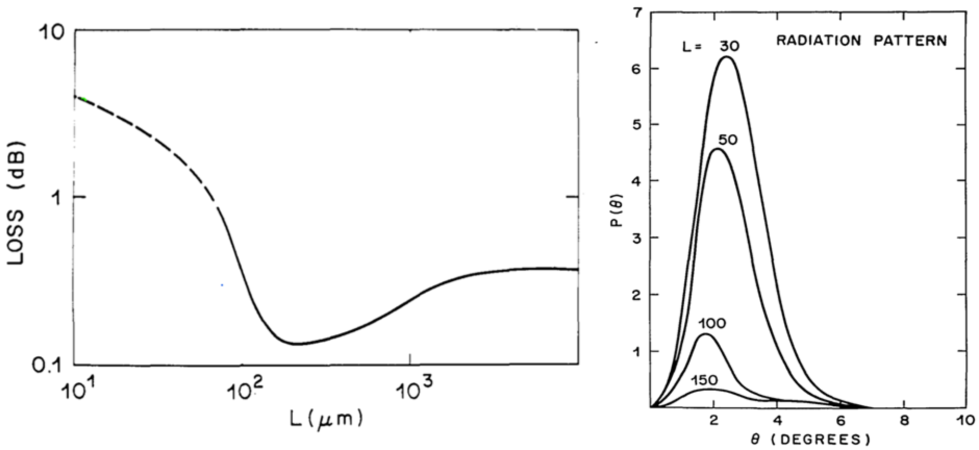

Figure 6.2. (a) Radiation loss in dB of tapering waveguide with respect to its length[45]. (b) Radiation power of the channel waveguide for various taper lengths[45].

6.2. MC-LED with the bottom mirror of dielectric DBRs

One good option of bottom mirror is dielectric DBRs. Normally, the DBRs are applied to vertical cavity surface-emitting lasers (VCSELs) as high reflection top and bottom mirrors. Since the dual dielectric DBRs have wide stopband and high reflectivity, the VCSELs using the dual dielectric DBRs have been demonstrated in UCSB[64]. Kearns et al. deposited 12 pairs of SiO_2 and Ta_2O_5 as top DBRs and 16 pairs of those as bottom DBRs. From the 1D transmission matrix model, the reflectivities are 99.939% for top the mirror and 99.995% for the bottom mirror, respectively[64]. Figure 6.3 shows the light intensity plot and the schematic of the MC-LED with the bottom DBRs. In figure 6.3(a), the geometrical cavity thickness of 143 nm MC-LED has high LEE of 33% when the critical angle is 23° between the GaN and air interface. By using the dielectric DBRs with pairs of SiO_2 and Ta_2O_5, we could expect several differences in operation of device. First of all, the reflectance is better with the DBRs than metal mirror. From the previous works, the 12 pairs of DBRs of SiO_2/Ta_2O_5 have the reflectance of 99.939%[64] while the Ag has the reflectance of 97%[63]. As it mentioned in the previous work[22], the LEE improves with the higher reflectance of mirror. When the mirror reflectance of 83% was applied in the simulation of LEE, the LEE was only 24% while the mirror reflectance of 97% has the LEE of 31%. Therefore, to achieve the better LEE, the highly reflective mirror needs to be chosen. Second, the DBR MC-LED will have longer effective cavity length at the wavelength of 420 nm. We have considered the phase shift by the Ag metal contact which added the effective cavity length as 58 nm at the 420 nm wavelength. When the DBRs are applied, we roughly expect additional cavity length as ~120 nm which is the optical thickness of a pair of two quarter wavelength layers of SiO_2, Ta_2O_5. With the high refractive index difference between SiO_2, 1.47 and Ta_2O_5, 2.18 and multiple pairs of the DBRs, the DBRs allow only a pair of those layers as penetration depth of the light. Though the MC-LED with bottom DBRs shows double effective thickness increment, it could be feasible because of recent demonstration of ultra-short MC-LEDs with 113 nm cavity length. We have already achieved this 113 nm epitaxial wafer without any problem, which means the thin enough epitaxial wafer is available to compensate the additional thickness increment. Third, the light absorption is much less in the MC-LED with DBRs. While Ag is good reflector for the emission wavelength, it absorbs the light and causes heating since the metal absorption is severe in this kind of short device. However, the dielectric DBRs have no such absorption. Lastly, Ag has electromigration problem which is detrimental for device in electrical operation aspect. The electrons in silver are removed, and Ag gets ionized. The ionized Ag gradually moves to the cathode, which causes the silver line. But the DBRs MC-LED doesn’t have the problem.

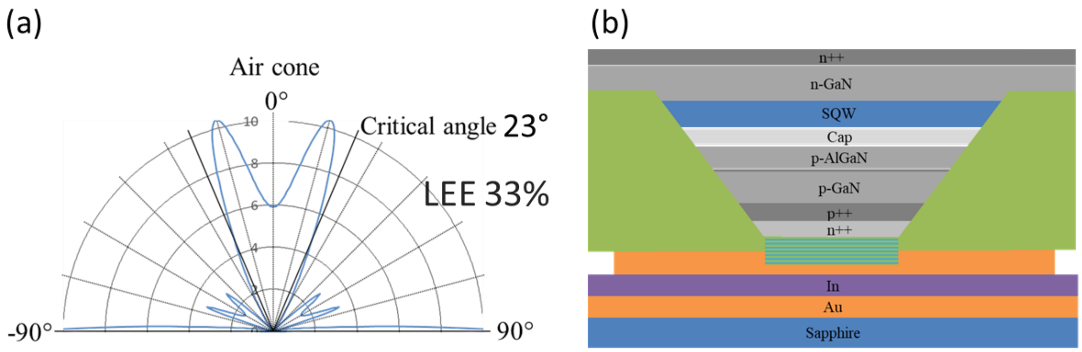

Figure 6.3. (a) the light intensity plot of MC-LED with the bottom DBRs when the geometrical cavity thickness of 143 nm. The LEE is 33% when the critical angle is 23° (b)Schematic of device cross-section of the bottom DBRs. The bottom mirror is replaced from Ag metal mirror to dielectric layer pairs of SiO_2/Ta_2O_5.

6.3. Device encapsulation

Using the encapsulation and optimized c-plane epitaxial wafer, we might reach 34% of EQE in this ultra-short MC-LEDs. Currently, there is no encapsulation on the device. The critical angle at this case is 23° and LEE is 31%. If the top of the device is covered by lower refractive material, such as the refractive index of 1.5, then the critical angle can be 37°. In figure 6.4(a), the LEE of that encapsulated device reaches 39% by extracting more light in the wider window of angle. As shown in the figure 6.4(b), the 205 nm MC-LED, EQE is 7.3%. Using the encapsulation of lower refractive index material on top, the LEE of the device could be increased as 39%. In that case, the EQE of the device can be 9.4% as shown in figure 6.4(b). Also, if we use the optimized c-plane epitaxial wafer having 87% of IQE[49], then the MC-LED with encapsulation from the epi could reach the 34% of EQE. Achieving the high performance MC-LEDs, the device processing needs to include the dielectric deposition. In addition, some epitaxial layer optimization on c-plane epi is needed to make it flip-chip process compatible as semipolar (20-2-1) epi.

(a)

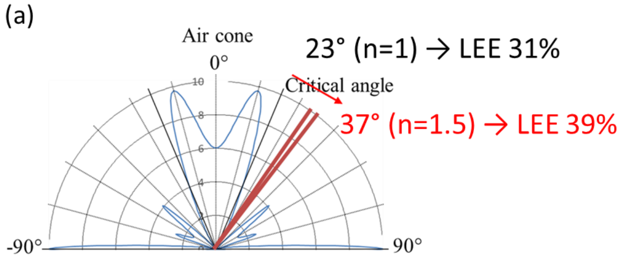

(b)

	IQE	LEE	EQE
Current 205 nm MC-LED	24%	31%	7.3%
With Encapsulation	24%	**39%**	9.4%
C-plane epitaxial wafer	**87%***	39%	**34%**

Figure 6.4. (a) the light intensity plot of MC-LED showing the two different critical angles determined by the lower refractive index materials, n=1 and n=1.5 (b) simplified result table of IQE, LEE, EQE in three kinds of MC-LEDs, current 205 nm MC-LED, the same MC-LED with encapsulation of n=1.5, and MC-LED using the optimized c-plane epitaxial wafer* and encapsulation of n=1.5[49].

6.4. Sidewall passivation using the ALD

One of the improvements can be made by sidewall passivation using the atomic-layer deposition (ALD). Wong et al. demonstrated high efficiency micro-LEDs with SiO_2 sidewall passivation in 2018[19]. Both plasma-enhanced chemical vapor deposition (PECVD) and ALD were performed in different samples. When the dielectric layer was deposited by ALD, the light emission was uniform and leakage current for all devices were lower than PECVD samples. The EQEs were 33% with ALD sidewall passivation, 24% without sidewall passivation, respectively. Therefore, using the ALD for the passivation will be one of options to improve electrical performances, such as uniform emission and leakage current prevention on MC-LEDs. If the Al_2O_3 layer is deposited on the sidewall by ALD instead of current Si_3N_4 sputtering, then the dielectric layer will passivate the dangling bonds on sidewall which are caused by dry etching damage during the aperture formation. Especially, it will reduce the leakage paths on ultra-short cavity length MC-LEDs, such as 113 nm design.

6.5. Device size reduction less than 10 μm

Shrinking the device dimensions less than 10 μm increase the LEE of MC-LEDs possibly. Recently, Ley et al[18]. and Smith et al[17]. demonstrated very small micro-LEDs with the sizes of 1~10 μm. Especially, Ley et al[18] showed that the EQEs of small devices with the diameters of 2 μm and 5 μm are higher than larger devices. From the Monte Carlo ray tracing studies, they have observed that the LEE is higher in small devices than large ones. It is because the inclined sidewall redirects the light rays beyond the critical angles to normal direction. Therefore, smaller diameter devices extract more light since its sidewalls are closer than that of larger devices.

However, De Neve et al. showed the opposite result in 1997[56]. The EQEs of small devices were lower than the large devices. They prepared GaAs LEDs with different aperture sizes and measured the light output power. The reason of output power reduction related to the device sizes was photon recycling. Therefore, there are two conflicting results which are worth to check.

6.6. Blue, green, and red MC-LEDs with porous layer

Last future work is applying the porous layer for longer emission wavelength MC-LEDs. Pasayat et al. demonstrated LEDs with porous layer in 2019[65]. They have achieved 45 nm redshift in PL emission from the InGaN MQWs regrown on relaxed InGaN buffer layer by porosification. This means the porosified under layer will possibly be useful to have more indium incorporation in the QW of MC-LEDs. Therefore, the emission wavelength in those devices will span from violet to red, instead of current violet range.

6.7. Conclusion

We have demonstrated the first short 200 nm cavity length MC-LEDs with low EQE of 0.8%. The substrate removal technique made the ultra-short cavity thickness design possible. However, during the following experiment, high efficiency 205 nm cavity length MC-LEDs with peak EQE of 7.3% were demonstrated. This was done by the sidewall treatment and dielectric layer replacement. Because the dry etching damage introduces the non-radiative recombination centers and leakage paths, the previous non-treated MC-LEDs showed low EQEs and leakage current. Dipping the samples in H_3PO_4 removed the dry etching damages from the wet etching. And sputtering the Si_3N_4 worked well as the protecting layer for QW in MC-LEDs from the KOH during the PEC etching than SiO_2. Also, in the recent comparison experiment, the shortest cavity length of 113 nm devices were demonstrated. Though there was leakage current during the operation of the ultra-short MC-LEDs, that will be solved easily by optimizing the process step. Since the top surface of the epitaxial wafers were not covered with any mask during the H_3PO_4 wet etch treatment, the thin 113 nm cavity length MC-LEDs which had very thin p-side layers could be formed the leakage paths through the pin holes of the epitaxial wafer. This type of over-etching issue is very critical to MC-LEDs. The reason is the device epitaxial layers need to be controlled strictly in this microcavity regime. There is no room for extra thickness on p-side layers to avoid the over-etching problem. There is already available epitaxial wafer, MC5, for 113 nm with QW position of

75% for the highest LEE as shown in table 5.2, the quick test results of various epi-wafers. By putting mask to prevent the unexpected damages during the wet process, we will be able to achieve the 113 nm cavity length MC-LEDs with highest LEE of 35%.

Appendix

A1. Process flow for 200 nm MC-LEDs

Step	Equipment	#	Details	Notes
Calibration and epitaxial growth				
Calibration growth	MOCVD	1	Grow ~100 nm of n-type or p-type layer on AlGaN layer of ~10 nm	Figure out AlGaN growth rate and composition of Al first
Measurement	MRD (XRD)	2	Measure the thickness and get the growth rate	Use Global fit software
Tray preparation	MOCVD	3	Bake the trays before the epi growth 1210 °C, 30 min	~1 hour (bake) +20 min (loading/unloading)
Epitaxial growth	MOCVD	4	Grow the epi structures	~1 hour 40 min (205 nm MCLED) + 20 min (loading/unloading)
Quick test and TJ growth				
Activation	MOCVD Oven	5	Load epi wafer 600 °C, 15 min	
Quick test	Quicktest lab	6	Measure output power, voltage, peak wavelength, FWHM @ 20 mA, output power @ 200 mA	Hard burn-in 200~300 mA for 5 sec (if epi is unstable, soft burn-in 20 mA for 20 sec and then hard burn-in)
Aqua regia	Acid bench	7	3:1 $HCl:HNO_3$ @ 120 °C, 5 min for pre-heat w/o sample, 10 min treatment w/ samples, repeat 3x	Pour HCl first, add HNO_3. Mix new batch each iteration
BHF dip	Acid bench	8	Buffered HF 5 min	
Vacuum seal	Vacuum sealer	9	Mode P1, vacuum 95, gas 0, sealing 2.5	Bag under the right valve
TJ growth	MOCVD	10	1. Run bake recipe when the previous growth includes p-type layer. 2. Epi with sapphire corral on flat puck	Grow at the same day of BHF treatment
Aperture etching				
Cleaning	Solvent bench	11	1. Pre-heated NMP 10 min with high sonication 2. DI rinse and N2 dry	Check with microscope. Clean again when it is dirty
Lithography	PR bench	12	1. Spin HMDS with spin recipe 5 2. SPR220-1.8 with spin recipe 5 3. Remove edge-bead using razor blade 4. Soft bake 115 °C, 90 sec	Recipe 5: speed 3k rpm, ramp 600 rpm/s, 30 sec
	SUSS MJB-3	13	Expose "APERTURE" 25 sec	
	PR bench	14	Hard bake 115 °C, 60 sec	
	Develop bench	15	AZ300-MIF 50 sec	Check with microscope. Develop 10 sec more when under-develop

Ashing	PE II-A	16	O2 300 mT, power 100 W, 30 sec	
Aperture etching	RIE 5	17	O2 clean 10 min and SiCl4 conditioning 2 min: "JB_O2_clean_SiCl4"	~35 min
	RIE 5	18	SiCl4 etch for designated depth using the recipe "JB_SiCl4_only"	Check etching result with microscope
Chemical treatment	HF bench	19	BHF 5 min for Si-residue removal and rinse with DI, N2 dry	
	Acid bench	20	H3PO4 30 min in RT and rinse DI, N2 dry	
	Solvent bench	21	NMP 10 min with sonication high	Check the surface with microscope or confocal microscope.
Checking depth	KLA Tencor P-7, Olympus LEXT	22	Check the etching depth with the Dektak or confocal microscope	Go back to step 11 when under-etched
TJ activation	Rapid Thermal Annealer	23	720 °C, 25 min, N2/O2 9.6/2.4 sccm (use recipe "720C_25min_N2_O2")	
Isolation deposition				
Lithography	PR bench	24	1. Spin HMDS with spin recipe 5 2. nLoF2020 with spin recipe 5 3. Remove edge-bead using razor blade 4. Soft bake 110 °C, 90 sec	Recipe 5: speed 3k rpm, ramp 600 rpm/s, 30 sec
	SUSS MJB-3	25	Expose "ISOL_NEG" 10 sec	
	PR bench	26	Hard bake 110 °C, 60 sec	
	Develop bench	27	AZ300-MIF 50 sec	Check with microscope. Develop 10 sec more when under-develop
Ashing	PE II-A	28	O2 300 mT, power 100 W, 30 sec	
Dielectric deposition	Sputter 3	29	120 nm SiNx deposition power 250 W, gun angle 4 mm Use recipe "SiN_250W_200nm_JB_RF3"	Load Si pilot to check the thickness
Lift off	Solvent bench	30	Dip 80 °C NMP 10 min with high sonication (place right side down in NMP)	Check with microscope. Sonicate 10 min more when lift off is not done
Mesa etching				
Lithography	PR bench	31	1. Spin HMDS with spin recipe 0 2. SPR220-7.0 with spin recipe 0 3. Remove edge-bead using razor blade 4. Soft bake 115 °C, 120 sec	Recipe 0: speed 3.5k rpm, ramp 700 rpm/s, 45 sec
	SUSS MJB-3	32	Expose "MESA" 60 sec	
	PR bench	33	Degas bake 60 °C, 120 sec	
	Develop bench	34	AZ300-MIF 90 sec	Check with microscope. Develop 15 sec more when under-develop

Ashing	PE II-A	35	O2 300 mT, power 100 W, 30 sec	
Mesa etching	RIE 5	36	O2 clean 10 min and Cl2 conditioning 2 min: "JB_O2_clean_Cl2"	~35 min
	RIE 5	37	Cl2 etch for designated depth using the recipe "JB_Cl2_etch"	Check whether it over-etches with microscope
Cleaning	Solvent bench	38	Dip 80 °C NMP 10 min with high sonication	Check with microscope. Sonicate 10 min more when lift off is not done
Depth measurement	KLA Tencor P-7, Olympus LEXT	39	Check the etching depth with the Dektak or confocal microscope	
p-side metal deposition				
Lithography	PR bench	40	1. Spin HMDS with spin recipe 5 2. nLoF2035 with spin recipe 5 3. Remove edge-bead using razor blade 4. Soft bake 110C, 90 sec	Recipe 5: speed 3k rpm, ramp 700 rpm/s, 30 sec
	SUSS MJB-3	41	Expose "P-METAL" 10 sec	
	PR bench	42	Hard bake 110 °C, 60 sec	
	Develop bench	43	AZ300-MIF 50 sec	Check with microscope. Develop 10 sec more when under-develop
Ashing	PE II-A	44	O2 300 mT, power 100 W, 30 sec	
Metal deposition	EBeam 1	45	1. Set the distance between top of rod and top plate as 12 cm 2. Ti/Ag/Ni/Au: thickness 6/500/333/3333 A, rate 0.1/0.2-0.5-1/0.5-1/1-1.5-2 A/sec	Target thickness of 20/1,500/1,000/10,000 A
Lift off	Solvent bench	46	Dip in 80C NMP 10 min with low sonication	Check with microscope. Sonicate 10 min more when lift off is not done
Edge cleaning	Develop bench	47	Remove edge metal deposition using razor blade	
Submount preparation				
Metal deposition	EBeam 1	48	Deposit Ti/Au: thickness 133/2000 A (target 640 nm) (same setting of #36) on SSP sapphire	
	Thermal evaporator 2	49	1. Set the distance between sample holder and shutter 11 cm 2. Deposit In/Au: thickness 5000/700 A (target 1.54 um) In boat (full of In tear drops) @ filament "1", Au boat (6 Au pellets) @ filament "3"	HVAC on ~2.5 min In deposition prog. 7, deposition rate ~10 A/sec Au deposition prog. 3, deposition rate ~8 A/sec
Depth measurement	KLA Tencor P-7, Olympus LEXT	50	Check the deposition with the Dektak or confocal microscope	
Flip-chip bonding and PEC etching (packaging lab)				

Bonding	230 °C oven	51	1. Set the oven @ 230 °C 2. Put the wafer's right side down on submount in fixture 3. Hand-tighten the fixture 4. Load and wait 2 hour in the oven	If it is not bonded, change the submount and try #40 again.
PEC etching	PEC setup	52	1. Pour 1M KOH in a beaker 2. Set the ice bath temperature @ -1.5 C and place the beaker 3. Submerge the sample in the KOH 4. Turn on the 405 nm lamp above the beaker 5. Rinse with DI and dry with N2	~12 hour
Swabbing and n-side metal deposition				
Swabbing	Develop bench	53	1. Swab in Tergitol detergent 10 times in each direction (total four directions of sample) 2. Rinse with DI and dry with N2	Not to hard on swabbing which causes missing devices
Check	Confocal microscope or SEM 1	54	Check the PEC etching yield	
Cleaning	Solvent bench	55	Dip 80 °C NMP 10 min with high sonication	Check with microscope. Sonicate 10 min more when lift off is not done
Lithography	PR bench	56	1. LOL2000 with spin recipe 5 2. Remove edge-bead using razor blade 3. Bake 170 °C, 5 min and cool 1 min 4. nLoF2035 with spin recipe 5 6. Remove edge-bead using razor blade 7. Soft bake 110 °C, 90 sec	Recipe 5: speed 3k rpm, ramp 700 rpm/s, 30 sec
	SUSS MJB-3	57	Expose "N-CONTACT" 10 sec	
	PR bench	58	Hard bake 110 °C, 60 sec	
	Develop bench	59	AZ300-MIF 50 sec	Check with microscope. Develop 10 sec more when under-develop
Ashing	PE II-A	60	O2 300 mT, power 100 W, 30 sec	
Metal deposition	EBeam 1	61	1. Set the distance between top of rod and top plate as 12 cm 2. Ti/ Au: thickness 133/2000 A, rate 0.2-0.5-1/1-1.5-2 A/sec	Target thickness of 400/6,000 A
Lift off	Solvent bench	62	Dip in 80 °C NMP 10 min with low sonication	Check with microscope. Sonicate 10 min more when lift off is not done
Test the devices				

References

[1] T. J. Flack, B. N. Pushpakaran, and S. B. Bayne, “GaN Technology for Power Electronic Applications: A Review,” *J. Electron. Mater.*, vol. 45, no. 6, pp. 2673–2682, 2016, doi: 10.1007/s11664-016-4435-3.

[2] E. A. Jones, F. F. Wang, and D. Costinett, “Review of Commercial GaN Power Devices and GaN-Based Converter Design Challenges,” *IEEE J. Emerg. Sel. Top. Power Electron.*, vol. 4, no. 3, pp. 707–719, 2016, doi: 10.1109/JESTPE.2016.2582685.

[3] C. Lee *et al.*, “Gigabit-per-second white light-based visible light communication using near-ultraviolet laser diode and red-, green-, and blue-emitting phosphors,” *Opt. Express*, vol. 25, no. 15, p. 17480, 2017, doi: 10.1364/oe.25.017480.

[4] J. Chen, S. Loeb, and J. H. Kim, “LED revolution: Fundamentals and prospects for UV disinfection applications,” *Environ. Sci. Water Res. Technol.*, vol. 3, no. 2, pp. 188–202, 2017, doi: 10.1039/c6ew00241b.

[5] A. David, N. G. Young, C. Lund, and M. D. Craven, “Review—The Physics of Recombinations in III-Nitride Emitters,” *ECS J. Solid State Sci. Technol.*, vol. 9, no. 1, p. 016021, 2020, doi: 10.1149/2.0372001jss.

[6] R. P. Green, J. J. D. McKendry, D. Massoubre, E. Gu, M. D. Dawson, and A. E. Kelly, “Modulation bandwidth studies of recombination processes in blue and green InGaN quantum well micro-light-emitting diodes,” *Appl. Phys. Lett.*, vol. 102, no. 9, pp. 1–5, 2013, doi: 10.1063/1.4794078.

[7] J. Day, J. Li, D. Y. C. Lie, C. Bradford, J. Y. Lin, and H. X. Jiang, “III-Nitride full-scale high-resolution microdisplays,” *Appl. Phys. Lett.*, vol. 99, no. 3, pp. 1–4, 2011,

doi: 10.1063/1.3615679.

[8] J. W. Raring *et al.*, "High-efficiency blue and true-green-emitting laser diodes based on non-c-plane oriented GaN substrates," *Appl. Phys. Express*, vol. 3, no. 11, 2010, doi: 10.1143/APEX.3.112101.

[9] A. Paranjpe, J. Montgomery, S. M. Lee, and C. Morath, "45-2: Invited Paper: Micro-LED Displays: Key Manufacturing Challenges and Solutions," *SID Symp. Dig. Tech. Pap.*, vol. 49, no. 1, pp. 597–600, May 2018, doi: 10.1002/sdtp.12414.

[10] M. S. Wong, S. Nakamura, and S. P. DenBaars, "Review—Progress in High Performance III-Nitride Micro-Light-Emitting Diodes," *ECS J. Solid State Sci. Technol.*, vol. 9, no. 1, p. 015012, 2020, doi: 10.1149/2.0302001jss.

[11] S. Nakamura, T. Mukai, M. Senoh, and N. Iwasa, "Thermal annealing effects on P-type Mg-doped GaN films," *Jpn. J. Appl. Phys.*, vol. 31, no. 2, pp. 139–142, 1992, doi: 10.1143/JJAP.31.L139.

[12] W. Götz, N. M. Johnson, J. Walker, D. P. Bour, H. Amano, and I. Akasaki, "Hydrogen passivation of Mg acceptors in GaN grown by metalorganic chemical vapor deposition," *Appl. Phys. Lett.*, vol. 67, no. 18, pp. 2666–2668, Oct. 1995, doi: 10.1063/1.114330.

[13] T. Fujii, Y. Gao, R. Sharma, E. L. Hu, S. P. DenBaars, and S. Nakamura, "Increase in the extraction efficiency of GaN-based light-emitting diodes via surface roughening," *Appl. Phys. Lett.*, vol. 84, no. 6, pp. 855–857, Feb. 2004, doi: 10.1063/1.1645992.

[14] M. Yamada *et al.*, "InGaN-Based Near-Ultraviolet and Blue-Light-Emitting Diodes with High External Quantum Efficiency Using a Patterned Sapphire Substrate and a Mesh Electrode," *Jpn. J. Appl. Phys.*, vol. 41, no. Part 2, No. 12B, pp. L1431–L1433,

Dec. 2002, doi: 10.1143/JJAP.41.L1431.

[15] Y. Zhao *et al.*, “30-mW-Class High-Power and High-Efficiency Blue Semipolar (10\bar1\bar1) InGaN/GaN Light-Emitting Diodes Obtained by Backside Roughening Technique,” *Appl. Phys. Express*, vol. 3, no. 10, p. 102101, Sep. 2010, doi: 10.1143/APEX.3.102101.

[16] F. Templier, “GaN-based emissive microdisplays: A very promising technology for compact, ultra-high brightness display systems,” *J. Soc. Inf. Disp.*, vol. 24, no. 11, pp. 669–675, Nov. 2016, doi: 10.1002/jsid.516.

[17] J. M. Smith *et al.*, “Comparison of size-dependent characteristics of blue and green InGaN microLEDs down to 1 μm in diameter,” *Appl. Phys. Lett.*, vol. 116, no. January, p. 071102, 2020, doi: 10.1063/1.5144819.

[18] R. T. Ley *et al.*, “Revealing the importance of light extraction efficiency in InGaN/GaN microLEDs via chemical treatment and dielectric passivation,” *Appl. Phys. Lett.*, vol. 116, no. 25, p. 251104, Jun. 2020, doi: 10.1063/5.0011651.

[19] M. S. Wong *et al.*, “High efficiency of III-nitride micro-light-emitting diodes by sidewall passivation using atomic layer deposition,” *Opt. Express*, vol. 26, no. 16, p. 21324, 2018, doi: 10.1364/OE.26.021324.

[20] E. Matioli and C. Weisbuch, “Impact of photonic crystals on LED light extraction efficiency: Approaches and limits to vertical structure designs,” *J. Phys. D. Appl. Phys.*, vol. 43, no. 35, p. 354005, Sep. 2010, doi: 10.1088/0022-3727/43/35/354005.

[21] Y. Zhao *et al.*, “High-Power Blue-Violet Semipolar (20-2-1) InGaN/GaN Light-Emitting Diodes with Low Efficiency Droop at 200 A/cm2,” *Appl. Phys. Express*, vol. 4, no. 8, p. 082104, Jul. 2011, doi: 10.1143/APEX.4.082104.

[22] J. Back, M. S. Wong, J. Kearns, S. P. DenBaars, C. Weisbuch, and S. Nakamura, “Violet semipolar (20-2-1) InGaN microcavity light-emitting diode with a 200 nm ultra-short cavity length,” *Opt. Express*, vol. 28, no. 20, p. 29991, Sep. 2020, doi: 10.1364/OE.401640.

[23] S. Lee *et al.*, “Smooth and selective photo-electrochemical etching of heavily doped GaN:Si using a mode-locked 355nm microchip laser,” *Appl. Phys. Express*, vol. 10, no. 1, pp. 8–11, 2017, doi: 10.7567/APEX.10.011001.

[24] B. P. Yonkee, E. C. Young, S. P. DenBaars, S. Nakamura, and J. S. Speck, “Silver free III-nitride flip chip light-emitting-diode with wall plug efficiency over 70% utilizing a GaN tunnel junction,” *Appl. Phys. Lett.*, vol. 109, no. 19, 2016, doi: 10.1063/1.4967501.

[25] Y. Kuwano *et al.*, “Lateral hydrogen diffusion at p-GaN layers in nitride-based light emitting diodes with tunnel junctions,” *Jpn. J. Appl. Phys.*, vol. 52, no. 8 PART 2, 2013, doi: 10.7567/JJAP.52.08JK12.

[26] L. Deillon, A. Hessler-Wyser, T. Hessler, and M. Rappaz, “Solid-liquid interdiffusion (SLID) bonding in the Au-In system: Experimental study and 1D modelling,” *J. Micromechanics Microengineering*, vol. 25, no. 12, 2015, doi: 10.1088/0960-1317/25/12/125016.

[27] E. Matioli *et al.*, “GaN-based embedded 2D photonic crystal LEDs: Numerical optimization and device characterization,” *Phys. Status Solidi Curr. Top. Solid State Phys.*, vol. 6, no. SUPPL. 2, pp. 675–679, 2009, doi: 10.1002/pssc.200880987.

[28] Y. Jung *et al.*, “Chemical Etch Characteristics of N-Face and Ga-Face GaN by Phosphoric Acid and Potassium Hydroxide Solutions,” *J. Electrochem. Soc.*, vol. 159,

no. 2, pp. H117–H120, Jan. 2011, doi: 10.1149/2.039202jes.

[29] M. S. Wong *et al.*, “Size-independent peak efficiency of III-nitride micro-light-emitting-diodes using chemical treatment and sidewall passivation,” *Appl. Phys. Express*, vol. 12, no. 9, p. 097004, Sep. 2019, doi: 10.7567/1882-0786/ab3949.

[30] C. C. Pan *et al.*, “High-power, low-efficiency-droop semipolar (202$\bar{1}\bar{1}$) single-quantum-well blue light-emitting diodes,” *Appl. Phys. Express*, vol. 5, no. 6, pp. 3–6, 2012, doi: 10.1143/APEX.5.062103.

[31] D. F. Feezell, J. S. Speck, S. P. Denbaars, and S. Nakamura, “Semipolar 2021 InGaN / GaN Light-Emitting Diodes for High-Ef fi ciency Solid-State Lighting,” vol. 9, no. 4, pp. 190–198, 2013, [Online]. Available: https://www.osapublishing.org/jdt/abstract.cfm?URI=jdt-9-4-190.

[32] C. A. Forman *et al.*, “Continuous-wave operation of m -plane GaN-based vertical-cavity surface-emitting lasers with a tunnel junction intracavity contact,” *Appl. Phys. Lett.*, vol. 112, no. 11, p. 111106, Mar. 2018, doi: 10.1063/1.5007746.

[33] S. Lee *et al.*, “GaN-based vertical-cavity surface-emitting lasers with tunnel junction contacts grown by metal-organic chemical vapor deposition,” *Appl. Phys. Express*, vol. 11, no. 6, p. 062703, Jun. 2018, doi: 10.7567/APEX.11.062703.

[34] J. A. Kearns, J. Back, N. C. Palmquist, D. A. Cohen, S. P. DenBaars, and S. Nakamura, “Inhomogeneous Current Injection and Filamentary Lasing of Semipolar (2021¯) Blue GaN-Based Vertical-Cavity Surface-Emitting Lasers with Buried Tunnel Junctions,” *Phys. status solidi*, vol. 217, no. 7, p. 1900718, Apr. 2020, doi: 10.1002/pssa.201900718.

[35] K. Mehta *et al.*, “Lateral current spreading in III-N ultraviolet vertical-cavity surface-

emitting lasers using modulation-doped short period superlattices," *IEEE J. Quantum Electron.*, vol. 54, no. 4, 2018, doi: 10.1109/JQE.2018.2836667.

[36] F. Ma and X. Liu, "Phase shift and penetration depth of metal mirrors in a microcavity structure," *Appl. Opt.*, vol. 46, no. 25, pp. 6247–6250, 2007.

[37] E. Kudo *et al.*, "Optical properties of highly stable silver thin films using different surface metal layers," *Thin Solid Films*, vol. 660, pp. 730–732, Aug. 2018, doi: 10.1016/j.tsf.2018.03.086.

[38] L. Macht, J. J. Kelly, J. L. Weyher, A. Grzegorczyk, and P. K. Larsen, "An electrochemical study of photoetching of heteroepitaxial GaN: Kinetics and morphology," *J. Cryst. Growth*, vol. 273, no. 3–4, pp. 347–356, 2005, doi: 10.1016/j.jcrysgro.2004.09.029.

[39] D. H. van Dorp, J. L. Weyher, M. R. Kooijman, and J. J. Kelly, "Photoetching Mechanisms of GaN in Alkaline S_2O_8 2 − Solution Solution," *J. Electrochem. Soc.*, vol. 156, no. 10, p. D371, Jul. 2009, doi: 10.1149/1.3183807.

[40] S. W. Lee *et al.*, "Origin of forward leakage current in GaN-based light-emitting devices," *Appl. Phys. Lett.*, vol. 89, no. 13, p. 132117, Sep. 2006, doi: 10.1063/1.2357930.

[41] D. Hwang, A. J. Mughal, M. S. Wong, A. I. Alhassan, S. Nakamura, and S. P. Denbaars, "Micro-light-emitting diodes with III-nitride tunnel junction contacts grown by metalorganic chemical vapor deposition," *Appl. Phys. Express*, vol. 11, no. 1, p. 012102, 2018, doi: 10.7567/APEX.11.012102.

[42] P. Li *et al.*, "Metalorganic chemical vapor deposition grown n-InGaN/n-GaN tunnel junctions for micro-light-emitting diodes with very low forward voltage," *Appl. Phys.*

Lett., p. submitted, 2020.

[43] A. David, "Ph.D. thesis," Ecole Polytechnique X, 2006.

[44] E. Matioli, "Embedded Photonic Crystals for High-Efficiency GaN-Based Optoelectronic Devices," University of California, Santa Barbara, 2010.

[45] D. Marcuse, "Radiation losses of step-tapered channel waveguides," *Appl. Opt.*, vol. 19, no. 21, p. 3676, 1980, doi: 10.1364/ao.19.003676.

[46] P. M. Pattison, A. David, R. Sharma, C. Weisbuch, S. DenBaars, and S. Nakamura, "Gallium nitride based microcavity light emitting diodes with 2λ effective cavity thickness," *Appl. Phys. Lett.*, vol. 90, no. 3, p. 031111, Jan. 2007, doi: 10.1063/1.2430913.

[47] Y.-S. Choi *et al.*, "Submicron-thick microcavity InGaN light emitting diodes," in *Proceedings of SPIE*, Feb. 2008, vol. 6910, pp. 69100R-1-69100R–8, doi: 10.1117/12.764696.

[48] J. Dorsaz, J.-F. Carlin, S. Gradecak, and M. Ilegems, "Progress in AlInN–GaN Bragg reflectors: Application to a microcavity light emitting diode," *J. Appl. Phys.*, vol. 97, no. 8, p. 084505, Apr. 2005, doi: 10.1063/1.1872197.

[49] D. Hwang, A. Mughal, C. D. Pynn, S. Nakamura, and S. P. DenBaars, "Sustained high external quantum efficiency in ultrasmall blue III–nitride micro-LEDs," *Appl. Phys. Express*, vol. 10, no. 3, p. 032101, Mar. 2017, doi: 10.7567/APEX.10.032101.

[50] F. Olivier, A. Daami, C. Licitra, and F. Templier, "Shockley-Read-Hall and Auger non-radiative recombination in GaN based LEDs: A size effect study," *Appl. Phys. Lett.*, vol. 111, no. 2, p. 022104, Jul. 2017, doi: 10.1063/1.4993741.

[51] S. S. Konoplev, K. A. Bulashevich, and S. Y. Karpov, "From Large-Size to Micro-

LEDs: Scaling Trends Revealed by Modeling," *Phys. status solidi*, vol. 215, no. 10, p. 1700508, May 2018, doi: 10.1002/pssa.201700508.

[52] Y. Yang and X. A. Cao, "Removing plasma-induced sidewall damage in GaN-based light-emitting diodes by annealing and wet chemical treatments," *J. Vac. Sci. Technol. B Microelectron. Nanom. Struct.*, vol. 27, no. 6, p. 2337, 2009, doi: 10.1116/1.3244590.

[53] X. A. Cao *et al.*, "Electrical effects of plasma damage in p-GaN," *Appl. Phys. Lett.*, vol. 75, no. 17, pp. 2569–2571, 1999, doi: 10.1063/1.125080.

[54] Y. Zhao *et al.*, "High optical polarization ratio from semipolar (202¯1¯) blue-green InGaN/GaN light-emitting diodes," *Appl. Phys. Lett.*, vol. 99, no. 5, p. 051109, Aug. 2011, doi: 10.1063/1.3619826.

[55] Y. Shao and F. G. Shi, "Exploring the critical thickness for maximum reflectance of optical reflectors based on polymer-filler composites," *Opt. Mater. Express*, vol. 6, no. 4, p. 1106, 2016, doi: 10.1364/ome.6.001106.

[56] H. De Neve, J. Blondelle, P. Van Daele, P. Demeester, R. Baets, and G. Borghs, "Recycling of guided mode light emission in planar microcavity light emitting diodes," *Appl. Phys. Lett.*, vol. 70, no. 7, pp. 799–801, Feb. 1997, doi: 10.1063/1.118226.

[57] H. Benisty, H. De Neve, and C. Weisbuch, "Impact of planar microcavity effects on light extraction - Part I: Basic concepts and analytical trends," *IEEE J. Quantum Electron.*, vol. 34, no. 9, pp. 1612–1631, 1998, doi: 10.1109/3.709578.

[58] P. Li *et al.*, "Metalorganic chemical vapor deposition grown n-InGaN/n-GaN tunnel junctions for micro-light-emitting diodes with very low forward voltage," *Semicond.*

Sci. Technol., vol. 35, no. 12, p. 125023, Dec. 2020, doi: 10.1088/1361-6641/abbd5b.

[59] C. Lalau Keraly, L. Kuritzky, M. Cochet, and C. Weisbuch, “Light Extraction Efficiency Part A. Ray Tracing for Light Extraction Efficiency (LEE) Modeling in Nitride LEDs,” in *III-Nitride Based Light Emitting Diodes and Applications, Topics in Applied Physics*, vol. 126, T.-Y. Seong, J. Han, H. Amano, and H. Morkoc, Eds. Dordrecht: Springer Netherlands, 2013, pp. 231–269.

[60] C. Weisbuch *et al.*, “Recent results and latest views on microcavity LEDs,” in *Proceedings of SPIE*, Jun. 2004, vol. 5366, p. 1, doi: 10.1117/12.537630.

[61] I. E. Titkov *et al.*, “Temperature-Dependent internal quantum efficiency of blue high-brightness light-emitting diodes,” *IEEE J. Quantum Electron.*, vol. 50, no. 11, pp. 911–920, 2014, doi: 10.1109/JQE.2014.2359958.

[62] G. Li *et al.*, “GaN-based light-emitting diodes on various substrates: a critical review,” *Reports Prog. Phys.*, vol. 79, no. 5, p. 056501, May 2016, doi: 10.1088/0034-4885/79/5/056501.

[63] J. Back, M. S. Wong, S. P. DenBaars, C. Weisbuch, and S. Nakamura, “High efficiency blue InGaN microcavity light-emitting diode with a 205 nm ultra-short cavity,” *Appl. Phys. Lett.*, vol. 118, no. 3, p. 031102, Jan. 2021, doi: 10.1063/5.0039773.

[64] J. A. Kearns, J. Back, D. A. Cohen, S. P. DenBaars, and S. Nakamura, “Demonstration of blue semipolar $(20\bar{2}\bar{1})$ GaN-based vertical-cavity surface-emitting lasers,” *Opt. Express*, vol. 27, no. 17, p. 23707, 2019, doi: 10.1364/oe.27.023707.

[65] S. S. Pasayat *et al.*, “Fabrication of relaxed InGaN pseudo-substrates composed of

micron-sized pattern arrays with high fill factors using porous GaN," *Semicond. Sci. Technol.*, vol. 34, no. 11, p. 115020, Nov. 2019, doi: 10.1088/1361-6641/ab4372.